Part IV

Nanocoatings and surface modification techniques

15

Nanotechnologies for coating and structuring of textiles

T. STEGMAIER, M. DAUNER, V. VON ARNIM, A. SCHERRIEBLE, A. DINKELMANN and H. PLANCK, ITV Denkendorf, Germany

15.1 Introduction

Fiber-based materials in technical applications are an increasing worldwide market and cover a wide area. Interesting applications for fibers with nano-scaled dimensions or nanostructured surfaces are in mobility (vehicles, aircraft, fuel cells), gas and liquid filtration, fiber reinforced materials (composites), protection and professional protective clothing. Tailoring and controlling of structures on a nano-scale level are considered to be key factors for the development of advanced materials or structural components and multifunctional applications. Nanotechnology is considered to increase the number, variety and effectivity of physical properties (electrical conductivity, magnetic susceptibility, interaction with light, photonics, corrosion protection, friction control, abrasion resistance, water and oil repellence, soil release, biocompatibility) of existing products and therefore act as an innovative base for new products.

The dimensional aspect for the use of the 'nanotechnology' term is not clearly defined. It is commonly the control over a structural range from a few nanometers up to 50 and 100 nanometers that defines 'nanotechnology'. In some cases the upper limit of the considered scale is regarded to be a few hundred nanometers or even 1 μm. In our research on nano-structured textiles we usually consider structural elements smaller than 100 nm. However, because 'nano' fibers with diameters of 100–500 nm are of great technological interest and need innovative fiber spinning techniques, these fibers are often included in the investigations of nanofibers.

There are many ways to implement nano-scale controlled properties into textiles. One is to give the fiber itself a nano-scale by fiber spinning. With novel fiber spinning technologies it is possible to spin fibers with diameters between 20 and 500 nm; 10–500 times thinner than fibers spinnable by traditional fiber spinning techniques. An aim is to make the production of fibers with diameters below 100 nm highly productive and state-of-the-art.

In order to achieve effects from nanostructures in the fiber bulk either

nanoparticle-filled polymer melts (e.g. pigments, TiO_2, ZnO, clay) or nanophase-separating polymeric systems (e.g. elastane) can be spun. Nanofillers such as clay have been known for decades, but the processing of those filled polymeric melts is challenging because agglomeration has to be avoided and the influence of nanoparticles on rheological properties can be great.

15.2 Production of nanofiber nonwovens using electrostatic spinning

Porosity and pore size are crucial properties of filter media, which determine efficiency as well as pressure drop and permeability. Small pore sizes at high porosity of a textile filter medium depend on the fiber size. A reduction of the pore size below the fiber diameter greatly reduces the porosity and diminishes the permeability, which means the filtration efficiency increases with a reduction in the fiber diameter.

The demand for filter media with high filter efficiency in the sub-micrometer range is increasing. The demand is based on the need for the filtration of aerosols and of industrially more and more important nanoparticles as well as on the requests for effective barrier effects against bacteria (<0.3 µm), viruses and other microorganisms. The diameter of natural as well as of synthetic fibers usually ranges from 10 to 20 µm. Microfibers and bi-component split fibers allow 3–7 µm. Melt blow and flash spinning end up with 1 µm fiber diameters.[1] Below that, in the sub-micrometer range, glass fibers are produced, but should not be used for many filtration applications. Figure 15.1 shows the relation between fiber diameter and the resulting fiber surface: a reduction from microfibers (10 µm) to nanofibers (100 nm) increases the fiber surface in a textile formation with a weight of 300 g/m^2 from 100 m^2 to 10 000 m^2.

15.2.1 Electrostatic spinning

The basic design of electrostatic spinning and its realization in most research laboratories is very simple (Fig. 15.2). A polymer solution is fed to a nozzle by a defined low pressure. An electrical field is applied between the nozzle and a collector (rotating mandrel or a conveyor belt). The application of the voltage on the nozzle or the carrier is not important initially. The application of positive or negative charges is mandatory. Independent of the polymer, solvent and the concentration of the solution, a voltage of 1 kV per centimeter between the nozzle and the collector of the spun fibers is useful. The nozzle diameter is usually about 100 µm.

Based on video recordings the mechanism leading to nanofibers was described at first as a multiple splaying similar to lightning.[2] Ten times

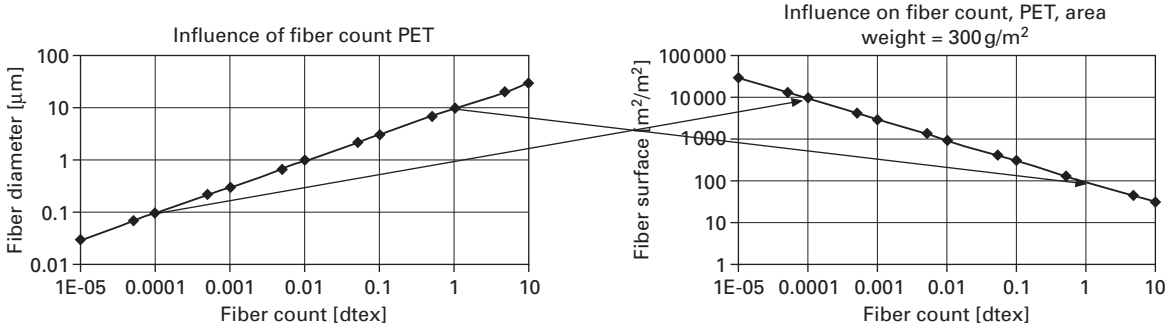

15.1 Increase of fiber surface through reduction of fiber diameter.

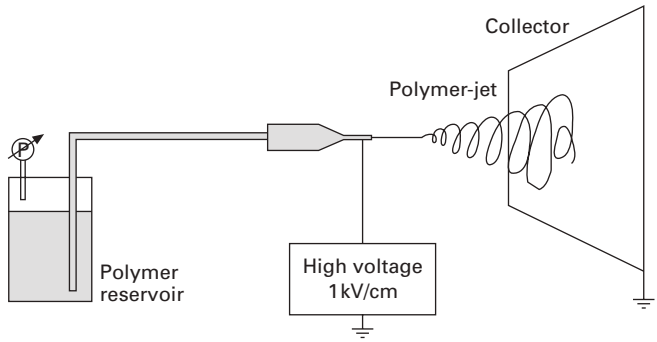

15.2 Apparatus for the electrostatic spinning, 'Whipping' mechanism from Ref. 3.

splaying of a 1 µm fiber leads to fibrils of about 0.3 µm in diameter. It can be easily calculated that an original single polymer solution jet needs to split into some 100 distinct jets in order to achieve nanofibers of 100 nm diameter. (In addition, the solvent extraction has to be taken in account.)

In 2000, Reneker and Chun published the scientific proof for another mechanism, so-called 'whipping', which was discovered thanks to an improved video-resolution: after leaving the nozzle the primary fiber stays stable on the way to the carrier as long as surface tension, electrical charging and external influences (such as friction in air) stay in equilibrium. Any perturbation leads to a deviation of the fiber until a new equilibrium is reached. At constant margins (feeding and winding speed) the fiber becomes stretched. Here again a draw ratio of 100 can be easily achieved, reducing the diameter from 1 to 0.1 µm.[2]

15.2.2 Polymers and solvents

The requirements on the polymer are comparable to other fiber-forming processes from solutions. Amorphous polymers result in regular nonwoven structures by use of the electrospinning process. Yet, according to our experiments and verified by literature data, nano-fibers could be produced only from crystallite-forming polymers. A further requirement for electrostatic spinning is that the polymer should be polar. Regular structures in the micrometer scale were produced from different polyurethanes and from co-polyesters (e.g. Fig. 15.3 and 15.4). Microporous surfaces have been produced by the electrospinning process using solutions from polylactides.[4] Using solutions from polyethyleneoxide (PEO), polyvinylalcohol (PVA) and polyacrylonitrile (PAN), as well as from polyimide, fibers in the nanometer scale were produced. The fiber diameter can be measured only by scanning electron microscope (SEM).

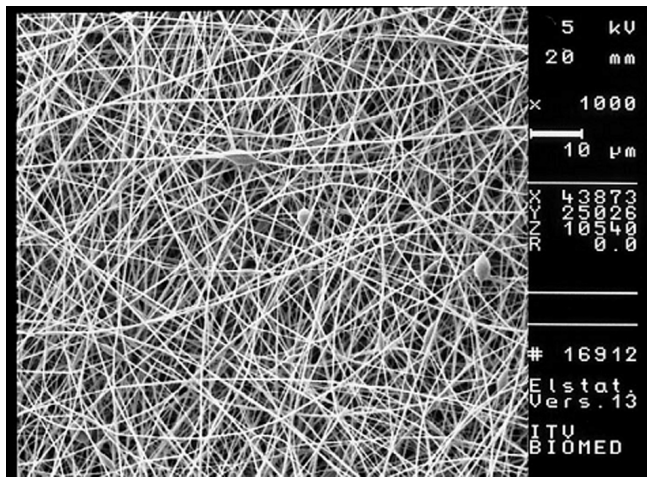

15.3 PVA in water, 1 kV/cm.

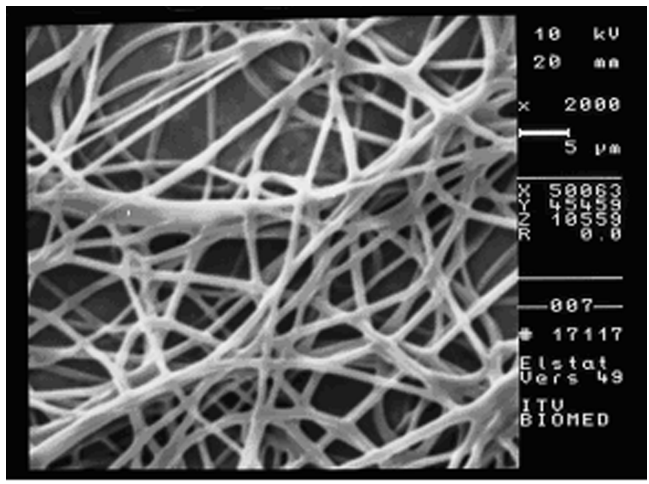

15.4 Polyurethane, $CHCl_3$/MeOH, 1 kV/cm.

As with the polymers, a high polarity of the solvent improves the electrostatic process. Further a high electrical conductivity of the solvent is required for the production of nano-fibers.[5] PVA and PEO are favorites for experiments as they can be processed from aqueous solutions and no special safety considerations have to be made regarding toxicity or explosivity. In addition, water is highly polar and most suitable for electrostatic spinning. (Their use for filters is limited, of course.) These are the main requirements on the solvents. In practice these ideal conditions will rarely be found. The use of chlorinated organic solvents is accepted when only small amounts are processed (e.g. for medical applications). It is difficult to obtain an operation permit for

large-scale production. Using inflammable organic solvents such as hydrocarbons carries risks of explosion, and safety concerns are substantial.

The vapor pressure of the solvent is a minor concern for processing by electrostatic spinning. Dimethylacetamide (DMAC) and dimethylformamide (DMF) with a low vapor pressure respectively can be very useful for the spinning of certain polymers. But the complete removal of the solvents may be a problem. On the other hand a high vapor pressure may cause problems due to the early evaporation of the respective solvent.

The appropriate concentration of the solutions depends of course on the polymer, its molecular mass and the solvent. Fibers do not form at very low concentrations. High concentrations hinder the feeding of the solution and its filtration. Good results are obtained at 5–20 vol.% with the best results in between.

15.2.3 Production methods

Investments of tens of millions euros per year are made worldwide for the development of electrostatic spinning. The United States, Korea and Japan are particularly heavy investors. Within Europe, Germany is one of the leading countries in R & D on electrospinning.

At INDEX 2005 in Geneva, Switzerland, the Czech start-up company Elmarco, Liberec presented a technology for the productive spinning of nano-fiber webs. This technology, which avoids the use of needle tips or nozzles, has been filed for patents by other companies before, yet is without commercial use. The process is based on a rotating roll dipping in a bath of polymer solution. Roll and bath are electrically on ground. The high-voltage electrode is placed at some distance above the roll. Nano-fibers can be continuously collected on a web which runs in the space between the roll and the electrode.

15.2.4 Productivity

A general problem of electrostatic spinning is the poor productivity. There are technologies that do not use a nozzle system – as reported in most of the publications from scientific laboratories – but convey the polymer solution by distribution on a surface like a rotating rod. Productivity is measured by the polymer volume delivered per time unit by a spinning pump. This works with the nozzle system only. Here the concentration of the solution must be considered, which is the proportion of the fiber-forming polymer and the delivered solution. It directly influences the viscosity of the solution. Measuring the throughput of the polymer solution is currently the only way to determine the productivity of an electrospinning process in-line. The production speed (m^2/min) at constant area weight of the nanofiber web as a measure for

productivity is needed. However, because of the extremely low weight of the nanofiber webs the electrospun web is difficult to weigh in-line.

The first suggestion derived from basic research to technical products was to multiply the nozzles. The practical distance of the nozzles at which the meta-stable rotating fibers do not touch each other has been determined in our trials to be 5 mm. The linear order technical production lines will have an array of nozzles. Clearly the production speed depends on the nozzle numbers. Yet the effort needed to deliver a homogeneous solution to the nozzles and to clean them is increased as well.

The approach to improve the nano-fiber formation by using fine capillary holes (100 µm) was found to be impractical, because the solvent evaporated too fast, which resulted in obstruction of the capillaries. An additional problem was caused by the parallel order of the capillaries. If they are closed, they will not be opened by a low processing pressure; the polymer solutions only run through open holes. This results in an inhomogeneous fiber diameter distribution and an unstable fiber manufacturing process with large maintenance efforts. One solution may be the cyclic automatic cleaning of the capillaries, but this greatly increases the cost of the equipment. Thus a diameter of the capillaries of 500 µm has been chosen, which is easier to handle in the production and processing stages. An *L/D* ratio of 20:1 enhances the orientation of the molecules, yet here as well problems of production occur after about 20–30 min. Even with a 50 capillary nozzle a spin pump (0.6 cm^3/min) could not be used because of the extremely low throughput at which fibers were formed. The throughput could be increased and the spinning pump could run at its lowest turns by supporting the fiber formation and the evaporation of the solvent by an air stream blown concentrically around each capillary.

The delivery is best made by gear pumps, which guarantees a constant volume flow of the conveyed solution independent of the pressure. The volume flow acts as a process parameter to determine the area weight produced.

The alternative state-of-the-art process to produce fine nonwovens is the melt-blow process. A comparison of melt-blow and electrospinning with respect to productivity is therefore of interest. In order to produce 2 µm thin fibers by the melt-blow process using 1250 capillaries per meter, a throughput of 3000 cm^3/m h is typical. An electrospinning set-up with 500 mm width and 50 capillaries in one row delivers about 1 cm^3/m h polymer. In order to achieve the same throughput as the melt-blow example, the electrospinning set-up needs to be scaled up to an array of over 10 000 capillaries in 12–13 rows, with 100 capillaries per meter working width.

15.2.5 Centrifuge spinning

Like electrostatic spinning, centrifuge spinning per se is not a new technology. Glass to sub-micrometer fibers, pitch to carbon fibers, melamin to the Basofil

fibers are some examples in which the technology has been used or at least tested. Yet no literature is known reporting the production of polymeric fibers below 1 μm.

In cooperation with Reiter, Winnenden, Germany, ITV Denkendorf has established equipment having as the core unit a high-speed rotor up to 50 000 rpm driven by pressurized air. The polymer solution is delivered via the hollow axis. By centrifugal forces the solution is accelerated and sprayed. An air stream helps to bundle the fiber cone. Here electrostatic charging is not used for fiber formation but for fiber collection to a web.

Depending on the process parameters one rotor covers about 330 mm. Thus, three rotors are required at least per 1 m working width. Based upon the equipment in planning a polymer volume of 500 cm^3/m h can be processed to fibers in the range of 0.3 μm. Taking into account a linear dependency of productivity to the fiber diameter, the productivity of centrifuge spinning meets that of melt-blown.

15.2.6 Comparing technologies

For laboratory use, electrostatic spinning using manifolds is superior in its simplicity. However, scaling up for production use is impaired by its low productivity, which can be increased only through considerable mechanical effort. Only with a controlled mass transport per capillary can the formation of the desired fine fibers be ensured. Automatic cleaning means are required to guarantee open capillaries. The use of an air stream can increase the productivity, but is limited by fiber fineness and diameter distribution. The centrifuge spinning requires a highly developed technology with more than 40 000 rpm. Reiter developed this many years ago for varnishing. The productivity is comparably high. The delivery of the polymer solution by a spin pump as well as the distribution of the fibers on the width of the substrate are important for a homogeneous fiber web. Electrostatic spinning may use spin pumps with nozzle manifolds for technical applications, yet obstruction of the nozzles will disturb the homogeneity.

Homogeneous fiber distribution over the length and the width, as well as the effective area weight, requires an extensive means of control. The common very low area weight of the nanofiber web of about 0.1 to 1 g/m^2 should be considered. Centrifuge spinning allows the online determination of the area weight by one pump per rotor. The centrifugal technology by itself ensures the homogeneous distribution of the fibers. The area weight can be controlled by appropriate means.

The question of how to control the laminate strength of the web with the substrate for filtration use is common to all technologies. In addition to engineering measures knowledge of the chemistry is required and must be elaborated for each substrate and each application. Also common to all these

technologies is the tendency already known from melt-blown: finer fibers can be achieved best by reduction of the polymer mass processed per time, i.e. to reduce the productivity. For polymer solutions the reduction of polymer mass can mean reduced throughput as well as reduction of the polymer concentration in the solution.

15.3 Anti-adhesive nanocoating of fibers and textiles

The textile finishing industry increasingly makes use of functional nanoparticles in order to achieve new or improved properties of textiles. Nanoparticles such as antimicrobial silver, photo-active TiO_2, conductive or magnetic metals or metal oxides as well as UV-absorbing particles (ZnO) are utilized in textile functionalization.[6] The interest in nanoparticles to functionalize textiles also results from the micro-structured nature of most textile products because the thickness of functional coatings on micro-scaled fibers should be in the region of submicrometers. Therefore, beside all new functions, the trend towards even thinner fiber creates a need for thin nano-scaled or nano-structured finishing coatings in order to maintain the small fiber diameter and to make use of its related properties.

One often desired textile property of huge interest is liquid repellence. Although the finishing of textiles with oil- and water-repelling resin-based fluorocarbons (FC) is state-of-the art (Scotchguard® and others), there are still attempts to increase production efficiencies and to improve the product properties. Simplified, an FC finishing process in textile production can be considered as a nanocoating process. A typical thickness of an FC finishing coating layer on a microfiber (10 µm fiber diameter) is 50 nm. By decreasing the diameter of the fiber to 1 µm, but keeping textile weight and liquor pick-up in a padding machine/padder constant, the coating thickness on each fiber will decrease to 10 nm and lower. The theoretical models predict even an FC monolayer on sub-micrometer fibers. Figure 15.5 shows the calculated dependence between FC layer thickness and fiber diameter for a polyester textile, assuming typical finishing conditions.

There are different approaches to improve the effects of an FC finishing of textiles. The approach discussed next, plasma technology, takes into account that it is a waste of energy to dry off 99% of the applied finishing fluid to leave an FC layer that is a few nanometers thin on the fiber. Another approach that will be discussed later is based on the roughness dependence of wetting and aims at the generation of ultra-water-repelling surfaces by nano-structured rough surfaces with low surface energy.

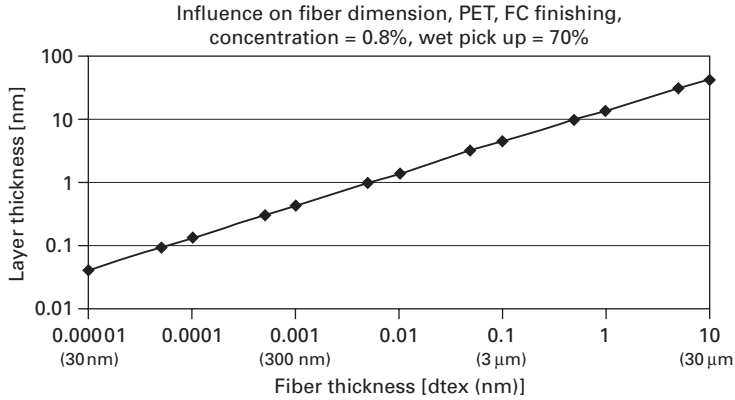

15.5 Dependence between estimated fluorocarbon layer thickness and fiber thickness.

15.4 Water- and oil-repellent coatings by plasma treatment

Plasma-based modifications are dry processes and therefore an interesting alternative to the traditional wet textile finishing systems for economic reasons. They make use of gases whose reactivity has been raised by electrical discharges in strong electric fields between electrodes. Atmospheric pressure plasma systems can be integrated easily in continuously running textile production and finishing lines. If the discharge energy is sufficiently controlled and the gas temperature is kept in the range of room temperature, it is called cold or low-temperature plasma and the plasma treatment is generally applicable to nearly all kind of fibers. Further advantages of plasma treatments are modifications of surface properties without changing the properties of the fiber bulk. They are water-free processes with a minimum consumption of chemicals going along with elimination of energy-intensive drying processes. Therefore, plasma processes can be highly environmentally friendly processes.

Plasma treatment changes properties such as friction coefficient, surface energy and antistatic behavior. The technological basis of the wide applicability of atmospheric pressure processes in the textile industry was the enhancement of the established corona technology by coating both electrodes by a dielectric material (dielectrical barrier discharge, DBD), using an intermittent (pulsed) voltage source as well as by feeding defined gas mixtures into the discharge (Fig. 15.6). If reactive gases that are able to polymerize after excitation in the discharge are fed into the plasma zone, thin coatings can be deposited on the substrate from a non-equilibrium plasma by, for example, radical polymerization.

The morphology of the coating and the deposition rate are controlled by the reaction mechanism and reaction rate. Readily polymerizing systems

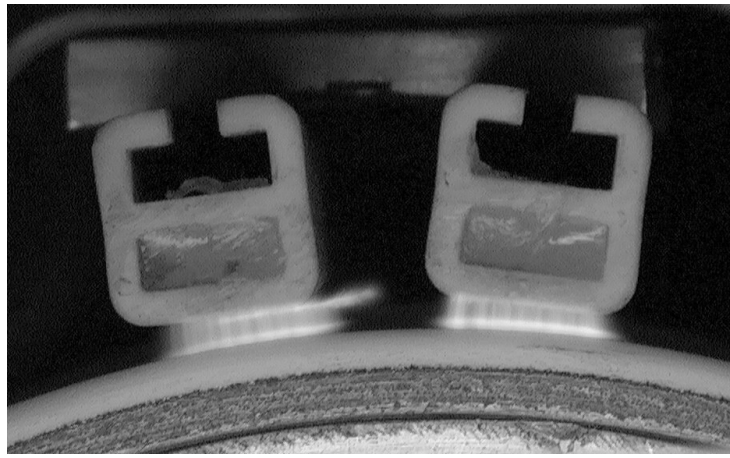

15.6 Dielectric barrier discharge (DBD) in air.

form particles within the discharge which can be deposited on the substrate. However, for textile treatments, these dust-forming plasmas are less relevant because the particles typically lie loosely on the surface.

Of very great interest are polymerization processes that predominantly take place at the substrate surface by forming a permanent functional surface coating. For example, highly cross-linked layers with varying surface energies, depending on the chemical composition, can be deposited from non-equivalent plasmas. Plasma polymerization processes need, in general, an encapsulated plasma device to control the plasma atmosphere. However, a continuous roll to roll and air to air process is still possible if either the plasma process runs within ambient air or gas-locks avoids the entry of air into the reactor chamber. The generation of water- and oil-repellent functional layers on textiles by plasma polymerization of fluorocarbons at atmospheric pressure under continuous inline conditions has been a major focus of collaborative research projects at ITV Denkendorf.[7, 8]

The structures achieved with plasma chemical deposited FC layers are characterized by a nanometer-scaled thickness and relatively high degree of cross-linking. Plasma polymerized layers with FCs in DBD show surface energies of 11 mN/m on polymeric films. These values are significantly lower than the typical value of PTFE with 18 mN/m.[9]

In encapsulated continuously working plasma units (Fig. 15.7), oil repellency grades of 5–6 (according to AATCC 118-1992) have been obtained on PET-Monofil fabric at a process speed of 0.5 m/min (Fig. 15.8). Better oil-repellent properties than those of PTFE were obtained, but the properties of water-based FC finishing have not been completely achieved until now. Oil repellencies on treated fabrics increase with decreasing process speeds, increasing fluorocarbon layer thicknesses. The thickness of plasma polymerized

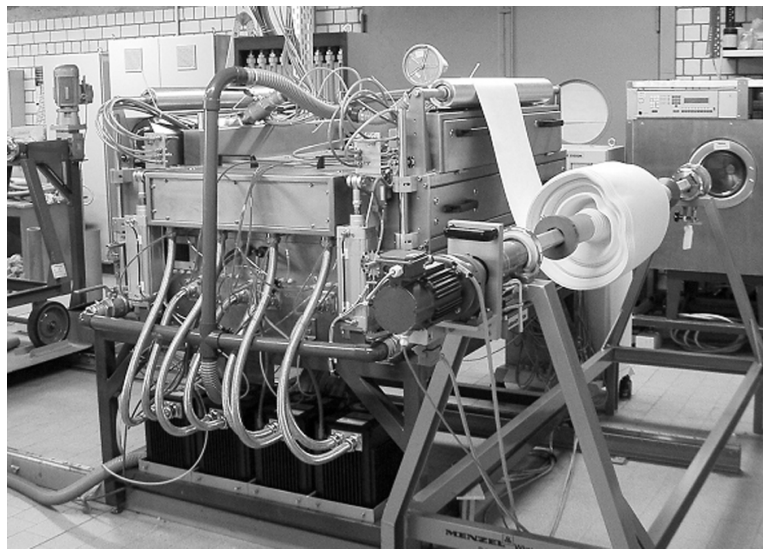

(a)

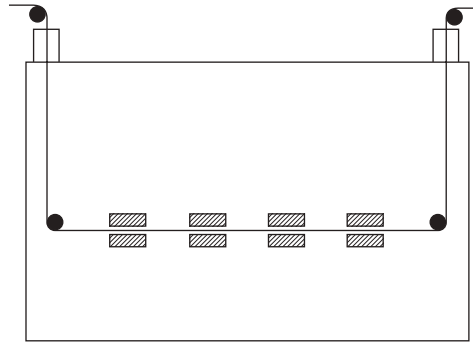

(b)

15.7 Encapsulated plasma unit for 1 m textile width.

FC layers on fibers of up to 14 nm was extrapolated from IR measurements on plasma-treated Si-wafers (Fig. 15.9). Deposition rates of up to 1 nm/s on fibers were achieved.

15.4.1 Aerosol and spraying applications

The use of aerosols in plasma technology increases the application spectrum of suitable chemicals enormously. With the help of aerosols in atmospheric pressure liquid chemicals, solutions and, in a limited way, dispersions can be used in plasma for surface modification. The potential of combinations from aerosols and spraying application in the DBD for the surface treatment of textiles is in the first development stage. Examples for current and future

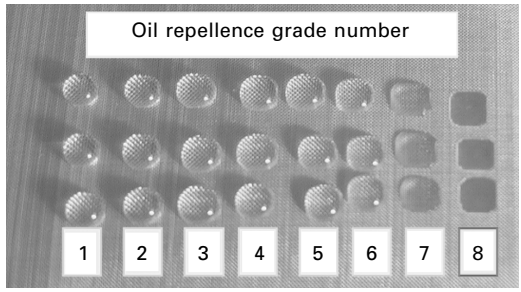

15.8 Demonstration of oil repellence of plasma-finished fabric.

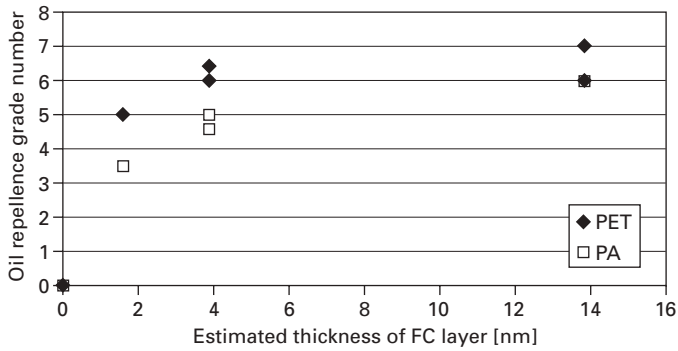

15.9 Dependence of oil repellence on plasma FC layer thickness.

applications are physical surface modification, e.g. generation of electret properties on filters,[10] chemical functionalization, energy saving finishing, and chemical and topographical nanostructuring.

15.5 Self-cleaning superhydrophobic surfaces

New products and new properties of products can be developed by learning from principles and functions in nature. ITV Denkendorf is working in basic and applied science in networks of botanic institutes, chemical companies, textile producers and consumers in different fields on bionic ideas.[11] One of the main focuses of current work with nanotechnology within these networks is the development of self-cleaning superhydrophobic surfaces on textiles.

15.5.1 Principles

The characteristic property of self-cleaning or so-called Lotus-Effect® surfaces[12] is the capacity of complete cleaning only by means of water, for example, in the form of rain. The attribute is often called the self-cleaning effect, as there

is no need for cleaning agents or additional mechanical support, beside the droplet momentum. This characteristic was discovered and investigated on natural surfaces of plants, such as leaf and blossom surfaces, but also on animal surfaces. The most famous and probably the most ideal representative from the plant world is the lotus plant that acts as the eponym. The main function of nano-structured superhydrophobic surfaces in nature is most likely protection against pathogenic organic contamination such as bacteria or spores.[13] These contaminants are completely removed from the leaves by rainfall.

The self-cleaning effect is based on low surface energy and the minimization of adhesion area to attaching agents by nano- and micro-scaled surface structures. SEM photographs show the superposed double structure of these organism surfaces. The results are extremely high contact angles of contacting water drops, rolling off at slight inclinations and removing attaching pollutions.

15.5.2 Transfer to fiber-based products

There is a variety of applications for fiber-based surfaces with self-cleaning characteristics. This includes outdoor applications, such as textile roofs for airports and railways, sunscreen textiles, outdoor clothing, but also indoor applications, which come into contact with water or water-based solutions (Fig. 15.10).[14]

One of the specific features of textiles in this context is that they readily bring rough structures with at least two topological structure elements represented by the filament's fiber arrangement within the yarn structure and the yarn arrangement within the fabric structure. Subsequent approaches to

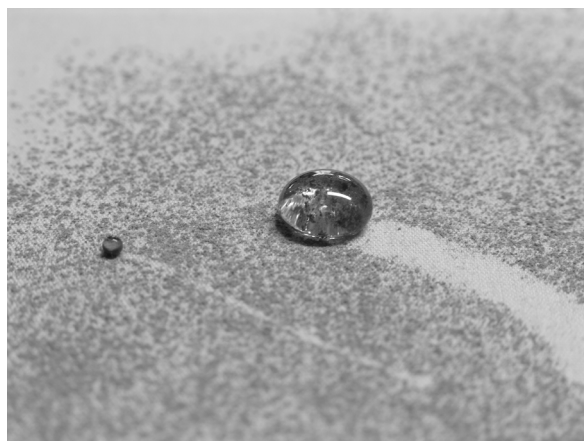

15.10 Honey droplet on a fabric with self-cleaning surface characteristic.

implement the self-cleaning effect on textile-based surfaces also implement fiber surface modification to low surface energies, the optimization of fabric and yarn construction structures. The alteration of textile surface finishing chemicals to meet the above-mentioned requirements can, for example, consist of polymer-based dispersions with nanoparticle additives. Other products are organic–inorganic hybrid materials on the basis of sol–gel chemistry, eventually also with nano-filler additives. In order to be transferred to modern textile production lines, the finishing systems should be water-based. Processes to apply the chemicals consist of standard textile finishing processes such as padding, face padding or spraying. Another attempt that is being investigated at ITV Denkendorf is to modify the fiber surface coating by the yarn.[15] This process is especially interesting if finishing processes after fabric construction are limited or for sewing thread. However, dyeing processes have to be applied before the yarn finishing, such as yarn dyeing or spin dyeing.

The textile construction also plays a crucial role for the effects of self-cleaning. In two ITV studies that were financially supported by the German Federal Ministry of Research and Technology the influence of textile structure on superhydrophobicity and self-cleaning was investigated. In the first study, to analyze the general feasibility of the development of extremely self-cleaning textiles, the influence of construction parameters on woven fabrics made of filament yarn was investigated. Particularly low wettability is measured for woven fabrics with open yarn structure. These fabrics have distinct micro-structured surfaces and show superhydrophobicity. High filament fineness supports hydrophobicity compared with yarns with thicker filaments, if the yarn is constructed with low compactness, so that the filaments lie side by side with an adequate distance between them. Aspect rates between 1 and 2 based on distance and height differences of adjacent filaments turn out to be especially favorable for high water repellence.

In the study to analyze the influence of structure and arrangement of staple fibers and filaments in fabrics of different types of constructions (knitted goods, nonwovens, warp knit fabrics and woven fabrics), various textile parameters (fiber material, yarn spinning method, filament and fiber construction and surface modification by mechanical and chemical methods) were varied. The investigations show significant influence of hairiness of the sample surfaces on the water repellence. Long, distant fibers, especially if present in samples made of ring-spun yarn, hinder the small water droplets of approximately 2 mm in diameter from rolling off and therefore result in poor repellence compared with equivalent samples made of open-end yarn and Vortex-yarn. In contrast to that the self-cleaning behavior is not affected by long, distant fibers and therefore an influence of the spinning method is not detected. The repellence is proportional to the fiber density of short distant fibers as the contact area decreases in the same way as when the

drop sits on the fiber endings like on flock-coated textiles, as shown in Fig. 15.11.

The same effect is observed in the opposite way with singeing or calendering, which results in smoother surfaces. On the other hand for such surfaces that have fewer undercutting structures the accessibility of dirt particles and therefore self-cleaning ability is enhanced. The implementation of nano-dimensional structures on the fibre surfaces enhances superhydrophobicity and the self-cleaning effect. This is shown in Fig. 15.12.

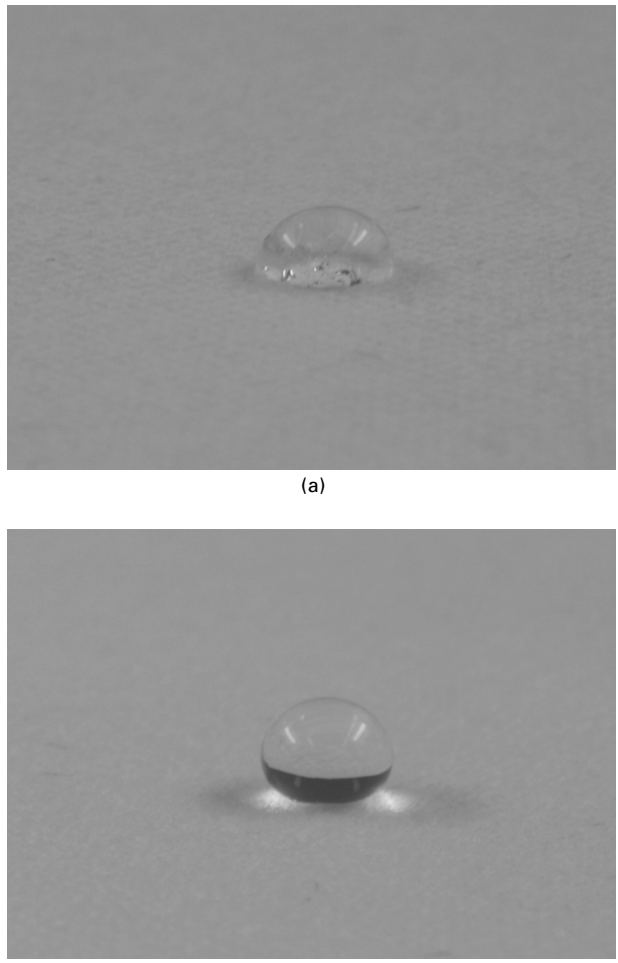

15.11 Static wetting behavior of water drops on hydrophobic flock textiles with varied surface roughness roughness: (a) low surface roughness, (b) high surface roughness.

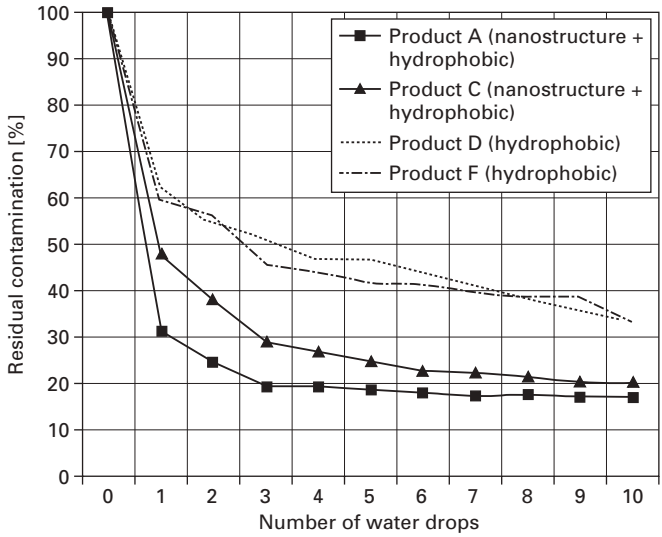

15.12 Residual contamination with soot particles after impact of water drops; multifilament fabric with nano-structured rough superhydrophobic coating (products A and C) and respectively smooth hydrophobic finishing (products D and F).

15.5.3 Testing methods

Methods to test superhydrophobicity and self-cleaning have been newly developed or adapted for textile applications at ITV Denkendorf. These methods were developed to sensitively differentiate between conventional soil-repellent finished textile samples that have a smooth fiber surface on the one hand and textiles that are finished with products that impose nano-dimensional structures on the fiber surface on the other hand. The rate of superhydrophobicity is measured by determining the so-called repellent power, which was invented by Dr Keller BASF, Ludwigshafen, Germany, via the determination of the dynamic roll-off angle. The static dynamic contact angle used for the characterization of even surfaces such as foils is applicable to textiles only in special cases. When dealing with micro-rough surfaces, especially where distant fibres dominate the surface structures, the contact angles cannot be measured satisfactorily with optical testing methods. The dynamic roll-off angle represents the boundary value at which a liquid droplet with a defined volume that is placed on the inclined sample surface from a defined height rolls off the sample. Correlations of roll-off angle and contact angles are given by Furmidge.[16] Self-cleaning efficiency is measured via testing methods with dirt that is known from other textile testing standards and consists of mixtures of different components or of single component particles such as carbon black. Dirt mixtures that are used for testing consist exemplarily of silica, mineral oil, olive oil and carbon black. In the applied

test method the dirt is mechanically rubbed into the textiles' surface to simulate strong impact. After contamination the sample is sprayed with water.

Evaluation of remaining contamination is either done qualitatively by standardized rating in comparison to the gray scale according to the norm DIN EN 20105 A02/A03 or with quantitative methods in which the residual contaminants are detected and quantified at a microscope with image processing and subsequent particle detection software.

15.5.4 The Denkendorf quality mark

In order to prove the superhydrophobic and self-cleaning effect of textile products, ITV issues the quality mark 'self-cleaning – inspired by nature' that makes use of the foregoing testing methods (Fig. 15.13). Additionally, in the testing procedure to this seal of approval the fiber's filament surface is examined with an SEM to qualify the surface structures, underlining the prerequisite of nano-scaled structures for the self-cleaning effect.

Recent research and development work in the field of nano-scaled surfaces on textiles at ITV Denkendorf aims strongly at the optimization of the mechanical abrasion resistance of such surfaces. The durability of these surfaces has to be measured depending on the application of the product. Awning fabric, tested in climate exposure test cabinets with high UV penetration for 1000 h and intermediate application-dependent mechanical load in the form of grinding, exhibited better self-cleaning behavior than awning fabric prepared with conventional finishing systems. The ability for recovery of impaired surfaces is an important feature of further development activities.

15.13 Quality mark for self-cleaning textiles.

15.6 Sources of further information and advice

www.lotus-effect.de
www.selfcleaning.eu
www.nanopartikel.info

15.7 References

1. Dauner, M., Production of nano fiber nonwovens using electrostatic spinning; *7th Symposium 'Textile Filter'*, Chemnitz, 2–3 March, 2004
2. Reneker, D. H., Chun, I., Nanometer diameter fibers of polymer, produced by electro spinning; *Nanotechnology* **7** (1995), 216–223
3. Reneker, D. H. *et al.*, Bending instability of electrically charged liquid jets of polymer solutions in electro spinning; *J. Appl. Phys.* **87** (9), (2000), 4531–4547
4. Bognitzki, M. *et al*., Nanostructured fibers via electro spinning; *Adv. Mater*. **13** (1), (2001), 70–72
5. Böbel, J., *Entwicklung von nanostrukturierten Oberflächen für das Tissue Engineering auf Basis des Elektrospinnens*; Studienarbeit, DITF/Universität Stuttgart, 2003
6. Soane, D. S., *et al.*, US Patent 6,607,994 B2 2003
7. Stegmaier, T., Arnim, V. V., Dinkelmann, A., Planck, H., Behandlung von laufenden Textilbahnen im Atmosphärendruckplasma, *Melliand textilberichte* **6** (2004), 476–481
8. Arnim, V. V., Stegmaier, T., Praschak, D., Bahners, T., Lunk, A., *et al.*, Continuous plasma treatment of textiles under atmospheric pressure; *Proceedings of the 29th Aachen Textile Conference*, 2002
9. Lunk, A., Vinogradov, I. P., Dinkelmann, A., Deposition of fluorocarbon polymer films in a dielectric barrier discharge(DBD); *Surface Coatings Technol.* **174–175** (2003), 509–514
10. Ernst, M., Stegmaier, T., Planck, H., Elektretcoatings for Nonwovens; *7th Symposium 'Textile Filter'*, Chemnitz, 2–3 March, 2004
11. Stegmaier, T., Milwich, M., Scherrieble, A., Geuer, M., Planck, H., Bionik developments based on textile materials for technical applications, *Bionik 2004 – International Conference*, Hannover Messe, 22–23 April, 2004
12. Barthlott, W., Self-cleaning surfaces of objects and process for producing same; Patent specification EP0772514B1, 1997
13. Barthlott, W., Neinhuis, C., Purity of the sacred lotus, or escape from contamination in biological surfaces; *Planta* **202** (1997), 1–8
14. Stegmaier, T., Dauner, M., Dinkelmann, A., Scherrieble, A., von Arnim, V., Schneider, P., Planck, H., Nanostructured fibers and coatings for technical textiles; *Techn. Textiles* **47** (2004), 142–146
15. Stegmaier, T., Abele, H., Ernst, M., Hager, T., Scherrieble, A., Schneider, P., Witt, M.-U., Wunderlich, W., Planck, H., Functionalisation of filaments and fibres by coatings; *Techn. Textiles* **48** (2005), 16–19
16. Furmidge, C. G. L., Studies at phase interfaces. I. The sliding of liquid drops on solid surfaces and a theory for spray retention, J. *Colloid Sci.* **17** (1962), 309–324

16

Electrostatic self-assembled nanolayer films for cotton fibers

G. K. HYDE and J. P. HINESTROZA,
Cornell University, USA

16.1 Introduction

The use of multilayered polymeric films offers the possibility of creating multicomposite molecular assemblies with great levels of reproducibility and controlled molecular architectures. While these high levels of control have been reached in planar and homogeneous surfaces such as silicon, glass, gold and other synthetic materials, their realization in natural fibers has not been achieved. Natural fibers offer unique challenges as not only are their cross-sections irregular, but their surfaces are chemically and physically heterogeneous. However, having the ability to control the surface of a natural fiber offers great rewards that go far beyond pure economics as natural fibers are renewable and biodegradable resources.

16.2 Principles of electrostatic self-assembly for creating nanolayer films

The Langmuir–Blodget (LB) technique allows monolayers to be created by using a non-solvent as a substrate. Once the monolayers have formed over the surface of a non-solvent system, they can be transferred onto a solid support. This technique, pioneered in the 1960s, is believed to be the first synthetic nano-scale heterostructure. These LB experiments were the first true nanomanipulations and they offered unprecedented control of the deposition of individual molecular layers. The creation of LB films requires the use of specialized equipment that is often expensive and difficult to maintain, and it is not compatible with existing fiber manufacturing techniques. Furthermore, the technique is limited by the size and topology of the substrate, making it unfeasible for large-scale robust manufacturing.[1]

Starting in the early 1990s, Gero Decher's group pioneered work on a robust method to create nanolayer structures using electrostatic self-assembly (ESA) principles.[2–5] The use of electrostatic interactions was selected as it offered the least steric demand of all self-assembly methods. Decher's initial

work was focused on rod-like molecules containing ionic groups at both ends, polyelectrolytes and various other charged materials in aqueous solutions.[1]

The ESA process has greatly increased in popularity due to the method's simplicity and the fact that not only polyelectrolytes but also almost any type of charged nanomoieties can be used to create the nanolayers in a controlled manner.[6] Figure 16.1 illustrates the process. In this example, a positively charged substrate, cotton, adsorbs a polyanion. This adsorption step is followed by a rinsing or excess removal procedure. The coated substrate, which now possesses an outer layer of a polyanion, can now adsorb a polycation. A surface charge reversal occurs with each adsorption step, leading to the formation of a layered structure.[1] The strong electrostatic attraction between charged surfaces and oppositely charged molecules in solution is believed to be the dominant factor in the adsorption of the polyelectrolytes.[2, 7–10] In theory, the adsorption of molecules possessing more than one equal charge allows for charge reversal on the surface. This behavior implies that (1) equally charged molecules will be repulsed, allowing for adsorption self-regulation and restriction of the deposition to a single layer, and (2) an oppositely charged molecule can be adsorbed in a second step on top of the first one.

Multilayer films may be composed of polyions, charged molecular objects and/or colloidal objects. In theory, there are no limitations with respect to

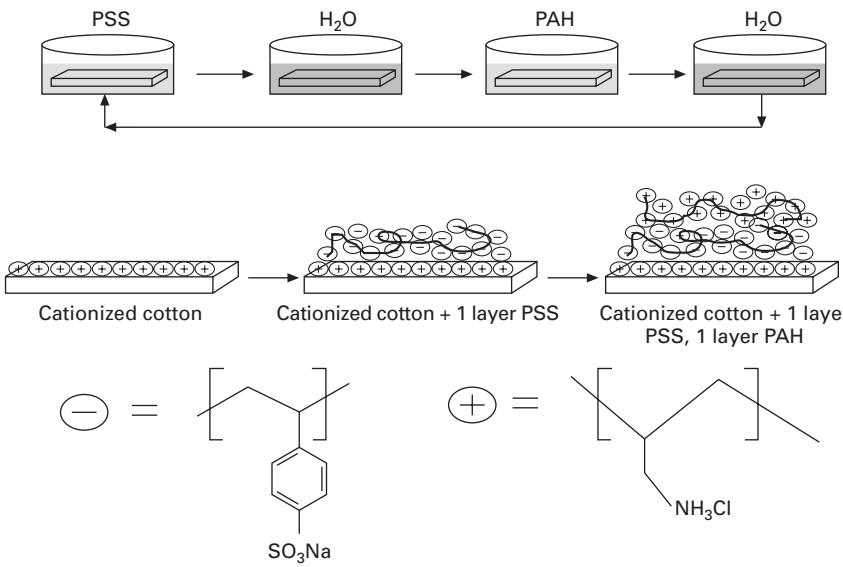

16.1 Schematic detailing deposition of anionic poly(styrene sulfonate) (PSS) and cationic poly(allylamine hydrochloride) (PAH) on cationized cotton fabric.

substrate size and topology as most of the time the process involves adsorption from an aqueous solution. Nanolayer films have been created on objects of a variety of sizes.[11–15] Although good adhesion of a layer to the base substrate requires a particular number of ionic bonds, the overcompensation of the surface charge by the incoming layer is found to be more dependent on the properties of the polymer than on those of the substrate. The use of polyelectrolytes allows for the formation of bridges over individual underlying defects. This unique feature of ESA enables the creation of self-healing structures as the conformation of the polymer over the surface of the substrate can be controlled by manipulating the adsorption operating conditions.[1] Numerous studies have validated this observation by demonstrating a linear increase of film thickness with the number of deposited layers independent of the nature of the initial substrate.[11, 16–20]

16.2.1 Deposition conditions

Nanolayer films are normally deposited using adsorbate concentrations of several milligrams per milliliter. While these concentrations are greater than those needed to reach a plateau in an adsorption isotherm, the excess prevents depletion of the solutions during the deposition of multilayered structures.[1] Washing or excess removal steps are often used after each adsorption step. The rinsing step is aimed at avoiding cross-contamination with the next adsorption solution as well as to remove weakly adsorbed polymer layers, hence stabilizing the multilayer structure.[18] Adsorption times per layer can range from minutes for polyelectrolytes to hours for certain colloids. The magnitude of the adsorption times is a process limited by mass transfer and hence depends on factors such as the molar mass and concentrations of the polyelectrolyte solutions as well as deposition conditions such as mixing.[1, 18]

Several factors influence the composition of the multilayer film as well as the characteristics of the individual layers. The thickness of each layer appears to be dependent on both the characteristics of the immediately underlying surface and the deposition conditions. The nature and density of charged groups, their local mobility, and the surface roughness also appear to have an influence. Operational factors such as concentration, adsorption time, ionic strength, temperature, rinsing time, dipping speed and drying time also influence the nanolayer thickness.[21] For a given pair of strongly dissociated polycations and polyanions, the thickness of the nanolayers is proportional to the salt concentration in the solution.

Self-assembly of charged nanoparticles to oppositely charged substrate surfaces is governed by adsorption and desorption equilibria. While the efficient adsorption of the layers is the main objective of each immersion step, preventing the desorption or the rearrangement of the deposited layers during the rinsing process is of equal importance. The optimization of the

ESA process requires the selection of proper stabilizers and careful control of the deposition kinetics.[6, 22, 23]

16.3 Advantages and disadvantages of electrostatic self-assembly

The process of layer-by-layer adsorption exhibits several advantages over similar surface modification techniques aimed at the production of multilayered films. One of the main advantages is that film architecture is almost completely determined by the deposition conditions, making ESA a manufacturing-amenable process. Another advantage of layer-by-layer adsorption is that a wide variety of different materials can be used to create multilayer thin films, hence creating multicomposite or hybrid films.[1] Current examples of multicomposite films include structures that contain proteins, clay platelets, metals and gold colloids.[1, 24–27]

Despite the fact that ESA has become widely used in recent years, certain details of the process are still not clearly understood. For example, the existence of a minimum time required to complete the deposition process has not been fully explained from first principles. The dynamics of the intermediate washing and drying steps have not been well characterized either.

A quantitative evaluation of the assembly process will be necessary to make ESA a practical commercial method.[28] ESA is also influenced by a variety of factors that may be difficult to control, such as polymer entropy, charge transfer interactions and hydrogen bonding.[29] No single theory has been developed to completely describe the deposition process. However, a variety of seminal studies have clarified many aspects of the ESA method.[7, 30, 31]

The ease of preparation and the high degree of versatility render self-assembled films useful to a large variety of applications. Self-assembled films can function as barriers, with controllable levels of permeability, for gases, liquids, covalent molecules, ions and electrons. These properties have been used for the construction of insulators, passivators, sensors and modified electrodes. Self-assembled nanolayers are also suitable for the construction of devices based on molecular recognition. Molecules or nanoparticles within a self-assembled layer can be aligned spontaneously, or by changing the temperature, pressure and pH, or by the application of external electric or magnetic fields. These characteristics allow for the formation of superlattices with a controllable architecture opening a new avenue for the development of a number of photonic, electronic, magnetic and non-linear optical devices. When insulators, conductors and magnetic, ferroelectric and semiconductor nanoparticulate films are deposited using the layer-by-layer process, hybrid heterostructures can be constructed with molecular precision.

By manipulating the size and the interparticle distances of monodispersed nanoparticles within self-assembled films, novel optic devices may be

developed.[32–35] Self-assembled nanolayers have been used to create polymer light-emitting diode devices with improved performance characteristics.[36] Furthermore, controlling some of the solution parameters such as surface charges and pair combinations has opened the possibility of creating new light-sensitive materials and optical devices.[37] The self-healing capability of ESA nanolayers provides an increased tolerance to defects. This self-healing ability sets the electrostatic method apart from other self-organization techniques.[6] The electrostatic method can be used on substrates with non-uniform surfaces and compensates for defects caused during the adsorption process.[28, 38]

16.4 Substrates used for electrostatic self-assembly

Synthetic substrates such as glass, quartz, mica, gold, silver and a wide array of polymers have been extensively used as base substrates for ESA deposition.[6, 19, 22, 39–42] Both hydrophilic (fluorine, glass and silicon) and hydrophobic (silanized glass) substrates have also been successfully used to support nanolayer thin films.[43] The choice of substrates has often been determined by their convenience for different analysis techniques. Glass and quartz are used so the deposition can be monitored using UV-VIS spectroscopy and optical microscopy.[6] Silicon wafers have been used for ellipsometric studies.[25, 44] and the smooth surfaces of quartz, mica and glass are the preferred choices for X-ray reflectivity studies.[19, 20, 45]

16.4.1 Influence of substrate characteristics

Owing to the characteristics of the layer-by-layer deposition technique, the adsorption of the polyelectrolytes is dependent on the surface charge of the substrate rather than its topology.[46] However, during the initial deposition steps the topology may play a major role.[4, 13, 47–50] The amount of adsorbed polymer and the chemical composition of the outermost layer normally exhibit larger variations during the initial deposition steps before reaching a plateau.[13, 17, 33] The surface charge density of the substrate usually determines how many deposition steps are required to reach this steady state. However, constant growth is eventually reached despite the substrate characteristics as long as the polyelectrolytes complement each other, creating electrostatic equilibrium.[12, 47, 51]

Previous work has been able to elucidate the influence of surface charge on the deposition of ESA layers. For example, Fou and Rubner used microscopic glass slides with hydrophilic, hydrophobic, negatively charged and positively charged surfaces as substrates. The surface charge of the substrates was found to have a great influence on the deposition time, layer thickness and layer uniformity.[52] However, the topology of the substrate itself was found to have a negligible effect on the adsorption of the individual layers.[46]

16.4.2 Polymers as substrates for layer-by-layer deposition

The majority of the early work involving the layer-by-layer process involved inorganic substrates such as quartz and silicone since it was thought that the process required flat clean surfaces.[20, 26, 29] Later on polymer films and other organic materials were used as substrates.[53, 54] Some of the most studied polymers include poly(propylene) (PP), poly(isobutylene) (PIB), poly(styrene) (PS), poly(methyl methacrylate) (PMMA), poly(ethylene terephthalate) (PET), poly(phenylene oxide) (PPO) and poly(ether imide) (PEI).[13]

Delcorte and others used surface analysis techniques to demonstrate that alternate polyelectrolyte thin films could be built up on polymeric substrates. PP, PIB, PS, PMMA, PET, PPO and PEI were evaluated as substrates. Semicrystalline PET as well as polymers containing carbonyl groups and/or benzene rings were identified as the most promising substrate choices.[13]

PET is of particular interest to the textile industry. It can be surface modified using a variety of techniques including plasma, corona discharge, ion beam, laser treatment, photo-initiated graft polymerization, saponification, aminolysis, reduction and entrapment of poly(ethylene oxide). PET is a suitable substrate for several reasons. It contains carbonyl groups that are capable of hydrogen bonding. The surface can be readily hydrolyzed to introduce carboxylic acid, as well as alcohol, it is able to support negative charges (PET-CO_2^-) in a sufficiently basic solution and the PET surface can react with polyamines to incorporate amine functionality capable of introducing positive charges (PET-NH_3^+) in a non-basic solution.[11]

Chen and McCarthy conducted a study involving the modification of PET with layer-by-layer deposition. Poly(sodium styrenesulfonate) and poly(allylamine hydrochloride) were used as polyelectrolytes for surface modification. Contact angle analysis and X-ray photoelectron spectroscopy (XPS) were used to illustrate the structure of the outermost layers as well as the thickness of each individual layer.[11] Furthermore, XPS and contact angle data indicated that the layers were stratified and that the wettability of the multilayer assemblies could be controlled by the identity of the outer- most polyelectrolyte layer. The individual layers were found to be extremely thin (2–6 Å) and it was demonstrated that the thickness of each layer could be controlled by adjusting the ionic strength of the polyelectrolyte solutions. The stoichiometry of the deposition process (ammonium ion:sulfonate ion ratio) was also affected by the substrate chemistry and solution ionic strength. This observation was particularly appealing as it indicated that the layer-by-layer deposition process was quite forgiving and could be done under a variety of conditions. Peel tests further showed that the multilayer assemblies deposited over the PET films exhibited good mechanical properties as no failures were observed in the multilayers.[11]

16.4.3 Surface modification techniques

Surface modification techniques used to charge the substrates on which the nanolayers are to be deposited can be categorized as physical or chemical. Chemical modification techniques include surface patterning, photobleaching or plasma treatment.[5, 12, 55, 56] Methods of physical modification primarily use Langmuir–Blodgett films or layers of charged polyelectrolytes as primers for the deposition of multilayers.[4, 57–59] While these techniques are fully demonstrated on synthetic substrates, there is little literature on their use to modify the surface of natural fibers.

Several attempts have been made to add functionality to cotton fibers. One of the most viable methods includes the creation of cationic sites by using controlled epoxy-based chemical reactions. It has been previously reported that reacting cotton with 2,3-epoxypropyltrimethylammonium chloride forms cationic charges on the surface of the fibers. While this process was originally developed to improve the affinity of cotton for anionic dyes, it has been recently used to provide the cotton fabric with a positive surface charge aimed at supporting polyelectrolyte nanolayers.[60]

16.5 Polyelectrolytes used for electrostatic self-assembly

Aqueous solutions of polyelectrolytes are commonly preferred for depositing layer-by-layer assemblies. However, organic solvents have proven to be useful as well.[6] Since the ESA method is mainly based on the attraction of opposite charges, it is necessary that the layer-forming compounds have at least a minimal number of charged groups. Below this minimum charge, the layer-by-layer deposition process no longer works. Past studies have led to the belief that large hydrophobic fragments found in polyelectrolytes could be detrimental to the layer-by-layer deposition technique as they reduce their charge density and they can interfere with ion–ion interactions. Experiments involving weak polyelectrolytes support this theory.[18, 61] These observations illustrated that a minimum charge level is required before the polyelectrolytes will engage in self-assembly patterns. However, recent studies have successfully used polyelectrolytes with very low charge densities by manipulating other types of molecular interactions capable of reducing the minimum charge required for the layers to be adsorbed.[16, 47, 62–66]

16.5.1 Synthetic polyelectrolytes

A large number of synthetic polyelectrolytes have been used to create a variety of nanostructured thin film coatings.[1, 23, 67–69] Some of these polyelectrolytes include poly(ethyleneimine), poly(allylamine),

poly(diallyldimethylammonium chloride), poly(styrene sulfonate), poly(vinyl sulfate), poly(acrylic acid) and poly[*N*-vinyl-(4-(39-carboxy-49-hydroxyphenylazo) benzene sulfonamide)].[6]

One of the most studied and well-understood systems consists of poly(allylamine) (PAA) and poly(styrene sulfonate) (PSS).[11, 19, 70–72] A number of more complex, functionalized polyelectrolytes have also been used, based on their ability to form structured coatings, and whether or not they can enable secondary chemical modifications. One of the greatest advantages of the layer-by-layer deposition technique is that almost any polyelectrolyte can be used as long as the appropriate oppositely charged partner polyelectrolyte is chosen.[6]

A large number of functional polymers have also been studied, including electrical and ionic conducting and light-emitting polymers.[14, 73–81] Past experiments have also used non-conjugated redox-active polymers, reactive polymers and polymeric complexes.[82–91] Standard polyelectrolytes modified with small numbers of functional groups have also been used for labeling purposes and for molecular recognition studies.[12, 92–94] Polyelectrolytes labeled with dyes and fluorescent probes have been used in an effort to better understand the adsorption of the layers as well.[13, 33, 95–100] Complementary chromophores have also been used to monitor multilayer adsorption on real time via UV-VIS spectroscopy and colorimetric methods.[6]

16.5.2 Modified and natural polyelectrolytes

Charged nano-objects, usually referred to as rigid polyelectrolytes, such as stable colloidal dispersions of charged silica, metal oxides, microcrystallites, and metal colloids have been deposited using the layer-by-layer (LbL) technique.[25, 95, 101–110] Most of the deposition work involves the use of fully charged polyelectrolytes. PSS and poly(allylamine hydrochloride) (PAH) are examples of polyelectrolytes that have often been deposited at pH values less than 7.0. Recent studies have aimed at depositing multilayers composed of weak polyelectrolytes. Weak polyelectrolytes are attractive as their charge density can be controlled by adjusting the pH of the solutions.[23, 111] In addition, weak polyelectrolytes such as PAA and PAH allow for a more precise control over the physical characteristics of the multilayers. Weak polyelectrolytes can be deposited with a high percentage of the chains making loops and tails under pH conditions of incomplete charge. This is in contrast to strong polyelectrolytes which often deposit as molecularly thin layers (about 5 Å). Layer thicknesses greater than 80 Å have been achieved when using weak polyelectrolyte solutions of PAA/PAH.[23, 111]

Natural polyelectrolytes such as nucleic acids, proteins and polysaccharides have also been used for LbL ESA.[112–114] Studies involving natural polyelectrolytes have aimed at gaining deeper understanding of the biological

functions of film and their ability to simulate biological processes. LbL does not require chemical modification and should in theory maintain normal protein behavior.[115–117] Cyclic compounds, dendrimers and hyperbranched polyelectrolytes such as poly(ethyleneimine) have all been used with success, indicating the robustness of the LbL method.[44, 118–120]

16.6 Analyzing self-assembled nanolayer films on cotton

Since the introduction of the ESA method, a variety of techniques have been adapted to assess self-assembled nanolayers. Recent work by Akin and collaborators illustrates the use of the most common analysis techniques namely XPS, X-ray reflectivity and atomic force microscopy (AFM).[121] Self-assembled nanolayer films have also been characterized using infrared (IR) spectroscopy, UV-VIS spectroscopy, ellipsometry, planar optical wave guide systems and quartz crystal microgravimetry (QCM).[22] Surface plasmon resonance (SPR) measurements have also been used to characterize multilayer thin films adsorbed onto gold and other noble metal substrates. SPR monitors the reflectivity of an incident light beam from a thin film that is attached to a glass prism as a function of the incident angle and it can be several orders of magnitude more sensitive than QCM measurements.[122] Several other techniques used include gel permeation chromatography, nuclear magnetic resonance (NMR) spectroscopy, and end group titration. However, IR and XPS appear to be the most commonly used as they can easily identify the chemical functionality of the end groups in the outermost layer.[123]

Recent work by our research group, Hyde *et al*.,[124] has demonstrated that the LbL deposition of oppositely charged polyelectrolytes can be used as a method of surface modification for cotton fibers and fabrics. The cotton fibers were functionalized by reacting 2,3-epoxypropyltrimethylammonium chloride with the hydroxyl groups of cellulose to create cationic charges. These cationic charges were used to deposit subsequent layers of PSS and PAH.

XPS and transmission electron microscopy (TEM) were used to characterize the multilayer structures over the cotton fibers. XPS spectra provided an analysis of the chemical groups present on the outermost layer of the samples. Specifically the presence of nitrogen and sulfur was monitored as it related to the deposition of PSS and PAH respectively. The ratio of N/S on the outermost layer was found to be in quantitative agreement with previously published work that deposited PSS and PAH on synthetic substrates.

Figure 16.2 compares the XPS survey spectra for samples of cationically charged woven cotton fabric and fabric supporting layers of PSS and PAH. Sharp peaks can be observed at 281.91 eV for carbon and 528.91 eV for oxygen. A small amount of nitrogen, believed to be generated during the cationization process, was detected at 398.91 eV for the cationized fabric.

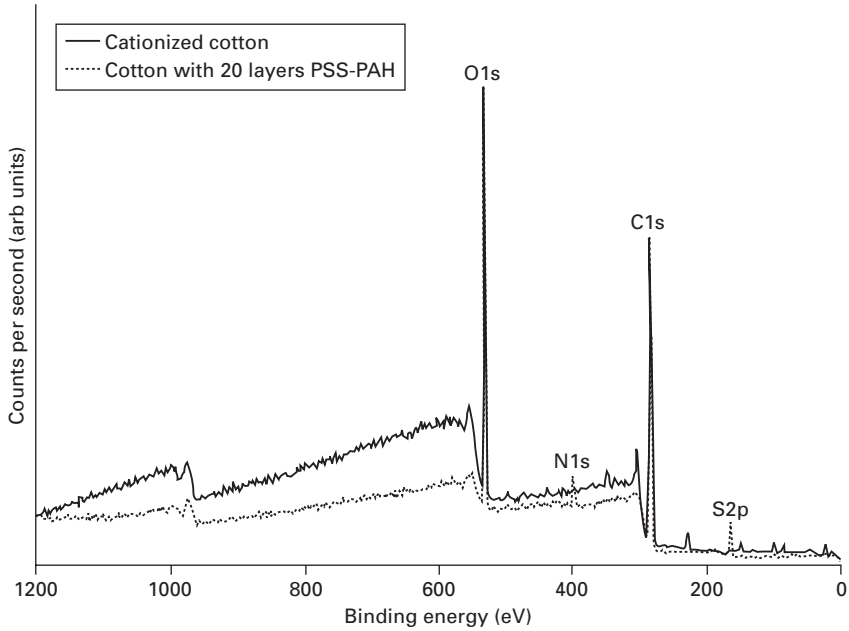

16.2 XPS survey spectra of cationized cotton and cotton supporting 20 alternating layers of PSS and PAH.

The figure also shows a survey spectrum of a 20-layer PSS/PAH multilayer film deposited on a woven cationic cotton substrate. It can be seen that the peaks at 398.91 and 164.91 eV have increased in magnitude in comparison with those present in the cationic cotton sample, indicating the presence of a multilayer film. The peaks correspond to nitrogen and sulfur respectively.

TEM was used to obtain direct evidence of the presence of the layers and their ability to provide a fully conformal coating over the cotton fibers. Figure 16.3 shows a TEM image of a cotton fiber supporting 20 layers. The cuticle of the cotton fiber can be seen on the right side of the image. The multilayer film provides a uniform, conformal coating to the surface of the fiber with a thickness between 325 and 375 nm. Since 20 layers were deposited, it can be speculated that each layer may be 16–19 nm thick. Figure 16.4 provides an enhanced image of the outermost layer of the multilayer structure, confirming that each layer had a thickness around 20 nm.

Our research group has also investigated the use of LbL deposition as a method of surface modification for cotton fibers and fabrics. The wool fibers were functionalized by using 2,3-epoxypropyltrimethylammonium to create cationic charges. These cationic charges were used to deposit subsequent layers of PSS and PAH.

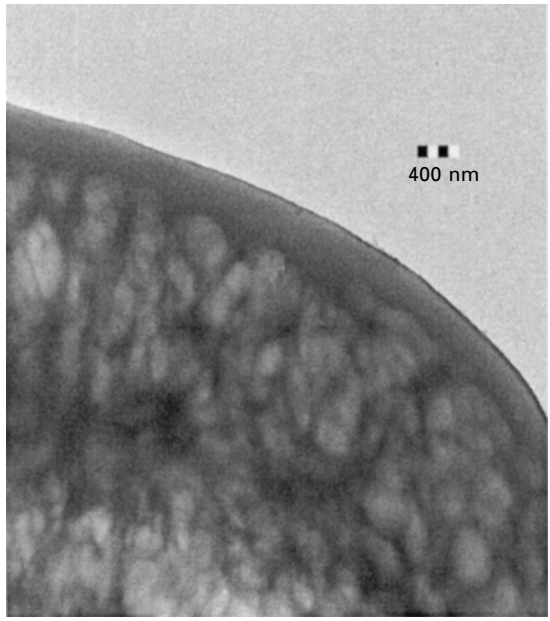

16.3 TEM image of cotton fiber with 20-layer film of PSS/PAH.

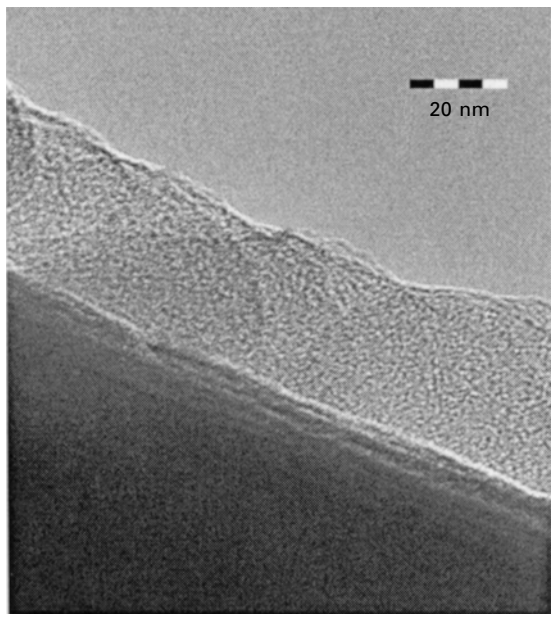

16.4 TEM image of outermost layer in 20-layer film of PSS/PAH.

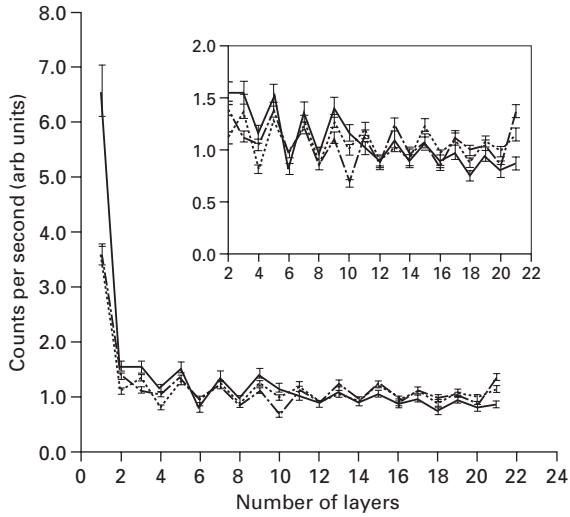

16.5 N/S evolution ratio for wool substrate supporting a 20-layer film of PSS/PAH. Three different specimens are presented, illustrating robustness and reproducibility of the ESA procedure. The inset provides a closer look at the N/S ratio at the outer layers.

XPS analysis was used to analyze the chemical groups present on the outermost layers of the wool samples. Specifically the presence of nitrogen and sulfur was monitored as it related to the deposition of PSS and PAH respectively. Figure 16.5 provides the N/S ratio for a wool sample supporting a 20-layer film of PSS/PAH. The variance in initial layers occurs because of the uneven nature of the wool substrate. As the number of layers increases, the variance levels out appropriately. The alternating trend seen is similar to that for the cotton substrates.

16.7 Conclusions: functional textiles for protection, filtration and other applications

Any number of different textile fibers and fabrics could possibly be used as substrates for the electrostatic self-assembly of nanolayers as far as they could hold charges on their surfaces. Possible candidates include polyamides as well as hemp, silk and many others.

Several papers have been published recently detailing new methods of LbL assembly, highlighting reduced deposition times and improved layer uniformity. For example, Kim *et al.* devised a new technique for LbL deposition called dynamic LbL assembly. This process makes use of the basic LbL deposition process and fluidic devices to create well-defined multilayer polyelectrolyte films that can be quickly and easily fabricated on a specific

area of a substrate. Using this procedure multilayer films can be fabricated in just 90 s of processing time. The resulting films are similar in terms of film thickness and roughness when compared with samples produced by the conventional LbL dipping process.[125]

Porcel *et al*. developed a novel method that simultaneously sprays polyanion and polycation solutions onto a vertically oriented charged surface. This process creates a uniform film that grows with time. The vertical position leads to continuous drainage and helps removing any material that is not fixed on the surface of the outermost layer. This deposition technique, much like the conventional technique, does not include a drying step allowing for a continuous removal of any excess materials and improving the uniformity of the film.[126]

The ESA deposition process has been used to deposit alternate nanolayers of PSS and PAH on substrates of cotton and wool fabric. Treatment of the samples with 2,3-epoxypropyltrimethylammonium chloride was proven to be an effective procedure to create a substrate able to support multilayer thin films. XPS and TEM provided direct and indirect evidence of the efficacy of the deposition process. In addition, quantitative agreement of the XPS data with previously published data using several synthetic substrates corroborates that the LbL deposition process can be used as a method for the modification of textile fibers and fabrics. The experimental results also show that ESA is more dependent on the nature of the polyelectrolytes than that of the original substrate.

LbL deposition is a process that could be used to potentially develop functional textiles for protective clothing and selective filtration applications. Using nanolayer films as a method of textile modification will allow increases in the functionality of a variety of textile products. It is also possible that ESA could be easily integrated into existing textile manufacturing processes.

16.8 References

1. Decher, G., Fuzzy nanoassemblies: toward layered polymeric multicomposites. *Science*, 1997. **277**: p. 1232–1237.
2. Lvov, Y., Decher, G. and Moehwald, H., Assembly, structural characterization, and thermal behavior of layer-by-layer deposited ultrathin films of poly(vinyl sulfate) and poly(allylamine). *Langmuir*, 1993. **9**: p. 481–486.
3. Lvov, Y., Decher, G. and Sukhorukov, G., Assembly of thin films by means of successive deposition of alternate layers of DNA and poly(allylamine). *Macromolecules*, 1993. **26**: p. 5396–5399.
4. Lvov, Y., Essler, F. and Decher, G., Combination of polycation/polyanion self-assembly and Langmuir–Blodgett transfer for the construction of superlattice films. *J Phys Chem*, 1993. **97**: p. 13773–13777.
5. Lvov, Y., *et al*., Assembly of polyelectrolyte molecular films onto plasma-treated glass. *J Phys Chem*, 1993. **97**: p. 12835–12841.

6. Bertrand, P., *et al*., Ultrathin polymer coatings by complexation of polyelectrolytes at interfaces: suitable materials, structure and properties. *Macromol Rapid Commun*, 2000. **21**: p. 319–348.
7. Hammond, P., Recent explorations in electrostatic multilayer thin film assembly. *Curr Opin Coll Inter Sci*, 2000. **4**: p. 430–442.
8. Phuvanartnuruks, V. and McCarthy, T., Stepwise polymer surface modification: chemistry-layer-by-layer deposition. *Macromolecules*, 1998. **31**: p. 1906–1914.
9. Tieke, B., *et al*., Ultrathin self-assembled polyelectrolyte multilayer membranes. *Eur Phys J E*, 2001. **5**: p. 29–39.
10. Ulman, A., Formation and structure of self-assembled monolayers. *Chem Rev*, 1996. **96**: p. 1533–1554.
11. Chen, W. and McCarthy, T., Layer-by-layer deposition: A tool for polymer surface modification. *Macromolecules*, 1997. **30**: p. 78–86.
12. Decher, G., *et al.*, New nanocomposite films for biosensors – layer-by-layer adsorbed films of polyelectrolytes, proteins or DNA. *Biosensors Bioelectronics*, 1994. **9**(9–10): p. 677–684.
13. Delcorte, A., *et al*., Adsorption of polyelectrolyte multilayers on polymer surfaces. *Langmuir*, 1997. **13**(19): p. 5125–5136.
14. Liang, Z.Q. and Wang, Q., Multilayer assembly and patterning of poly(*p*-phenylenevinylene)s via covalent coupling reactions. *Langmuir*, 2004. **20**(22): p. 9600–9606.
15. Poptoshev, E., Schoeler, B. and Caruso, F., Influence of solvent quality on the growth of polyelectrolyte multilayers. *Langmuir*, 2004. **20**: p. 829–834.
16. Cooper, T.M., Campbell, A.L. and Crane, R.L. Formation of polypeptide–dye multilayers by an electrostatic self-assembly technique. *Langmuir*, 1995. **11**(7): p. 2713–2718.
17. Dubas, S. and Schlenoff, J., Factors controlling the growth of polyelectrolyte multilayers. *Macromolecules*, 1999. **32**: p. 8153–8160.
18. Hoogeveen, N.G., *et al.*, Formation and stability of multilayers of polyelectrolytes. *Langmuir*, 1996. **12**(15): p. 3675–3681.
19. Losche, M., *et al*., Detailed structure of molecularly thin polyelectrolyte multilayer films on solid substrates as revealed by neutron reflectometry. *Macromolecules*, 1998. **31**: p. 8893–8906.
20. Schmitt, J., *et al*., Internal structure of layer-by-layer adsorbed polyelectrolyte films: a neutron and X-ray reflectivity study. *Macromolecules*, 1993. **26**: p. 7058–7063.
21. Decher, G., 'Polyelectrolyte multilayers, an overview', in G. Decher and J. Schlenoff, Editors. *Multilayer Thin Films,* 2003, Wiley-VCH. p. 1–46.
22. Caruso, F., *et al.*, Ultrathin multilayer polyelectrolyte films on gold: construction and thickness determination. *Langmuir*, 1997. **13**: p. 3422–3426.
23. Yoo, D., Shiratori, S. and Rubner, M., Controlling bilayer composition and surface wettability of sequentially adsorbed multilayers of weak polyelectrolytes. *Macromolecules*, 1998. **31**: p. 4309–4318.
24. Feldheim, D.L., *et al*., Electron transfer in self-assembled inorganic polyelectrolyte/metal nanoparticle heterostructures. *J Amer Chem Soc*, 1996. **118**: p. 7640–7641.
25. Keller, S.W., Kim, H. and Mallouk, T.E., Layer-by-layer assembly of intercalation compounds and heterostructures on surfaces: toward molecular 'beaker' epitaxy. *J Amer Chem Soc*, 1994. **116**: p. 8817–8818.

26. Lvov, Y., *et al.*, Assembly of multicomponent protein films by means of electrostatic layer-by-layer adsorption. *J Amer Chem Soc*, 1995. **117**: p. 6117–6123.
27. Lvov, Y., *et al*., Formation of ultrathin multilayer and hydrated gel from montmorillonite and linear polycations. *Langmuir*, 1996. **12**(12): p. 3038–3044.
28. Lvov, Y., *et al*., A careful examination of the adsorption step in the alternate layer-by-layer assembly of linear polyanion and polycation. *Coll Surf A*, 1999. **146**: p. 337–346.
29. Delcorte, A., *et al*., ToF-SIMS study of alternate polyelectrolyte thin films: chemical surface characterization and molecular secondary ions sampling depth. *Surface Sci*, 1996. **366**: p. 149–165.
30. Fogden, A. and Ninham, B.W., Electrostatics of curved fluid membranes: the interplay of direct interactions and fluctuations in charged lamellar phases. *Adv Coll Int Sci*, 1999. **83**: p. 85–110.
31. Ninham, B.W., Kurihara, K. and Vinogradova, O.I., Hydrophobicity, specific ion adsorption and reactivity. *Coll Surf A*, 1997. **123–124**: p. 7–12.
32. Advincula, R., Fells, E. and Park, M., Molecularly ordered low molecular weight azobenzene dyes and polycation alternate multilayer films: aggregation, layer order, and photoalignment. *Chem Mater*, 2001. **13**: p. 2870–2878.
33. Decher, G., Lvov, Y. and Schmitt, J., Proof of multilayer structural organization in self-assembled polycation–polyanion molecular films. *Thin Solid Films*, 1994. **244**: p. 772–777.
34. Fendler, J., Preparation and utilization of self-assembled ultrathin films composed of polyelectrolytes, nanoparticles and nanoplatelets. *Croatica Chim Acta*, 1998. **71**: p. 1127–1137.
35. Kato, N., *et al*., Thin multilayer films of weak polyelectrolytes on colloid particles. *Macromolecules*, 2002. **35**: p. 9780–9787.
36. Advincula, R., Supramolecular strategies using the layer-by-layer sequential assembly technique: applications for PLED and LC display devices and biosensors. *IEICE Trans Electron*, 2000. **E83-C**: p. 1104–1111.
37. Advincula, R., *et al*., Photo-induced alignment of polymer ultrathin films fabricated by alternate self-assembly solution adsorption of polyelectrolytes and small azo dye chromophores. *ACS Polymer Preprints*, 1999. **Spring**: p. 1–2.
38. Lvov, Y., *et al*., Thin film nanofabrication via layer-by-layer adsorption of tubule halloysite, spherical silica, proteins, and polycations. *Coll Surf A*, 2002. **198–200**: p. 375–382.
39. Cassagneau, T. and Fendler, J. Preparation and layer-by-layer self-assembly of silver nanoparticles capped by graphite oxide nanosheets. *J Phys Chem B*, 1999. **103**: p. 1789–1793.
40. Artyukhin, A.B., *et al.*, Layer-by-layer electrostatic self-assembly of polyelectrolyte nanoshells on individual carbon nanotube templates. *Langmuir*, 2004. **20**(4): p. 1442–1448.
41. Caruso, F., *et al.*, Quartz crystal microbalance and surface plasmon resonance study of surfactant adsorption onto gold and chromium oxide surfaces. *Langmuir*, 1995. **11**: p. 1546–1552.
42. Lu, C.H., *et al*., Au nanoparticle micropatterns prepared from self-assembled films. *Langmuir*, 2004. **20**(3): p. 974–977.
43. GirardEgrot, A.P., Morelis, R.M. and Coulet, P.R., Direct influence of the interaction between the first layer and a hydrophilic substrate on the transition from Y- to Z-

type transfer during deposition of phospholipid Langmuir–Blodgett films. *Langmuir*, 1996. **12**(3): p. 778–783.
44. Watanabe, S. and Regen, S.L., Dendrimers as building-blocks for multilayer construction. *J Amer Chem Soc*, 1994. **116**(19): p. 8855–8856.
45. Tronin, A., Lvov, Y. and Nicolini, C., Ellipsometry and x-ray reflectometry characterization of self-assembly process of polystyrenesulfonate and polyallylamine. *Colloid Polym Sci*, 1994. **272**(10): p. 1317–1321.
46. Sano, M., Lvov, Y. and Kunitake, T., Formation of ultrathin polymer layers on solid substrates by means of polymerization-induced epitaxy and alternate adsorption. *Ann Rev Mat Sci*, 1996. **26**: p. 153–187.
47. Lutt, M., Fitzsimmons, M.R. and Li, D., X-ray reflectivity study of self-assembled thin films of macrocycles and macromolecules. *J Phys Chem B*, 1998. **102**: p. 400–405.
48. Bergbreiter, D.E., Franchina, J.G. and Kabza, K., Hyperbranched grafting on oxidized polyethylene surfaces. *Macromolecules*, 1999. **32**(15): p. 4993–4998.
49. Schlenoff, J.B., Ly, H. and Li, M., Charge and mass balance in polyelectrolyte multilayers. *J Amer Chem Soc*, 1998. **120**(30): p. 7626–7634.
50. Ferreira, M., Cheung, J.H. and Rubner, M.F., Molecular self-assembly of conjugated polyions – a new process for fabricating multilayer thin-film heterostructures. *Thin Solid Films*, 1994. **244**(1–2): p. 806–809.
51. Kleinfield, E. and Ferguson, G., Healing of defects in the stepwise formation of polymer/silicate multilayer films. *Chem Mater*, 1996. **8**: p. 1575–1578.
52. Fou, A.C. and Rubner, M., Molecular-level processing of conjugated polymers. 2. Layer-by-layer manipulation of *in situ* polymerized p-type doped conducting polymers. *Macromolecules*, 1995. **28**: p. 7115–7120.
53. Brynda, E. and Houska, M., Multiple alternating molecular layers of albumin and heparin on solid surfaces. *J Colloid Interface Sci*, 1996. **183**(1): p. 18–25.
54. Godinez, L.A., *et al*., Multilayer self-assembly of amphiphilic cyclodextrin hosts on bare and modified gold substrates: controlling aggregation via surface modification. *Langmuir*, 1998. **14**(1): p. 137–144.
55. Riccardi, C., *et al.*, Surface modification of poly(ethylene terephthalate) fibers induced by radio frequency air plasma treatment. *Appl Surface Sci*, 2003. **211**: p. 386–397.
56. Hammond, P.T. and Whitesides, G.M., Formation of polymer microstructures by selective deposition of polyion multilayers using patterned self-assembled monolayers as a template. *Macromolecules*, 1995. **28**(22): p. 7569–7571.
57. Advincula, R. and Knoll, W., Supramolecular thin films via the Langmuir–Blodgett–Kuhn (LBK) technique. *Colloids Surfaces A–Physicochem Eng Aspects*, 1997. **123**: p. 443–455.
58. Advincula, R., *et al*., *In situ* investigations of polymer self-assembly solution adsorption by surface plasmon spectroscopy. *Langmuir*, 1996. **12**(15): p. 3536–3540.
59. Gao, M.Y., *et al.*, Constructing Pbi2 nanoparticles into a multilayer structure using the molecular deposition (Md) method. *J Chem Soc–Chem Commun*, 1994. (**24**): p. 2777–2778.
60. Hauser, P.J. and Tabba, A.R., Improving the environmental and economic aspects of cotton dyeing using a cationised cotton. *Coloration Technol*, 2001. **117**: p. 282–288.
61. Kolarik, L., *et al*., Building assemblies from high molecular weight polyelectrolytes. *Langmuir*, 1999. **15**: p. 8265–8275.

62. Cochin, D., *et al*., Layered nanostructures with LC-polymers, polyelectrolytes, and inorganics. *Macromolecules*, 1997. **30**: p. 4775–4779.
63. Linford, M.R., Auch, M. and Mohwald, H., Nonmonotonic effect of ionic strength on surface dye extraction during dye–polyelectrolyte multilayer formation. *J Amer Chem Soc*, 1998. **120**: p. 178–182.
64. Ariga, K., Lvov, Y. and Kunitake, T., Assembling alternate dye–polyion molecular films by electrostatic layer-by-layer adsorption. *J Amer Chem Soc*, 1997. **119**: p. 2224–2231.
65. Li, D., *et al.*, Preparation, characterization and properties of mixed organic and polymeric self-assembled multilayers. *J Amer Chem Soc*, 1998. **120**: p. 8797–8804.
66. Kurth, D.G. and Osterhout, R., *In situ* analysis of metallosupramolecular coordination polyelectrolyte films by surface plasmon resonance spectroscopy. *Langmuir*, 1999. **15**: p. 4842–4846.
67. Onda, M., *et al*., Sequential actions of glucose oxidase and peroxidase in molecular films assembled by layer-by-layer alternate adsorption. *Biotechnol Bioeng*, 1996. **51**(2): p. 163–167.
68. Onitsuka, O., *et al*., Enhancement of light emitting diodes based on self-assembled heterostructures of poly(*p*-phenylene vinylene). *J Appl Phys*, 1996. **80**(7): p. 4067–4071.
69. Wu, A., *et al*., Solid-state light-emitting devices based on the tris-chelated ruthenium(II) complex: 3. High efficiency devices via a layer-by-layer molecular-level blending approach. *J Amer Chem Soc*, 1999. **121**(20): p. 4883–4891.
70. Arys, X., *et al*., Ordered polyelectrolyte multilayers. Rules governing layering in organic binary multilayers. *J Amer Chem Soc*, 2003. **125**(7): p. 1859–1865.
71. Arys, X., Laschewsky, A. and Jonas, A.M. Ordered polyelectrolyte 'multilayers'. 1. Mechanisms of growth and structure formation: a comparison with classical fuzzy 'multilayers'. *Macromolecules*, 2001. **34**(10): p. 3318–3330.
72. Cho, J. and Char, K., Effect of layer integrity of spin self-assembled multilayer films on surface wettability. *Langmuir*, 2004. **20**(10): p. 4011–4016.
73. Dhanabalan, A., *et al*., A study of Langmuir and Langmuir–Blodgett films of polyaniline. *Langmuir*, 1997. **13**(16): p. 4395–4400.
74. Facchetti, A., *et al*., Design and preparation of zwitterionic organic thin films: self-assembled siloxane-based, thiophene-spaced *N*-benzylpyridinium dicyanomethanides as nonlinear optical materials. *Langmuir*, 2001. **17**(19): p. 5939–5942.
75. Hillebrandt, H., *et al*., High electric resistance polymer/lipid composite films on indium–tin-oxide electrodes. *Langmuir*, 1999. **15**(24): p. 8451–8459.
76. Joly, S., *et al.*, Multilayer nanoreactors for metallic and semiconducting particles. *Langmuir*, 2000. **16**(3): p. 1354–1359.
77. Park, M.K., *et al*., Self-assembly and characterization of polyaniline and sulfonated polystyrene multilayer-coated colloidal particles and hollow shells. *Langmuir*, 2003. **19**(20): p. 8550–8554.
78. Ram, M.K., *et al.*, Physical properties of polyaniline films: assembled by the layer-by-layer technique. *Langmuir*, 1999. **15**(4): p. 1252–1259.
79. Raposo, M. and Oliveira, O.N., Adsorption of poly(*o*-methoxyaniline) in layer-by-layer films. *Langmuir*, 2002. **18**(18): p. 6866–6874.
80. Wu, D.G., *et al*., Photosensitized electron injection from an ITO electrode to trichromophore dyes deposited on Langmuir–Blodgett films. *Langmuir*, 1999. **15**(21): p. 7276–7281.

81. Yuan, C.W., *et al.*, Insertion of polypyrrole into arachidic acid Langmuir-Blodgett-films. *Langmuir*, 1995. **11**(1): p. 5–7.
82. Koetse, M., *et al.*, Ultrathin coatings by multiple polyelectrolyte adsorption/surface activation (CoMPAS). *Macromolecules*, 1998. **31**(26): p. 9316–9327.
83. Wu, A.P., Lee, J. and Rubner, M.F., Light emitting electrochemical devices from sequentially adsorbed multilayers of a polymeric ruthenium (II) complex and various polyanions. *Thin Solid Films*, 1998. **329**: p. 663–667.
84. Arys, X., *et al.*, Ultrathin multilayers made by alternate deposition of ionenes and polyvinylsulfate: from unstable to stable growth. *Thin Solid Films*, 1998. **329**: p. 734–738.
85. Arys, X., *et al.*, Structural studies on thin organic coatings built by repeated adsorption of polyelectrolytes. *Prog Organic Coatings*, 1998. **34**(1–4): p. 108–118.
86. Lee, J.K., Yoo, D. and Rubner, M.F. Synthesis and characterization of an electroluminescent polyester containing the Ru(II) complex. *Chem Mater*, 1997. **9**(8): p. 1710–1712.
87. Hodak, J., *et al.*, Layer-by-layer self-assembly of glucose oxidase with a poly(allylamine)ferrocene redox mediator. *Langmuir*, 1997. **13**(10): p. 2708–2716.
88. Yoo, D., *et al.*, New electro-active self-assembled multilayer thin films based on alternately adsorbed layers of polyelectrolytes and functional dye molecules. *Synthetic Metals*, 1997. **85**(1–3): p. 1425–1426.
89. Ninham, B.W. and Yaminsky, V., Ion binding and ion specificity: the Hofmeister effect and Onsager and Lifshitz theories. *Langmuir*, 1997. **13**(7): p. 2097–2108.
90. Keller, S.W., *et al.*, Photoinduced charge separation in multilayer thin films grown by sequential adsorption of polyelectrolytes. *J Amer Chem Soc*, 1995. **117**(51): p. 12879–12880.
91. Keller, S.W. *et al.*, Photochemically induced charge separation in electrostatically constructed organic–inorganic multilayer composites, in Nocera D.G. and Wishart, J.S. Editors, *Photochemistry and Radiation Chemistry: Complementary Methods for the Study of Electron Transfer*, 1998, Adv. Chem. Ser. 254 (*Photochemistry and Radiation Chemistry*), p. 359–379.
92. Anzai, J., *et al.*, Layer-by-layer construction of multilayer thin films composed of avidin and biotin-labeled poly(amine)s. *Langmuir*, 1999. **15**(1): p. 221–226.
93. Laschewsky, A., *et al.*, Molecular recognition by hydrogen bonding in polyelectrolyte multilayers. *Chem–A Europ J*, 1997. **3**(1): p. 34–38.
94. Decher, G., Hong, J.D. and Schmitt, J., Buildup of ultrathin multilayer films by a self-assembly process: III. Consecutively alternating adsorption of anionic and cationic polyelectrolytes on charged surfaces, *Thin Solid Films*, 1992. **210(2)**: p. 831–835.
95. Caruso, F., et al., Magnetic core–shell particles: preparation of magnetite multilayers on polymer latex microspheres. *Adv Mater*, 1999. **11**(11): p. 950–953.
96. Dante, S., *et al.*, Photoisomerization of polyionic layer-by-layer films containing azobenzene. *Langmuir*, 1999. **15**(1): p. 193–201.
97. Lvov, Y., Yamada, S. and Kunitake, T., Non-linear optical effects in layer-by-layer alternate films of polycations and an azobenzene-containing polyanion. *Thin Solid Films*, 1997. **300**(1–2): p. 107–112.
98. Ferreira, M. and Rubner, M.F., Molecular-level processing of conjugated polymers.1. layer-by-layer manipulation of conjugated polyions. *Macromolecules*, 1995. **28**(21): p. 7107–7114.
99. Saremi, F., *et al.*, Self-assembled alternating multilayers built-up from diacetylene

bolaamphiphiles and poly(allylamine hydrochloride) – polymerization properties, structure, and morphology. *Langmuir*, 1995. **11**(4): p. 1068–1071.
100. Lowack, K. and Helm, C.A., Polyelectrolyte monolayers at the mica/air interface – mechanically induced rearrangements and monolayer annealing. *Macromolecules*, 1995. **28**(8): p. 2912–2921.
101. Caruso, F. and Mohwald, H., Preparation and characterization of ordered nanoparticle and polymer composite multilayers on colloids. *Langmuir*, 1999. **15**(23): p. 8276–8281.
102. He, J.A., *et al.*, Electrostatic self-assembly of polydiacetylene nanocrystals: nonlinear optical properties and chain orientation. *J Phys Chem B*, 1999. **103**(50): p. 11050–11056.
103. Voigt, A., *et al.*, Membrane filtration for microencapsulation and microcapsules fabrication by layer-by-layer polyelectrolyte adsorption. *Ind Eng Chem Res*, 1999. **38**(10): p. 4037–4043.
104. Liu, Y.J., Rosidian, A. and Claus, R.O., Mechanical properties of electrostatically self-assembled Al2O3–ZrO2 nanocomposites prepared at room temperature. *J Cluster Sci*, 1999. **10**(3): p. 421–428.
105. Cheng, L., *et al.*, Electrochemical growth and characterization of polyoxometalate-containing monolayers and multilayers on alkanethiol monolayers self-assembled on gold electrodes. *Chem Mater*, 1999. **11**(6): p. 1465–1475.
106. Liu, Y.J. and Claus, R.O., Strong enhancement of optical absorbance from ionic self-assembled multilayer thin films of nanocluster Pt and polymer dye. *J Appl Phys*, 1999. **85**(1): p. 419–424.
107. Rosidian, A., Liu, Y.J. and Claus, R.O., Ionic self-assembly of ultrahard ZrO2/polymer nanocomposite thin films. *Adv Mater*, 1998. **10**(14): p. 1087–1091.
108. Yonezawa, T., Onoue, S.Y. and Kunitake, T., Growth of closely packed layers of gold nanoparticles on an aligned ammonium surface. *Adv Mater*, 1998. **10**(5): p. 414–416.
109. Chen, T.Y. and Somasundaran, P., Preparation of novel core–shell nanocomposite particles by controlled polymer bridging. *J Amer Ceramic Soc*, 1998. **81**(1): p. 140–144.
110. Ingersoll, D., Kulesza, P.J. and Faulkner, L.R., Polyoxometalate-based layered composite films on electrodes – preparation through alternate immersions in modification solutions. *J Electrochem Soc*, 1994. **141**(1): p. 140–147.
111. Shiratori, S.S. and Rubner, M.F., pH-dependent thickness behavior of sequentially adsorbed layers of weak polyelectrolytes. *Macromolecules*, 2000. **33**(11): p. 4213–4219.
112. He, J.A., *et al.*, Bacteriorhodopsin thin film assemblies – immobilization, properties, and applications. *Adv Mater*, 1999. **11**(6): p. 435–466.
113. He, J.A., *et al.*, Photoelectric properties of oriented bacteriorhodopsin/polycation multilayers by electrostatic layer-by-layer assembly. *J Phys Chem B*, 1998. **102**(36): p. 7067–7072.
114. He, J.A., *et al.*, Oriented bacteriorhodopsin/polycation multilayers by electrostatic layer-by-layer assembly. *Langmuir*, 1998. **14**(7): p. 1674–1679.
115. Brynda, E., *et al.*, The detection of human beta(2)-microglobulin by grating coupler immunosensor with three dimensional antibody networks. *Biosensors Bioelectronics*, 1999. **14**(4): p. 363–368.
116. Caruso, F., *et al.*, Characterization of polyelectrolyte–protein multilayer films by atomic force microscopy, scanning electron microscopy, and Fourier transform

infrared reflection-absorption spectroscopy. *Langmuir*, 1998. **14**(16): p. 4559–4565.
117. Kong, W., *et al*., Immobilized bilayer glucose-isomerase in porous trimethylamine polystyrene based on molecular deposition. *J Chem Soc Chem Commun*, 1994. **11**: p. 1297–1298.
118. Fischer, P., *et al*., Polyelectrolytes bearing azobenzenes for the functionalization of multilayers. *Macromolecular Symposia*, 1999. **137**: p. 1–24.
119. Dermody, D.L., *et al*., Chemically grafted polymeric filters for chemical sensors: hyperbranched poly(acrylic acid) films incorporating beta-cyclodextrin receptors and amine-functionalized filter layers. *Langmuir*, 1999. **15**(3): p. 885–890.
120. Laschewsky, A., *et al*., Polyelectrolyte multilayers containing photoreactive groups. *Macromol Chem Phys*, 1997. **198**(10): p. 3239–3253.
121. Akin, F., *et al*., Nanostructure of fluorocarbon films deposited on polystyrene from $C_3F_5^+$ ions. *J Phys Chem B*, 2004. **108**: p. 9656–9664.
122. Nelson, B., *et al*., Near-infrared surface plasmon resonance measurements of ultrathin films. 1. Angle shift and SPR imaging experiments. *Anal Chem*, 1999. **71**: p. 3928–3934.
123. Hanton, S.D., Mass spectrometry of polymers and polymer surfaces. *Chem Rev*, 2001. **101**: p. 527–569.
124. Hyde, K., Rusa, M. and Hinestroza, J., Layer-by-layer deposition of polyelectrolyte nanolayers on natural fibres: cotton. *Nanotechnology* 2005. **16**: S422–S428.
125. Kim, H.J., *et al*., Dynamic sequential layer-by-layer deposition method for fast and region-selective multilayer thin film fabrication. *Langmuir*, 2005. **21**(18): p. 8532–8538.
126. Porcel, C.H., *et al.*, Ultrathin coatings and (poly(glutamic acid)/polyallylamine) films deposited by continuous and simultaneous spraying. *Langmuir*, 2005. **21**(2): p. 800–802.

17

Nanofabrication of thin polymer films

I. LUZINOV, Clemson University, USA

17.1 Introduction

Surface structure and behavior of fiber materials are of the utmost importance for the properties of fibers and textiles in processing and use, since friction, abrasion, wetting, adhesion, adsorption and penetration phenomena are involved. Further advances in industrial textiles impose rigorous requirements for the surface modification: a given textile material, depending on the conditions under which it is utilized, has to be hydrophobic or hydrophilic, acidic or basic, conductive or nonconductive, and deliver or adsorb some species. In order to obtain textile materials with the desired performance, the fiber surface is often modified with polymer layers before use. Numerous surface modifications involving oxidation, reduction, elimination, addition, cyclization and condensation, and grafting of macromolecules have been described in the literature.[1] Among them, the grafting technique has several advantages over others,[2] including easy and controllable introduction of new polymer chains with a high surface density, precise localization of the chain at the surface and long stability of the grafted layers. Moreover, covalent attachment of the macromolecules onto a polymer surface can avoid their delamination in liquid media.

The polymer chains located at the interface can be anchored to the surface in several configurations. The macromolecules may form multiple connections with the substrate or be connected to the surface by one or both ends. Tethered polymer chains that are grafted to a solid substrate by one chain end may be definitely distinguished from other anchored polymer layers, since they form polymer brushes if relatively high grafting density is reached.[3, 4] Brush-like layers are formed due to the excluded volume effect, when the substrate is completely covered with a relatively dense monolayer of grafted chains stretched normal to the support. There are several major parameters that control the grafted layer properties: grafting density, chain length, polydispersity and chemical composition of the chains.[5, 6]

This chapter focuses on synthesis and characterization of the nanothick,

chemically grafted polymer films (polymer brushes) on inorganic and polymeric substrates including polymer fibers. The synthesis has been conducted employing the recently developed macromolecular anchoring layer approach.[7] The chapter also offers examples of the application of the polymer grafting technique for the generation of hydrophobic, hydrophilic and switchable fibrous materials.

17.2 Macromolecular platform for nanofabrication

The chemical grafting of polymers can be accomplished by either 'grafting to' or 'grafting from' methods.[5] According to the 'grafting to' technique, end-functionalized polymer molecules react with complementary functional groups located on the surface to form tethered chains. The 'grafting from' technique utilizes the polymerization initiated from the substrate surface by attached (usually by covalent bonds) initiating groups.

It is necessary to highlight that most of the developed grafting ('to' and 'from') methods require attachment of end-functionalized polymers or low molecular weight substances (e.g. initiators) to the substrate for the polymer brush synthesis. There are two common approaches for the attachment of polymerization initiators or end-functionalized polymers for the brush fabrication. The first one relies on the reactions between end-functionalized initiator/polymer and native functional groups originally present on the substrate surface.[8–10] A different approach involves the formation of a monolayer consisting of functional groups active towards terminally functionalized (e.g. epoxide, amine, anhydride or hydroxide) initiator/polymer.[11, 12] Silane and thiol chemistries have proved to be suitable for the grafting in this case. Usually the coupling methods are relatively complex and specific for certain substrate/(macro)molecule combinations. An alternative method for the attachment involves primary polymer anchoring (mono)layer with activity towards both surface and functionalized (macro)molecule.[13–16] The polymer is used for the initial surface modification as well as generation of the highly reactive primary anchoring layer. When deposited on a substrate, the primary layer first reacts with the surface through formation of covalent bonds (Fig. 17.1). The reactive units located in the 'loops' and 'tails' sections of the attached macromolecules are not connected to the surface.[17] These free groups offer a synthetic potential for the further chemical modification reactions and serve as reactive sites for the subsequent attachment of the functionalized (macro)molecules. If the polymer used for building the primary layer contains functional groups highly active in various chemical reactions, the primary layer approach becomes virtually universal towards both surface and end-functionalized species being used for the brush formation.

For the majority of the initial experiments on the surface grafting a silicon wafer was used as a substrate, since it is now a 'standard' surface (along with

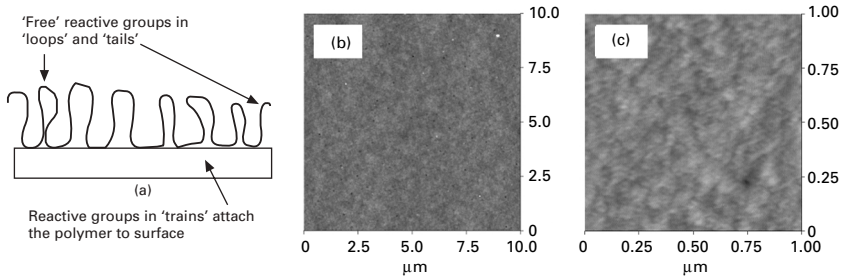

17.1 Schematic representation of reactive polymer attached to substrate (a). Atomic force microscopy (AFM) images showing topography of PGMA layer deposited by dip-coating on silicon wafer: (b) $10 \times 10\,\mu m^2$ and (c) $1 \times 1\,\mu m^2$.

mica) for the research in the field of thin polymer layers. A lot of brush investigations have been made using the wafer as a model surface, and thus we can compare our results with work of others. Poly(glycidyl methacrylate) (PGMA) was used as a primary anchoring polymer layer. A polymer with epoxy functionality was chosen, since the epoxy groups are quite reactive with carboxyl, hydroxyl, amino and anhydride functional groups. The versatile chemistry of the epoxy groups offered flexibility in selection of necessary initiators/macromolecules that are to be attached to the surface. The epoxy groups of the polymer chemically anchored PGMA to the surface.[13] The glycidyl methacrylate units located in the 'loops' sections of the attached macromolecules were not connected to the surface. These free groups served as reactive sites for the subsequent attachment of polymerization initiators and/or polymer with functional groups, which exhibit an affinity for the epoxy modified surface.

The attachment of PGMA to various surfaces was studied and it was found that the uniform and homogeneous epoxy containing polymer layer could be deposited on surfaces by adsorption or dip-coating.[7, 18–22] The epoxy containing polymer layer could be deposited as a monolayer on polymeric poly(ethyleneterephthalate) (PET), polyethylene, polypropylene (PP), silicon resin, nylon) and inorganic (silica, glass, titanium, alumina, gold, silver) surfaces. It was possible to regulate the thickness of the layer and consequently the amount of epoxy groups on the surface by varying the solvent characteristics and concentration of solution being used for the deposition. Layers with a thickness from 1 to 10 nm were obtained. It was found that the layer could not be removed from the wafer using a vigorous solvent treatment, suggesting that PGMA was chemically bonded to the surface. The PGMA layer was smooth (atomic force microscopy, AFM, roughness 0.3 nm) and uniformly covered the surface on nano- and micro-levels (Fig. 17.1b and c). To check the activity of the epoxy groups in the loops and tails of the adsorbed polymer,

a model reaction between the epoxy polymer layer and dodecyl amine (DA) was conducted.[19] The PGMA layer retained its epoxy functionalities, which could be used for further chemical modification reactions.

17.3 'Grafting from' technique for synthesis of polymer films

In the 'grafting from' technique the polymerization is initiated from the substrate surface by attached (usually covalently bonded) initiating groups. When exceptionally high grafting density is needed, the 'grafting from' approach is the only method for brush formation. The polymer brushes grown from the surface by the technique indeed possess extremely high density of the attached chains. Molecules of a monomer penetrate through the already grafted polymer layer easily and significant grafted amounts can be reached. This technique was used for the preparation of thick grafted layers of high grafting density on the surface. Anionic,[23, 24] cationic,[25, 26] controlled/living[27, 28] and conventional[29, 30] free radical polymerizations have been successfully used to synthesize tethered polymer layers on solid substrate surfaces. By appropriate choice of initiating system, temperature, monomer and concentration, it is quite possible to synthesize layers possessing different morphology, thickness and composition.[5] Thus, fine-tuning of the layer properties is possible.

To realize a 'grafting from' approach employing the PGMA platform the primary layer was used to synthesize an effective macroinitiator for controlled/'living' atom transfer radical polymerization (ATRP).[20, 21, 31] The controlled/'living' free radical polymerization has a number of advantages over traditional radical polymerization procedures. The main advantage of a 'living' process is that it provides reliable control over the polymer molecular weight and narrow polydispersities. Thus, the nature of the polymerization process permits structural characteristics of the grafted polymer brush to be readily varied and controlled. An added benefit is the frontal character of the chain growth on the surface. In this manner all chains have very similar history that may be translated in more predictable cooperative behavior of the chains and make the brush nearly 'defect free'. Numerous effective approaches have been reported for the synthesis of polymer brushes by the 'living' free radical polymerization.[5, 28, 32, 33]

17.3.1 Synthesis of macroinitiator

The synthesis of the ATRP macroinitiator included two major steps: deposition of the anchoring PGMA layer on the surface and attachment of bromoacetic acid (BAA) to the surface modified with the anchoring layer through the reaction between the carboxyl and epoxy functionalities. The reaction between

the epoxy groups and the carboxyl functionality of the BAA produces a bromoacetic ester derivative of the PGMA. Such α-bromoesters are known as effective initiators for ATRP of styrene, acrylic and some other vinyl monomers.[34] Therefore, the ATRP macromolecular initiator, covalently anchored to the silicon surface, was synthesized.

In order to prepare a thin layer of the PGMA macromolecular precursor, attached to the surface of silicon wafer, dip-coating from PGMA solution in methyl ethyl ketone (MEK) was employed. It was found that the thickness of PGMA layer is nearly proportional to the concentration of the solution, so the thickness of PGMA anchoring layers can be tuned easily by varying the concentration. After the dip coating, we observed not only smooth and uniform covering, but also stable reproducibility in the thickness of the reactive anchoring layer. Annealing of the adsorbed film for 20–40 min at 110 °C led to the permanent attachment of the deposited film to the substrate. The annealed PGMA layer was smooth and uniformly covered the substrate.

The PGMA film treated with BAA vapor produced macroinitiator possessing smooth and uniform surface morphology (Fig. 17.2a and b). Variation of the PGMA layer thickness allowed control over the amount of BAA attached to the surface. There was a nearly linear correlation between the quantity of the epoxy polymer attached to the surface and the amount of the initiator anchored (Fig. 17.2c). The kinetics of the BAA deposition process was also suitable for regulation of the BAA amount reacted with the anchoring PGMA layer. The PGMA layer was contacted with BAA vapor at two different temperatures (30 and 90 °C) for different times. The thickness of the anchoring layer was kept constant (4 nm) in this series of experiments. At the beginning of the BAA deposition the surface concentration of the attached molecules increased with time and then leveled off after 4–6 h. At higher temperature the reaction rate proceeded more rapidly. The maximum initiator concentration at 30 °C was around 10 molecules/nm^2, while at 90 °C it reached 28 molecules/nm^2.

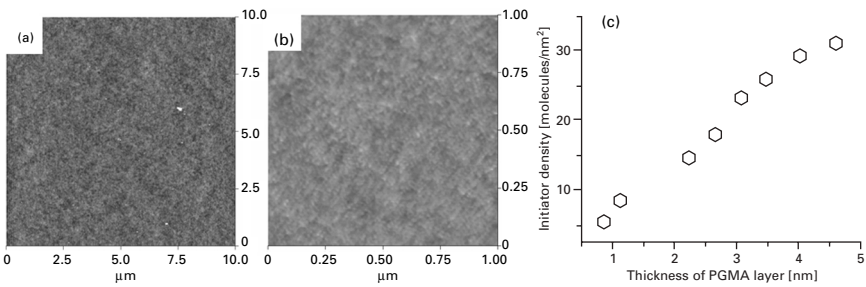

17.2 AFM images of PGMA/BAA macroinitiator. Image size: (a) 10 × 10 μm^2, (b) 1 × 1 μm^2. Vertical scale – 10 nm. (c) Surface density of attached BAA versus thickness of the annealed (12 h at 90 °C) PGMA layer.

17.3.2 Atom transfer radical polymerization from macroinitiator

The fundamental idea of ATRP is the halogen exchange in the polymerizing system between the halogen terminated growing polymer chain/Cu(I) dNbP complex and macroradical/Cu(II) dNbP complex.[34] Chain propagation is a first order process while termination is a second order reaction. For conventional bulk or solution ATRP the equilibrium is strongly shifted to the left. The free radical concentration is as low as 10^{-7}–10^{-8} mole/l and Cu(II) concentration is approximately 5% of that for Cu(I).[34] Consequently, the termination is diminished and all chains grow simultaneously during the polymerization without noticeable termination. An adequate concentration of Cu(II) is critical for effective reaction control. However, when the ATRP is initiated from the surface, the amount of the initiator located on the substrate is not sufficient to create the concentration of Cu(II) species required for polymerization control.[28, 35] There are two methods developed for maintaining the Cu(II) concentration for ATRP initiated from a surface: (a) simultaneous initiation of ATRP from the surface and in solution, and (b) addition of the necessary amount of Cu(II) at the beginning of the process.[5, 28] Both approaches were tested for the ATRP grafting from the PGMA/BAA macroinitiator adsorbed on the surface and successfully obtained the polymer brushes grafted to the silicon surface by the two methods.

Specifically, polystyrene (PS) brushes of different thicknesses were synthesized on the PGMA/BAA modified silicon wafer by ATRP. At the beginning of the polymerization process, a linear increase of polystyrene layer thickness was observed. Later, the rate of the grafting decreased and the brush thickness practically leveled off. Different surface concentrations of BAA were used in the grafting experiments to acquire knowledge about the relationship between amount of the initiator anchored to the surface through PGMA and rate of the brush formation. The increase in the surface density of the initiating moieties led to the increase in the grafting rate. However, a cutoff initiator concentration beyond which no increase of the thickness of the grafted layer was observed. From comparison between the surface densities of the initiator and the attached polymer it was determined that the efficiency of the initiation from the surface was in the level of 5–15%. It was also shown that other (than PS) polymer brushes could be successfully grown from the surface employing the macroinitiator based on the PGMA platform. *N*-isopropylacrylamide, poly(ethylene glycol) methyl ether methacrylate, butyl methacrylate and pentafluorostyrene were grafted to a substrate.

To prove the controlled nature of the polymerization initiated from the surface by the PGMA/BAA macroinitiator, polymerization of styrene was conducted using the already grown PS brush of 19 nm as an initiator. It was

found that the thickness of the grafted layer increased from 19 to 31 nm, indicating successful chain extension. The experiment demonstrated that the PS brush obtained with the PGMA/BAA macroinitiator is carrying active Br ends.

Following the polymerizations on the model silicon surface, the developed approach for the synthesis of the grafted layers on polymeric substrate was tested. The surface of the PET film was modified with a PGMA/BAA layer and ATRP of styrene initiated from the PET surface was carried out. As a result of the polymerization, a PS layer was firmly grafted to the PET surface. Figure 17.3 shows AFM images and values of water contact angles for virgin PET surface, PET surface covered with PGMA/BAA combination, and grafted PS layer. One can see that the surface morphology and wettability of the PET

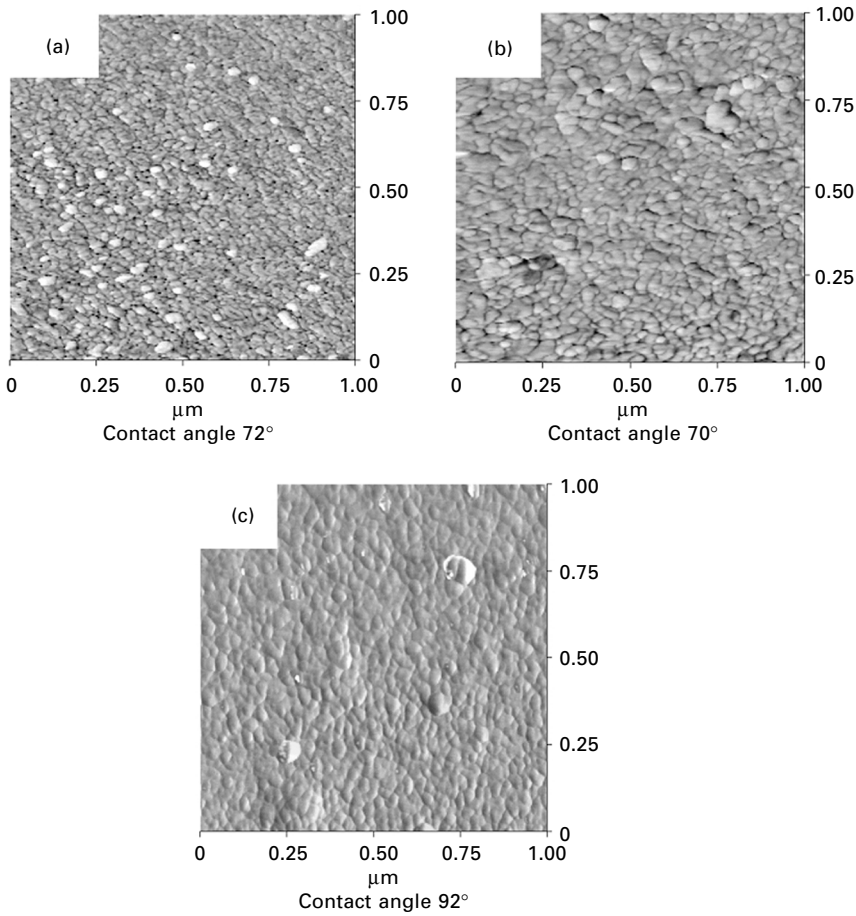

17.3 AFM phase images ($1 \times 1 \mu m^2$) of (a) virgin PET surface; (b) BAA layer attached to the PGMA layer; (c) PS layer obtained by ATRP initiated by attached BAA.

film was changed after the polymerization. The obtained result suggested applicability of the developed synthetic approach to surface modification of fibers and textile materials.

17.4 'Grafting to' technique for synthesis of polymer films

Synthesis of the polymer brushes can be readily accomplished by a 'grafting to' method.[36–38] In the 'grafting to' technique, end-functionalized polymer molecules react with complementary functional groups located on the surface to form tethered chains. End-functionalized polymers (with a narrow molecular weight distribution) can be synthesized by living, anionic, cationic, radical, group transfer and ring opening metathesis polymerizations. Thus the advantage of the method is that the well-defined end-functionalized polymers can be used for the grafting and, as a result, well-defined brushes can be readily obtained. The covalent bond formed between the polymer chain and the substrate makes the polymer brushes resistant to chemical environmental conditions. On the other hand, the technique has a constraint in terms of the maximum grafting that can be obtained, namely that the grafting is self-limiting.[37, 39] Polymer chains must diffuse through the existing polymer film to reach the reactive sites on the surface. This barrier becomes more pronounced as the tethered polymer thickness increases. Thus, the polymer brush obtained typically has low grafting density and low thickness.

The density of the brush obtained by the 'grafting to' method can be increased if the macromolecule attachment is conducted from a solution at Θ conditions[36] or from melt.[11, 37, 40, 41] Grafting from melt in particular offers potential advantages over grafting from solution, since the excluded volume interactions that make it difficult for chains to penetrate an initial grafted layer are screened out in the melt.[37] If the grafting is carried out from the melt, many polymer chains are already in locations from which they do not need to pass the potential barrier, since they are already adjacent to the surface. The macromolecules only need to reorient themselves within the first monolayer in order to expose the terminal groups to the surface functionalities.

An additional increase in grafting density for the attachment from the melt can be achieved when the PGMA anchoring layer is used for the introduction of reactive group on a substrate surface.[18, 19, 22, 42] Attachment of end-functionalized PS from melt to a 1 nm thick layer of PGMA, attached to silicon wafers was studied.[18] In fact, the free groups in the 'tails' and the 'loops' of the PGMA macromolecule (deposited on the substrate) served as reactive sites for the anchoring of the end-functionalized polymers. Comparison of the results for the grafting to the PGMA primary layer with published data[11] obtained for the epoxysilane (ES) monolayer suggested that there are

many similarities between these grafting processes. The same major trends were observed. However, the grafting to the PGMA layer was much more effective. In Fig. 17.4 the surface coverage, Γ is plotted versus the degree of polymerization (N) of the grafting polymer. The surface coverage initially increases for the range $43 < N < 440$, passes through a maximum at $N = 440$, and then decreases. The maximum is close to the critical entanglement molecular weight of PS, M_C, which is 31 200 g/mol ($N_C = 300$).[43] However, it is necessary to stress that the surface coverage and hence the thickness of the PS grafted to the PGMA layer is two- to three-fold greater than that obtained for the ES monolayer. It appeared that the epoxy groups located in the loops/tails of the adsorbed PGMA macromolecule were more accessible to the end-functional groups of PS when compared with epoxysilane with terminal epoxy groups located mainly at the monolayer surface. It was concluded that the high efficiency of PGMA in the grafting reactions was related to the high mobility of the epoxy reactive groups and to the formation of an interpenetrating zone at the PS/PGMA interface.

The grafting of end-functionalized polymers employing the macromolecular anchoring layer approach was further investigated considering the effect of the molecular weight and thickness of the PGMA layer.[42] The obtained experimental data indicated that, when the higher molecular weight PS chains are considered, neither the thickness nor the molecular weight of the PGMA layer have any significant influence on the grafting of the end-functionalized PS to the macromolecular anchoring layer. Conversely, the lower molecular weight PS sample does not follow the trend, since significantly higher amounts of the polymer can be grafted to the thicker anchoring layers. The high grafting in this case may be a result of formation of an extremely extended

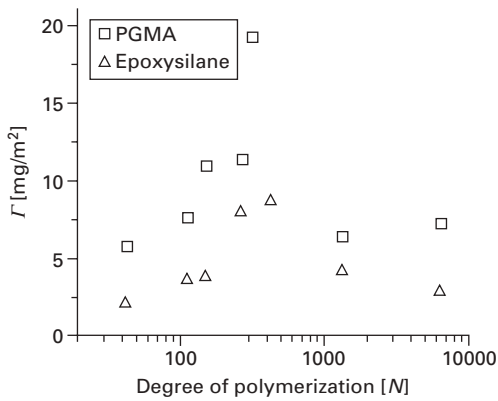

17.4 Surface coverage, Γ (mg/m^2) versus degree of polymerization (N) of grafted PS chains.

interphase between loops of the adsorbed PGMA and the low molecular weight PS.

The grafting of carboxylic acid end-functionalized poly(ethylene glycol) methyl ether (PEG) chains of different molecular weights from the melt onto a surface employing a PGMA anchoring layer was studied as well.[19, 22] The grafting led to the synthesis of the complete PEG brushes possessing exceptionally high grafting density. The maximum thickness of the attached PEG films was strongly dependent on the length of the polymer chains being grafted. The maximum grafting efficiency was close to the critical entanglement molecular weight region for PEG. AFM imaging revealed that the grafting process led to complete PEG layers with surface smoothness on a nanometric scale. Practically all the samples were partly or fully covered with crystalline domains that disappeared under water. The PEG hydrophilic nature meant that the surface with the grafted layer exhibited a low (up to 21°) water contact angle.

In general, it was shown that until a certain level of miscibility/compatibility between a polymer being grafted and the anchoring macromolecules (attached to a substrate) is reached, the effect of the layer thickness and molecular weight is not significantly pronounced. The same grafted layers were attached to relatively thin (1.0 nm) and thick (10 nm) PGMA films. If polymers to be grafted are miscible with PGMA, the grafted amount is strongly dependent on the anchoring layer thickness. In the case of such miscibility/compatibility the effect may become dramatic. Specifically, if end-functionalized polymer is miscible/compatible with the anchoring layer, the thickness and molecular weight of the anchoring layer must be seriously taken into account to avoid (or reach) the extensive interpenetration at the boundary.

The developed grafting approach was also employed for attachment of polymers to polymeric films and fibers. Hydrophilic/polar (PEG, polyacrylamide, polyacrylic acid) and hydrophobic (PS and polypentafluorostyrene) polymers were attached to PET, polyethylene, cotton and nylon. Figure 17.5a and b shows the morphology and wettability of a PET surface modified with PS and PEG grafted layers. The AFM images revealed that the polymeric surface was completely covered with the grafted layers and the polymer grafted dictated the surface properties of the polymer film. The synthesized layers could not be removed by multiple rinsing in hot solvents, including such strong solvent as *N*, *N*-dimethylformamide (DMF). The obtained results suggested that polymers possessing functional groups could be indeed grafted to polymeric surfaces modified with the PGMA anchoring layer. Polypentafluorostyrene and/or PS were also successfully grafted to PET, cotton and nylon fiber/textile materials utilizing the grafting approach developed. Highly hydrophobic materials were obtained as a result of the surface modification (Fig. 17.5c).

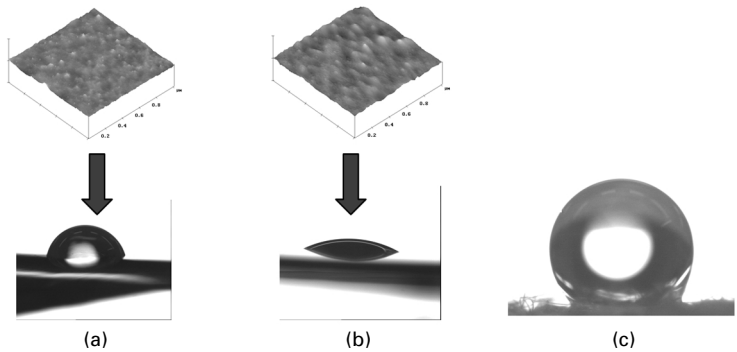

17.5 (a) and (b) AFM topography images ($1 \times 1 \mu m^2$) and wettability measurements for the PET surface modified with grafted polystyrene (a) and poly(ethylene glycol) (b). (c) Droplet of water on the surface of polyester textile material modified with grafted polystyrene layer. The polymers were grafted through the PGMA layer.

17.5 Synthesis of smart switchable coatings

Polymer coatings that are responsive to environmental conditions are of great interest for various advanced applications including generation of 'intelligent' fibers and textiles. The advantage of these 'smart' materials is the ability to switch and/or tune the surface properties of the coatings by applying external stimuli to vary, for example, adhesion, wettability, friction, roughness, reactivity, biocompatibility and selectivity. In recent years, various efforts have been reported on the development of such smart materials that can act in response to environmental stimuli, such as changes in electric potential, temperature, pH, or the presence of a specific chemical substance.[44–50] With the increasing demand for more sophisticated surfaces, one of the current targets is to fabricate and understand materials whose interfacial properties are capable of consistent reversible changes in their characteristics according to outside conditions or stimuli.[45]

17.5.1 Mixed polymer brushes

Recently, the new class of interfacially active responsive materials, mixed polymer brushes, has been developed.[50, 51] To generate the responsive brush, two or more different polymers have to be grafted to a surface (Fig. 17.6). Adaptive and responsive behavior of the thin film (chemically attached to a substrate) is based on phase segregation mechanism of two incompatible polymers constituting the mixed brushes. Upon outside stimuli (solvent quality, temperature, pH, ionic strength) the phase segregation results in switching of spatial distribution of functional groups within the ultrathin film and different chain fragments may be delivered to the brush exterior. The discovery of the

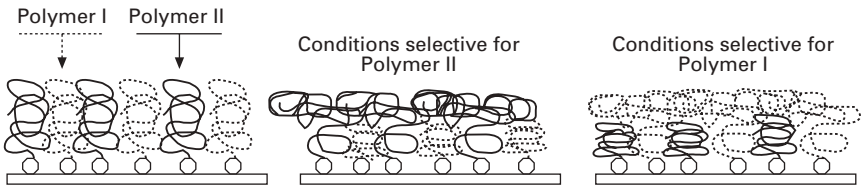

17.6 Schematic of morphology variation of mixed polymer brush situated in non-selective (left) and selective (right) conditions.

brush switchable behavior has offered novel virtually endless possibilities to generate adaptive/responsive surfaces/interfaces expressing a variety of unique properties. Moreover, the combination of two or more polymers in the brush does not act as a simple addition of different functions, but it affects a specific morphology of the film driven by a subtle interplay between increased numbers of interactions. Therefore, the difference between a brush of a random copolymer (when different functions can be combined in the same polymer chain by random distribution of two or more different monomer units in the polymer molecule) and binary or multicomponent brushes with different homopolymers randomly grafted to the same substrate should be emphasized. The principal difference is introduced by the structure of the film when different end-attached polymer chains can segregate into nanoscopic domains affecting a unique morphology of the film.

PS and poly(2-vinylpyridine) (PVP) switchable mixed brushes were synthesized employing the macromolecular anchoring layer used to activate the substrate boundary.[52] The 'grafting to' approach was used to attach the polymer chains to the substrate. The PS and PVP were deposited on the wafers in a sequential fashion to chemically graft PS in a first step, and subsequently graft PVP. The investigation has demonstrated that it is possible to synthesize mixed polymer brushes of various compositions by grafting to a silicon surface using PGMA as an anchoring interlayer. The mixed brush synthesized in this manner exhibits changes in surface energy as measured by contact angles. Specifically, these contact angle measurements follow the change in concentration of PS content well, and indicate switching between PS and PVP with toluene and ethanol, respectively.

Scanning probe microscopy (SPM) was used to visualize the sample surface morphology, observe microphase segregation within the brushes and sample roughness. Figure 17.7 shows how the surface morphology of the mixed brushes changes on content of PS and treatment with selective (ethanol and toluene) solvents. The surface topography of the mixed brushes showed a general trend toward smoother surfaces as the ratio of PS increases to the 95% composition. For samples with lower PS content, formation of clusters on the brush surface was observed, revealing pronounced phase segregation in the grafted film where grafted PS and PVP chains try to minimize their mutual contact.

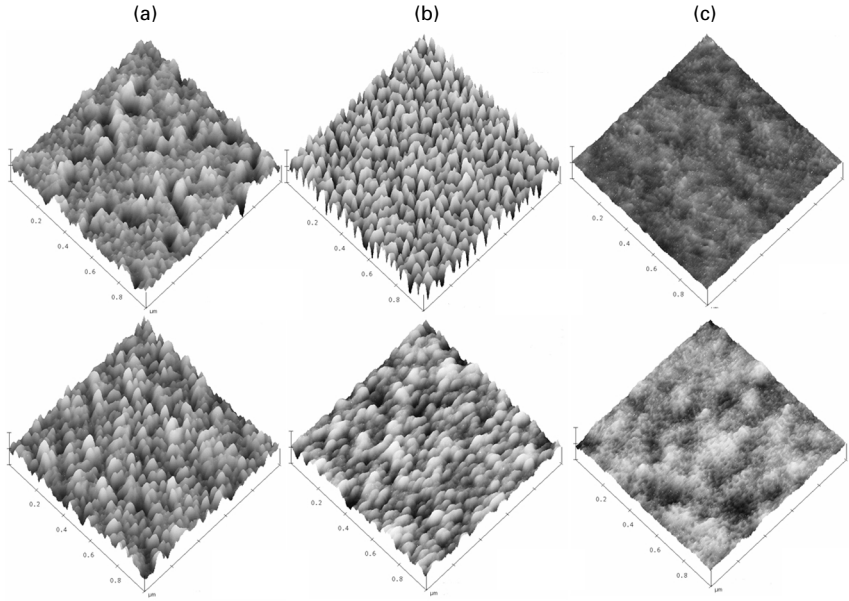

17.7 SPM topographical images of mixed PS-PVP brushes (grafted via PGMA anchoring layer) rinsed with ethanol (top row) and toluene (bottom row). Dimensions are $1 \times 1\,\mu m^2$ with a 5 nm vertical scale: (a) 31% PS, (b) 65% PS and (c) 94% PS.

In addition, an approach has been developed for fabrication of the stimuli-sensitive mixed brushes by 'one-pot' techniques, where all components of the smart nanolayers are simultaneously deposited on the surface and attached in one single step. Specifically, the one-step synthesis of PS-PVP mixed brushes was carried out. The end-functionalized PS and PVP were deposited on the surface (modified with PGMA) simultaneously from a joint solution in MEK. An initial study of the effect of depositing varying amounts of polymers indicated a preferential grafting of PVP at higher deposited amounts of polymer blend. However, the composition of the grafted nanolayer could be regulated by the ratio of the polymers in solution. Rinsing the mixed PS/PVP polymer brush in selective solvents allowed observation of the change in water contact angle as a function of the nanolayer composition. Using toluene and ethanol as the selective solvents the hydrophilic/hydrophobic nature of the brush–air interface changes was probed. In toluene, PS dominates the interface with larger contact angle values. Conversely, ethanol results in a PVP dominated surface and lower contact angle values. Changes in the roughness and structure of the nanolayer surface were also observed (by AFM), corresponding to the solvent treatment and the layer composition (Fig. 17.8). The phase imagery indicated a degree of segregation between the PS and PVP rich phases.

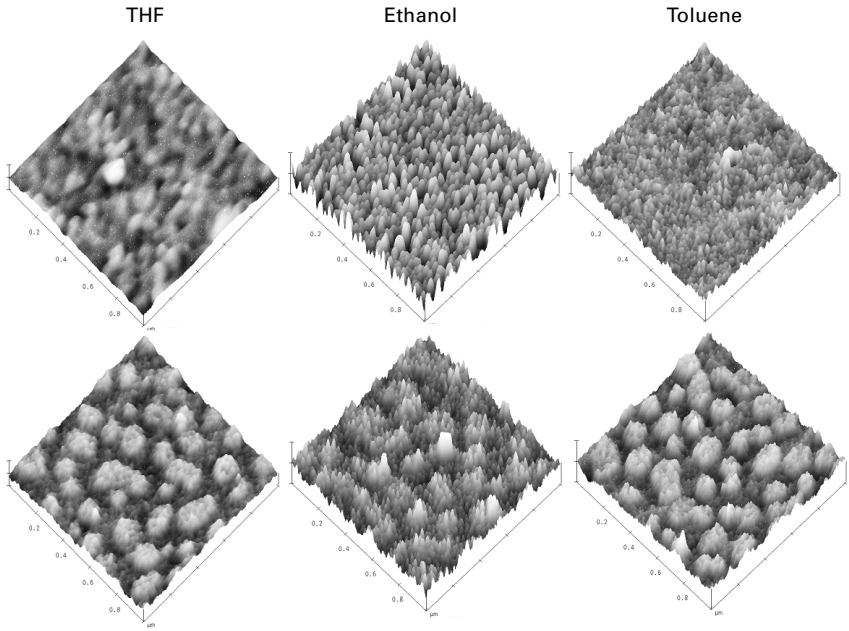

17.8 AFM topographical images of PS-PVP mixed brushes of different thicknesses in their hydrophobic (toluene treatment), hydrophilic (ethanol treatment), and neutral (tetrahydrofuran (THF) treatment) states ($1 \times 1\,\mu m^2$, vertical scale 5 nm). Thickness of the grafted layer: 9 nm (top row) and 5 nm (bottom row).

Switchable nanolayers were synthesized by combination of the grafting end-functionalized polymers ('grafting to') and polymerization initiated from the surface ('grafting from').[53] The combination allows synthesis of responsive nanolayers consisting of polymers that can only be attached by a certain grafting method. The synthesis was conducted according to the following procedure. BAA was used as an initiator of ATRP polymerization. Attachment of the BAA molecules to the surface covered with the PGMA film was conducted from gaseous phase. Next, the synthesis of the poly(*t*-butyl acrylate) PTBA brush was carried out by the 'grafting to' method utilizing PTBA with an end carboxyl functional group. The PTBA melt grafting buried the ATRP initiator under the polymer brush with a significant thickness of 12–20 nm. To complete the fabrication of the mixed brush, ATRP of styrene initiated by the PGMA/BAA macroinitiator was carried out. As a result of the developed process, the mixed polymer brushes with PTBA brush thickness 12–20 nm and PS layer 1–100 nm were obtained. Hydrolysis of PTBA to polyacrylic acid (PAA) was utilized to synthesize polymer layers possessing hydrophobic/hydrophilic properties. The brushes changed their surface morphology when they were exposed to solvent with different polarity (Fig. 17.9). For the best

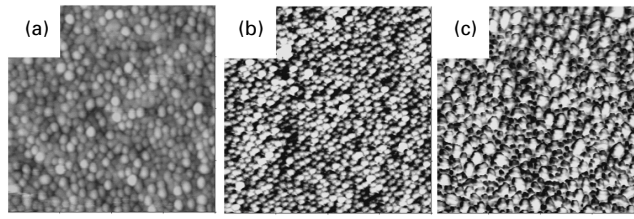

17.9 AFM topography images ($1 \times 1 \mu m^2$) of mixed PS–polyacrylic acid brushes treated with different solvent: (a) benzene (water contact angle 80°); (b) THF; (c) EtOH (water contact angle 40°). Thickness of PS/PAA 15/15 nm.

samples the contact angle was changed by 40° when the hybrid layer was exposed to the different environments.

17.5.2 Switchable unary polymer brush

The mobile epoxy groups located in the loops/tails of the adsorbed PGMA macromolecule are shown to be accessible to the functional groups of an end-functionalized polymer and thus available for grafting. The mobility of the loops/tails of PGMA could be also effectively used to develop a novel system, which is robust, and possesses wettability on demand. In fact, the responsive unary polymer brush (UPB) system described below benefited from the mobility of the PGMA loops effectively to switch surface properties.[54]

UPB can be described as a binary system consisting of an end-functionalized polymer grafted to a macromolecular anchoring layer. The UPB system developed (Fig. 17.10) consists of end-grafted PS and a PGMA anchoring layer. It was anticipated that the mobile loops/trains of the macromolecule could be effectively used to tailor surface properties between the favorable state for PS (non-polar) and the favorable state for PGMA (relatively more-polar).

AFM analysis of the substrates covered with UPB after solvent treatment (Fig. 17.10) showed a well-defined change in morphology for higher molecular weight PS. The surface changed from 'smooth' (toluene) to 'ripple' (MEK) after treatment with selective solvents. The phase segregation can be explained in terms of mobility of the free end of PS and restricted mobility of the 'loops' due to the anchored 'train' segments. The higher mobility of the PS chains indeed resulted in perpendicular segregation with one of the species enriched at the surface. This layered segregation resulted in the 'smooth' morphology after toluene treatment, while after MEK treatment, the restricted mobility of 'loops' prevented layer segregation of PGMA at the surface. This resulted in the two species self-assembling laterally into well-defined two-dimensional structures corresponding to the 'ripple' morphology. Contact

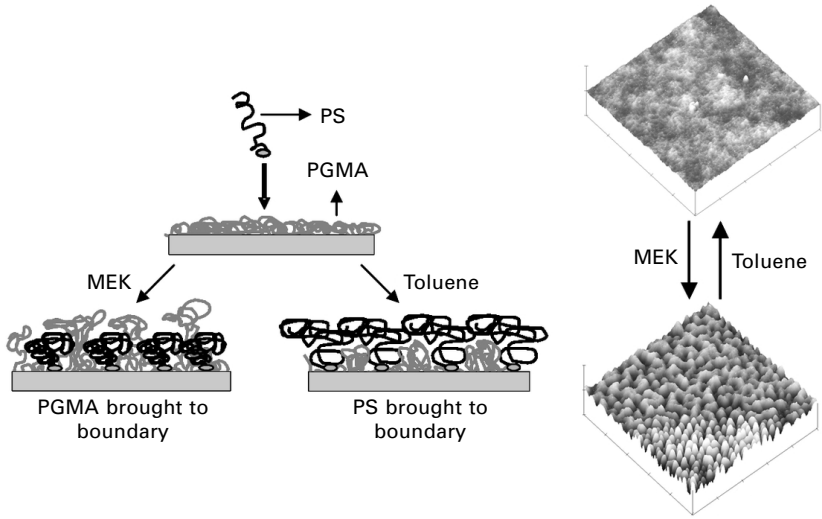

17.10 Left: Depiction of switchability of UPB system consisting of end-grafted PS and PGMA anchoring layer. Right: $1 \times 1\,\mu m^2$ AFM topography images of PS layers grafted to 3 nm PGMA after treatment with toluene and MEK. PS molecular weight: 672 000 g/mol. Vertical scale: 10 nm.

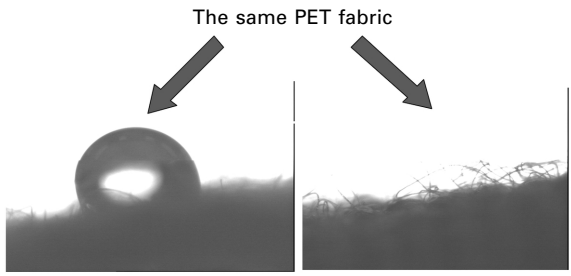

17.11 Wettability of PET fabrics covered with switchable UPB after treatment with different solvents. Left: treated with toluene. Right: treated with MEK.

angle measurements after solvent treatments indicated that the highest molecular weight PS (M_n = 672 000 g/mol) showed maximum switching (approx. 20°).

Using PGMA as an anchoring interlayer a switchable polymer nanolayer on the surface of PET textile material has been synthesized. The PET fabric changed the surface properties after being treated with different solvents (Fig. 17.11). When the fabric was exposed to toluene, it became hydrophobic and water did not penetrate the material. Conversely, water penetrated throughout the textile materials, if they were exposed to MEK. The wettability changes were reversible.

17.6 Synthesis of ultrahydrophobic materials

Water and soil repellency has been one of the major targets for fiber and textile scientists and manufacturers for centuries. Combinations of new materials for fiber production with a variety of surface treatments have been developed to reach the condition of limited wettability. Nevertheless, additional efforts has been needed to create fiber and textile materials with ideal repelling properties. Nature has already developed an elegant approach that combines chemistry and physics to create super-repellent surfaces.[55, 56] Lotus leaves are unusually water repellent and keep themselves spotless, since countless miniature protrusions, coated with a water-repellent hydrophobic substance, cover their surface. Water cannot spread out on the leaves and it rolls around as droplets, removing grime and soil as it moves.

The lotus effect is based on the surface roughness caused by different microstructures combined with hydrophobic properties of the wax covering the leaf surface.[55] The surface roughness is the key prerequisite for the lotus effect. Owing to the rough surface the wettability of the lotus leaves is decreased and the contact area for dirt particles is reduced.

A surface with both receding and advanced water contact angles above 150° is considered to be an ultrahydrophobic (or superhydrophobic) boundary.[57–59] The common way for enhancing the hydrophobicity is to lower the surface energy. However, even materials with the lowest surface energy (6.7 mJ/m^2 for a surface with regularly aligned closest-hexagonal-packed —CF_3 groups) gives a water contact angle of only around 120°. In fact, surfaces with water contact angle of more than 150° may be developed only by introducing proper roughness on material boundaries having low surface energy.

Classical works of Wenzel[60] and Cassie and Baxter[61] established that roughness as well as surface energy are the factors that determine wettability. Wenzel proposed a model describing the contact angle θ' at a rough surface:

$$\cos\theta' = r\cos\theta \qquad [17.1]$$

where r is a roughness factor, defined as the ratio of the actual area of a rough surface to the geometric projected area, and θ is the thermodynamic contact angle on a smooth surface of the material. Since r is always larger than unity, the surface roughness enhances both the hydrophilicity of hydrophilic surfaces and the hydrophobicity of hydrophobic ones. Cassie and Baxter proposed an equation describing the contact angle θ' at a surface composed of solid and air, assuming the water contact angle for air to be 180°:

$$\cos\theta' = f_1\cos\theta - f_2 \qquad [17.2]$$

where f_1 is the fraction of fluid area in contact with the material, and f_2 is the fraction of the fluid area in contact with air. The equation can be used for

hydrophobic surfaces that trap air in the hollows of the rough surface. It is possible to reach a transition from the Wenzel to the Cassie/Baxter regime (when the hysteresis is minute), if an optimum roughness is introduced to a hydrophobic substrate.[62] These optimized surface structures can trap air and exhibit ultrahydrophobic properties necessary to achieve the lotus effect.

17.6.1 Fabrication of ultrahydrophobic textile materials

For the fabrication of the lotus fibers two major requirements must be fulfilled: (1) the fibers need to have low surface energy and (2) the extended degree of roughness should be created. One of the methods to synthesize the rough and hydrophobic coating for fibers is utilization of a combination of a surface-attached polymer layer and nanoparticles. The surface layer consisting of a low surface energy polymer will bring hydrophobicity to the fiber surface whereas nanoparticles will create necessary topography.

The highly hydrophobic PET fabric was obtained by a combination of PS (low surface energy component) and silver nanoparticles (roughness initiation component). The desired ultrahydrophobic fabric was produced using a multi-step grafting approach. To begin with, a polyester fabric was rinsed in multiple solvents to remove contaminants. After cleaning and drying at ambient conditions the textile material substrate was subjected to plasma discharge and rinsed in tetrahydrofuran (THF) to remove low molecular weight remnants formed due to the chain scission process. Next, the fabric was dip coated with a 70/30 PGMA/PVP mixed solution in MEK. The modified substrate was annealed at 110 °C for 10 min to aid self-cross-linking of the epoxy groups of PGMA. (Cross-linking of PGMA stabilizes the microstructure of the blend.) The annealed substrate was treated with ethanol (a good solvent for PVP) to ensure the presence of PVP on the surface. The fabric was then exposed to a suspension of silver nanoparticles (110–130 nm in diameter) in deionized water overnight. The silver nanoparticle adsorbed surface was dip coated with a second layer of PGMA. This second layer entraps silver particles in a cage between the first PGMA/PVP layer and the PGMA layer. This sandwich layer is robust, since its integrity is maintained by the cross-linked epoxy functionalities. Carboxy terminated PS was grafted to the unreacted epoxy functionalities of the top layer at 150 °C. Unreacted PS was removed by multiple rinsing in toluene.

AFM study (images are not shown) demonstrated that PGMA/PVP blend (after treatment in ethanol) showed a typical dispersed morphology characteristic for the 70/30 immiscible polymer blend. The irregular PVP islands successfully immobilized particles (after overnight exposure to a suspension of silver nanoparticles in deionized water) due to the affinity of pyridyl groups to silver through the metal–ligand interactions of the nitrogen atoms. Varying the amount of PVP in the blend can regulate the density of

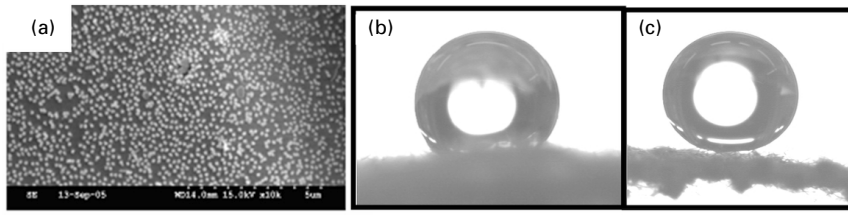

17.12 (a) Silver nanoparticles of size greater than 105 nm adsorbed on PET fiber surface. Magnification ×10 000. Static water contact angle on (b) control sample grafted with PS (no silver) and (c) ultrahydrophobic fabric.

silver nanoparticles adsorbed. The multilayered PS/PGMA/silver/PVP/PGMA system showed excellent mechanical integrity. The particles did not detach at high temperature (during PS grafting) or in toluene under ultrasonic treatment. Scanning electron microscope images of the polyester fabric surface after the modification are illustrated in Fig. 17.12a.

A typical static contact angle analysis was performed on polyester fabric modified with the 'silver/PS' approach and on a control fabric modified with only PS (no silver). The contact angle of the fabric increased from 113° ± 4° (Fig. 17.12b) for control surface to 157° ± 3° for PS/silver multilayer system (Fig. 17.12c). The increase in contact angle was due to the partial contact of water with PS and entrapped air between silver nanoparticles. This synergistic effect of the hydrophobicity of PS and the roughness caused by silver nanoparticles indeed resulted in a contact angle beyond the superhydrophobic boundary.

17.7 Conclusions

In this chapter, a series of recent results in surface modification of various surfaces employing the macromolecular anchoring layer approach was overviewed. It was demonstrated that the approach could be used as a virtually universal method for grafting of functional polymer brushes. The properties of the brushes can be controlled by polymer nature, structural and morphological factors, and external stimuli. The polymer grafting technique developed can be readily applied to surface modification of fibers and textiles, leading to generation of hydrophobic, hydrophilic and switchable fibrous materials.

17.8 Acknowledgments

The research presented has been supported by the National Science Foundation CTS-0456550 and DMR-0602528 grants, ERC Program of National Science Foundation under Award Number EEC-9731680, and Grants M01-CL03,

C05-CL01 and C04-CL06 from the Department of Commerce through the National Textile Center. The author would like to acknowledge present and former members of his research group: Viktor Klep, K. Swaminatha Iyer, Bogdan Zdyrko, Yong Liu, John Draper, Karthik Ramaratnam, and Oleksandr Burtovyy, who conducted most of the research presented. The author also acknowledges the participation of Professors P. J. Brown (Clemson University), G. Chumanov (Clemson University), S. Minko (Clarkson University) and M. Stamm (Institute for Polymer Research Dresden, Germany) and their research groups in the work outlined above.

17.9 References

1. Jagur-Grodzinski, J., *Heterogeneous Modification of Polymers: Matrix and surface reactions*, John Wiley & Sons, Chichester, 1997.
2. Uyama, Y., Kato, K., Ikada, Y., *Adv. in Polym. Sci.* 1998, **137**, p. 1.
3. Alexander, S., *J. Phys. (Paris)* 1977, **38**, 983.
4. de Gennes, P.-J., *Macromolecules* 1980, **13**, 1069.
5. Zhao, B., Brittain W. J., *Prog. Polym. Sci.* 2000, **25**, 677.
6. Laub, C. F., Koberstein, J. T., *Macromolecules* 1994, **27**, 5016.
7. Luzinov, I., Iyer, K. L. S., Klep, V., and Zdyrko, B., US patent 7,026,014 B2, 2006.
8. Husseman, M., Malmstrom, E. E., McNamara, M., Mate, M., Mecerreyes, D., Benoit, D. G., Hedrick, J. L., Mansky, P., Huang, E., Russell, T. P., Hawker, C. J., *Macromolecules* 1999, **32**, 1424.
9. Jones, D. M., Brown, A. A., Huck, W. T. S., *Langmuir* 2002, **18**, 1265.
10. Jones, R. A. L., Lehnert, R. J., Schonerr, H., Vancso, J., *Polymer* 1999, **40**, 525.
11. Luzinov, I., Julthongpiput, D., Malz, H., Pionteck, J., Tsukruk, V. V., *Macromolecules* 2000, **33**, 1043.
12. Kong, X., Kawai T., Abe, J., Iyoda, T. *Macromolecules* 2001, **34**, 1837.
13. Köthe, M., Müller, M., Simon, F., Komber, H., Jacobasch, H.-J., Adler, H.-J., *Colloids and Surfaces* 1999, **154**, 75.
14. Klep, V., Luzinov, I., *Polymer Preprints* 2002, **43**(2), 164.
15. Iyer, K. S., Klep, V., Luzinov, I., *Polymer Preprints* 2002, **43**(1), 455.
16. Liu, Y., Klep, V., Luzinov, I., *Polymer Preprints* 2003, **44**(1), 564.
17. Fleer, G. J., Cohen Stuart, M. A., Scheutjens J. M. H. M., Cosgrove, T., Vincent, B., *Polymers at Interfaces*, Chapman & Hall, New York, 1993.
18. Iyer, K. S., Zdyrko, B., Malz, H., Pionteck, J., Luzinov, I., *Macromolecules* 2003, **36**, 6519.
19. Zdyrko, B., Klep, V., Luzinov, I., *Langmuir* 2003, **19**, 10179.
20. Klep, V., Zdyrko, B., Liu, Y., Luzinov, I., in '*Polymer Brushes*', Advincula, Brittain, Caster, Ruhe editors, Wiley-VCH Verlag GmbH& Co., Weinheim, 2004, p. 69.
21. Liu, Y., Klep, V., Zdyrko, B., Luzinov, I., *Langmuir* 2004, **20**(16), 6710.
22. Zdyrko, B., Varshney, S. K., Luzinov, I., *Langmuir* 2004, **20**, 6727.
23. Jordan, R., Ulman, A., Kang, J. F., Rafailovich, M. H., Sokolov, J., *J. Am. Chem. Soc.* 1999, **121**, 1016.
24. Advincula, R., Zhou, Q., Park, M., Wang, S., Mays, J., Sakellariou, G., Pispas, S., Hadjichristidis, N., *Langmuir* 2002, **18**, 8672.
25. Zhao, B., Brittain, W. J., *Macromolecules* 2000, **33**, 342.

26. Jordan, R., West, N., Ulman, A., Chou, Y. M., Nuyken, O., *Macromolecules* 2001, **34** 1606.
27. Husseman, M., Malmstrom, E. E., McNamara, M., Mate, M., Mecerreyes, D., Benoit, D. G., Hedrick, J. L., Mansky, P., Huang, E., Russell, T. P., Hawker, C. J., *Macromolecules* 1999, **32**, 1424.
28. Matyjaszewski, K., Miller, P. J., Shukla, N., Immaraporn, B., Gelman, A., Luokala, B. B., Siclovan, T. M., Kickelbick, G., Vallant, T., Hoffmann, H., Pakula, T., *Macromolecules* 1999, **32**, 8716.
29. Luzinov, I., Minko, S., Senkovsky, V., Voronov, A., Hild, S., Marti, O., Wilke, W., *Macromolecules*, 1998, **31**, 3945.
30. Prucker, O., Rühe, J., *Langmuir* 1998, **14**, 6893.
31. Liu, Y., Klep, V., Zdyrko, B., Luzinov, I., *Langmuir* 2005, **21**, 11806.
32. Kim, J.-B., Bruening, M. L., Baker, G. L., *J. Am. Chem. Soc.* 2000, **122**, 7616.
33. Shah, R. R., Merreceyes, D., Husemann, M., Rees, I., Abbott, N. L., Hawker, C. J., Hedrick, J. L., *Macromolecules* 2000, **33**, 597.
34. Matyjasewski, K., *in Controlled Radical Polymerization 1998*; ACS Symposium Series No. 685, ACS, Washington, DC, Chapter 16, 258.
35. Jeyaprakash, J. D., Samuel, S., Dhamodharan, R., Rühe, J., *Macromol. Rapid. Commun.* 2002, **23**, 277.
36. Karim, A., Tsukruk, V. V., Douglas, J. F., Satija, S. K., Fetters, L. J., Reneker, D. H., Foster, M. D., *J. Phys. II France* 1995, **5**, 1441.
37. Jones, R. A. L., Lehnert, R. J., Schonerr, H., Vancso, J., *Polymer* 1999, **40**, 525.
38. Auroy, P., Auvray, L., Leger, L., *Macromolecules* 1991, **24**, 5158.
39. Jordan, R., Ulman, A., Kang, J. F., Rafailovich, M. H., Sokolov, J. S., *J. Am. Chem. Soc.* 1999, **121**, 1016.
40. Clarke, C. J., Jones, R. A. L., Clough, A. S., *Polymer* 1996, **37**, 3813.
41. Clarke, C. J., *Polymer* 1996, **37**, 4747.
42. Iyer, K. S, Luzinov, I. *Macromolecules* 2004, **37**, 9538.
43. Wool, R. P., *Polymer Interfaces: Structure and strength*, Hunser Publishers, Munich, 1995, p. 102.
44. Anastasidis, S., Retsos, H., Pispas, S., Hadjichristidis, N., Neophytides, S., *Macromolecules* 2003, **36**, 1994.
45. Russel, T. P., *Science* 2002, **297**, 964.
46. Lahann, J., Mitragotri, S., Tran, T.-N., Kaldo, H., Sundaram, J., Chol, I. S., Hoffer, S., Somorjai, G. A., Langer, R., *Science* 2003, **299**, 371.
47. Zhao, B., Brittain, W. J., *Macromolecules*, 2000, **33**, 8813.
48. Minko, S., Patil, S., Datsyuk, V., Simon, F., Eichhorn K.-J., Motornov, M., Usov, D., Tokarev, I., Stamm, M., *Langmuir*, 2002, **18**, 289.
49. Minko, S., Usov, D., Goreshnik, E., Stamm, M., *Macromol. Rapid Commun.* 2001, **22**, 206.
50. Sidorenko, A., Minko, S., Schenk-Meuser, K., Duschner, H., Stamm, M., *Langmuir* 1999, **15**, 8349.
51. Luzinov, I., Minko, S., Tsukruk, V., *Prog. Polym Sci*., 2004, **29**(7), 635.
52. Draper, J., Luzinov, I., Minko, S., Tokarev, I., Stamm, M., *Langmuir* 2004, **20**, 4064.
53. Klep, V., Minko, S., Luzinov, I., *Polymeric Mater. Sci. Eng.* 2003, **89**, 248.
54. Iyer, K. S, Luzinov, I., *in 'Responsive Polymer Materials: Designs and applications*', Sergiy Minko editor, Blackwell Publishing, Ames, 2006, p. 101.
55. Barthlott, W., Neinhuis, C., *Planta* 1997, **202**, 1.
56. Von Baeyer, H. C., *The Sciences* 2000, **January/February**, 12.

57. Miwa, M., Nakajima, A., Fujishima, A., Hashimoto, K., Watanabe, T., *Langmuir* 2000, **16**, 5754.
58. Youngblood, J. P., McCarthy, T. J., *Macromolecules* 1999, **32**, 6800.
59. Quere, D., *Nature Mater.* 2002, **1**, 14.
60. Wenzel, R. N., *Ind. Eng. Chem.* 1936, **28**, 988.
61. Cassie, A. B. D., Baxter, S., *Trans. Faraday Soc.* 1944, **3**, 16.
62. Nakajima, A., Hashimoto, K., Watanabe, T., *Chem. Monthly* 2001, **132**, 31.

18

Hybrid polymer nanolayers for surface modification of fibers

S. MINKO and M. MOTORNOV,
Clarkson University, USA

18.1 Introduction: smart textiles via thin hybrid films

A combination of several ingredients in the same hybrid material is useful in achieving a number of desirable properties, sometimes contra-properties. Very often we would like to switch between different properties of the material depending on the situation. Such behavior will be valuable for textiles, especially for cloth. Depending on environmental conditions or the state of our body the textile may change its properties to adapt to the situation in a desired way. These kinds of textiles are and cloth are known as 'smart textiles/cloth'. The term 'smart textile' refers to two different major functions: (1) responsive textiles that change their physical/chemical properties upon external stimuli and (2) 'information/communication textiles' with built-in sensors that monitor the human body and environmental conditions and provide, send and exchange information. This chapter deals with the first type. However, it is noteworthy that the smart textile will combine both kinds of function and a suit of the future will use the information and responsive functions to demonstrate a smart response regulated by a computer chip.

Switching of physical and chemical behavior of smart textiles is needed to regulate the temperature of the body and the humidity of the skin surface to evacuate excessive perspiration, to protect the skin from irradiation, aggressive chemicals and microbes (including chemical and biological threats), and to protect the cloth from becoming contaminated with dust and stains of foods, beverages and oil. At the same time the textile should be stable, resistant to washing/cleaning, demonstrate good feel and be attractive. That is a very complex task and doubtless such a textile will have a complex structure. In this case *hybrid material* is a key word. The use of an appropriate design of hierarchically arranged functional elements which are capable of rearranging upon external stimuli/signals is the way to the solution of this complex task. All levels of the organization in textile materials should be considered: structure of fibers, yarns, woven fabrics and their coatings. This chapter focuses on

one of the structural elements of the textile: thin hybrid coatings. Although thin coatings cannot perform all the above functions of the smart textiles, the responsive coating is a very important component of complex smart materials to regulate wetting, adhesion and permeability.

18.2 Mechanisms of responsive behavior in thin polymer films

Materials respond to external stimuli via various mechanisms.[1] For example if we set a match to a thin organic film the film will be burned out immediately. This kind of response appears uninteresting. However, if the film contains iodine isotopes which are captured in the smoke and reach a radioactivity detector, this mechanism can be used to activate a fire alarm. Thus, a definition of responsiveness depends on the type of response being produced. Here we consider responsiveness as an ability to reverse and adjust the changes of textile properties which help to regulate transport of aqueous solutions, dispersions and emulsions (of various origins) through the textile materials. We consider the application of thin polymer films (typically from 5 to 100 nm thick films) for such a regulation as a robust approach exploring interfacial interactions. Thin polymer films could switch surface composition upon external stimuli.[2] Consequently, all relevant properties of the thin film such as wetting, adhesion, adsorption and reactivity will be switched at the same time. In this way a range of very important functions of textiles (water permeability, self-cleaning, stain resistance, antimicrobial properties) can be regulated and adjusted.

18.2.1 Responsiveness of polymer chains to their environment

Responsiveness of thin polymer films is based on a phase segregation mechanism.[2] It can be either intramolecular segregation of homopolymers and copolymers with a complex architecture when different segments of blocks are incompatible and segregate to avoid unfavorable interactions, or intermolecular segregation when two or more dissimilar polymers segregate to microscopic or macroscopic phases. The phase segregation in thin films can be regulated by their environment represented in terms of a solvent quality change and confinement effects of the interfaces. For example, two samples of a dry and a wet thin film can be considered as the materials introduced in two different environmental conditions created by two different solvents: air for the dry sample (a very poor solvent) and water for the wet sample. A change of pH or salt concentration in the aqueous solution which wets the film may affect solubility of polymers in water. Interfaces (polymer–substrate, polymer–air or polymer–water) may greatly alter the properties of the thin

polymer films. In a typical example one of the polymers (or polymer segments) preferentially adsorbs at the interface. Changes of the film environment may change polymer adsorption at the interface. Hydrophilic segments will adsorb at the polymer film–water interface, while hydrophobic segments tend to adsorb at the polymer film–dry air interface. Humidity may also affect the adsorption. The driving force for the change in the phase segregation is the change in balance between polymer–polymer and polymer–environment interactions due to the changes in the thin film environment.

Polymer chains are very sensitive to their environment. This can be illustrated by conformational transition of single poly(2-vinylpyridine) (P2VP) chain *vs*. pH of aqueous solutions studied using *in situ* atomic force microscopy (AFM) (Fig. 18.1).[3] P2VP is a weak polyelectrolyte, thus the degree of ionization depends on pH. At low pH values, (pH < 3) P2VP chains are highly protonated and possess an extended coil conformation (Fig. 18.1a) due to electrostatic repulsion of charged segments. An increase of pH value close to pH 4 results in the coil-to-globule phase transition when the P2VP chains form compact conformations (Fig. 18.1c). The ionization degree drops

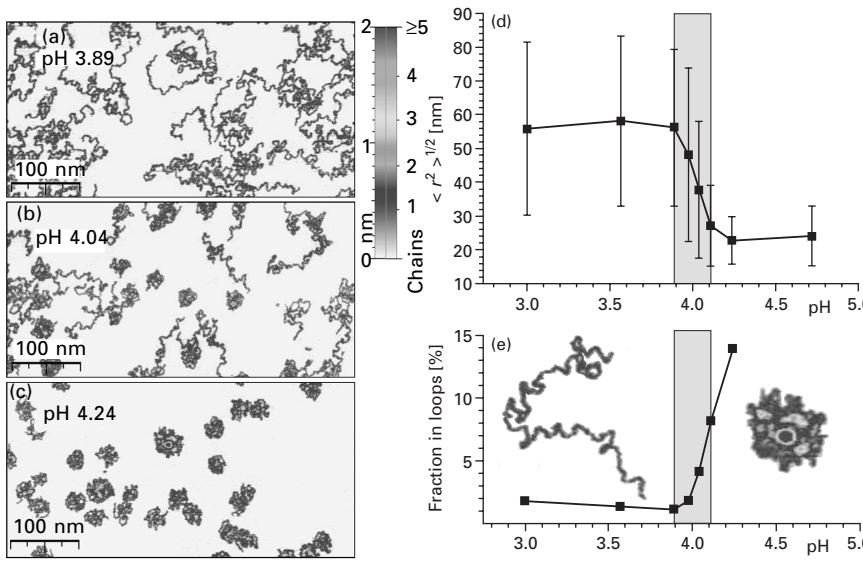

18.1 AFM-visualized conformations of adsorbed P2VP molecules: (a) pH 3.89, extended coils; (b) pH 4.04, intermediate state; (c) pH 4.24, compact coils. *Z*-scale bar shows a number of superposed chains assuming the height increment of 0.4 nm. (d) Directly measured values of root mean square (rms) end-to-end distance of P2VP single molecules adsorbed on mica surface versus pH. (e) Fraction of monomer units in loops versus pH. The gray zone in (d) and (e) is a pH range of the conformation transition. Reprinted with permission from Ref. 3. Copyright 2003 American Chemical Society.

and the hydrophobic effect pushes the hydrophobic backbone to attain a compact conformation. The transition is very sharp. The characteristic size of the molecules (gyration radius) changes by a factor of two (Fig. 18.1d).

In thin films polymer chains are highly concentrated. Assemblies of polymer chains respond cooperatively to their environment and form segregated domains. The sizes of the domains depend on interfacial tension and on the effects of constraints (for example, for chains grafted to a solid substrate, the polymer segments cannot move from the grafting point for a distance larger than the end-to-end distance of the polymer chain). Below we consider how the phase segregation mechanisms in thin polymer films can be explored for the fabrication of responsive materials.

18.2.2 Polymer brushes

The systematic study of the surface restructuring of polymer materials began two decades ago.[4–7] It was shown that the surfaces of polymer materials can rearrange and adapt their interfacial composition to approach a minimal interfacial tension. For example, polymers with specially tailored architecture (end functional groups, copolymers, segmented polymers, block–copolymers)[8–13] expose to the interface their polar fragments in contact with water, and non-polar fragments in air. For bulk polymers the restructuring is a slow process (from minutes to hours). Much faster reorganization can be obtained for thin polymer films. Solvents soak into or evaporate from monolayers of polymer chains (of moderate molecular weight) very quickly (time scale of seconds). However, thin polymer films are not stable. They typically de-wet substrates and can be easily and rapidly dissolved. The solution to the problem was approached by grafting polymers to the substrate surface. The best result was found with polymer brushes. Polymer brushes are monolayers of end-tethered polymer chains (Fig. 18.2), in which the distance between grafting points is smaller than the chain end-to-end distance. That causes polymer chains to stretch away from the grafting surface due to the excluded volume effect. The stretching degree is balanced by entropic

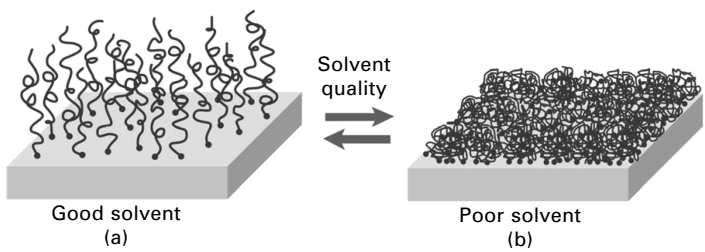

18.2 Homopolymer brush constituted of end-tethered chains stretched in good solvent (a), and collapsed in poor solvent (b).

elasticity of the polymer coils.[14] Polymer brushes are stable thin films because they are covalently (sometimes electrostatic or hydrophobic effects are used for the grafting) bound to the substrate. Brushes respond to their environment rapidly via conformational changes.

Polymer chains of different architectures were used to design polymer brushes.[15,16] Polymer brushes made up of homopolymer chains (homopolymer brushes) respond to their environment by expansion–contraction in good and poor solvents, respectively. At moderate grafting densities, homopolymer brushes segregate into spherical domains in a poor solvent, which allows them to minimize unfavorable interactions with the solvent. Thus, the transition between a good and a poor solvent is the driving force of the brush responsiveness. Polyelectrolyte homopolymer brushes respond to electrostatic interactions (Fig. 18.3)[17] in a similar way to that of bulk polyelectrolyte chains. (This difference is caused by the tethered chain architecture and a high local concentration of ionizable groups in polyelectrolyte brushes which affects the local ionization degree.[18])

Although homopolymer brushes demonstrate very pronounced responsiveness in terms of switching their properties between good and poor interactions with their environment, the composition of the interface is not changed qualitatively. In other words, independent of the environment, the polymer exposed to the interface remains unchanged in its chemical nature. Thus, the switching of the thin film properties is limited by the constitution of the given polymer.

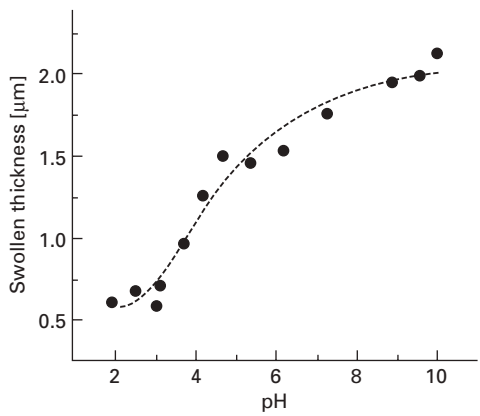

18.3 Swollen thickness of a 20 nm (dry thickness) poly(methacrylic acid) (PMAA) brush on a La-prism as a function of the pH of solution ('salt-free'). The brush was prepared by polymerization of methacrylic acid (bulk; t = 1.5 h; T = 60 °C). After the polymerization the PMAA brush was extracted with methanol and water for 15 h. The solid line is a guide to the eye. Reprinted with permission from Ref. 17. Copyright 2002, American Institute of Physics.

The largest response can be obtained if two very different polymers or polymers and nanoparticles are combined in the same hybrid thin film. In this case, the difference in the response of two different species may result in a very strong alternation of the thin film properties because either one or another polymers could be exposed to the top of the thin film. We discuss the mechanisms of responsiveness of such systems below.

18.2.3 Mixed polymer brushes

In *mixed brushes* (Fig. 18.4)[19] two or more different polymers are grafted to the same substrate. The mechanism of responsiveness of the mixed brushes originates from the dependence of the incompatibility of two polymers on their environment. Polymers in the mixed brush segregate into nanoscopic phases. The size of the nanophase is related to the size of polymer molecules. In a nonselective solvent, the phase segregation is a lateral segregation when unlike polymers form spherical (dimples) or elongated (lamellar-like or ripples) clusters tethered to the substrate. Both of the polymers are exposed on the top of the brush (Fig. 18.4a). If selectivity of a solvent (solvent dissolves one polymer better than another polymer) increases, the mixed brush structure tends to form a layered structure (Fig. 18.4b) and the resulting morphology is a combination of lateral and layered segregation mechanisms.[20] In selective

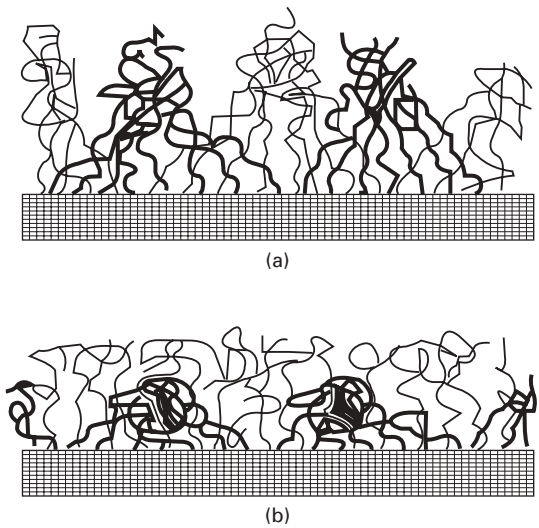

18.4 Schematic illustration of two possible morphologies of mixed brush irreversibly grafted to solid substrates (cross-section of the layer): lamellar morphology in a nonselective solvent (a); cluster morphology in a poor solvent for the black chains (b). Reprinted with permission from Ref.19. Copyright 2003 American Chemical Society.

solvents one polymer preferentially segregates to the top of the brush, while another polymer forms clusters segregated to the grafting surface. The most important difference of the mixed brush response compared with the homopolymer brush is that not only the transitions between stretched and collapsed conformations but also a change of the composition profile takes place. In other words, the surface composition of the brush is switched by changes in its environment (Fig. 18.5).

The responsiveness of *mixed polyelectrolyte brushes* is modified by electrostatic interactions which can be used to regulate the mechanism of the phase segregation. *Weak mixed polyelectrolyte brushes* are of special interest since the electrostatic interactions can be affected by pH and ionic strength of aqueous environment and the surface composition of the mixed polyelectrolyte brush can be switched just by a change of external pH.[21–23]

Typically, two or more unlike polymers are grafted *randomly* to the substrate in mixed polymer brushes. A special case is represented by *Y-shaped* amphiphilic brushes which combine two dissimilar polymer chains attached to a single focal point or a leg.[24, 25] Although the responsive behavior of

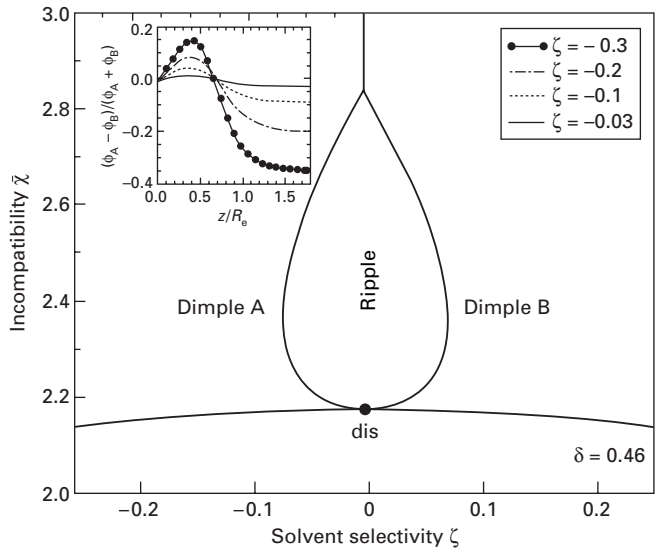

18.5 Phase diagram of a mixed brush as calculated in self-consistent field theory as a function of solvent selectivity. In addition to a laterally homogeneous (disordered) phase (below the line marked with dis), the phase diagram comprises a ripple phase (see Fig. 18.4a) and dimples (see Fig. 18.4b). The inset presents the laterally averaged composition profile expressed by fraction of monomers A(ψ_A) and B(ψ_b) vs. extension of the brush (Z) normalized by the Gaussion chains end-to-end distance (R_e); δ-is the degree of chain stretching in the brush. Reprinted with permission from Ref. 20. Copyright 2002, American Physical Society.

mixed and Y-shaped brushes can be explained by the same mechanism, the difference between randomly mixed polymer brushes and Y-shaped brushes is in the polymer distribution on the surface. The Y-shaped brushes could form more regular structures because the grafting of two different polymers is always coupled due to the Y-shaped architecture.

18.2.4 Block–copolymer brushes

In *block–copolymer brushes* (Fig. 18.6)[26] two or more chemically different polymers (typically two or three different blocks) constitute a polymer brush with block–copolymer architecture. Responsiveness of these brushes is determined by phase segregation of unlike polymer blocks; however, the structure of the brush layer depends on whether the AB block copolymer is tethered by the more (A) or the less (B) soluble block.[27, 28] In poor solvents

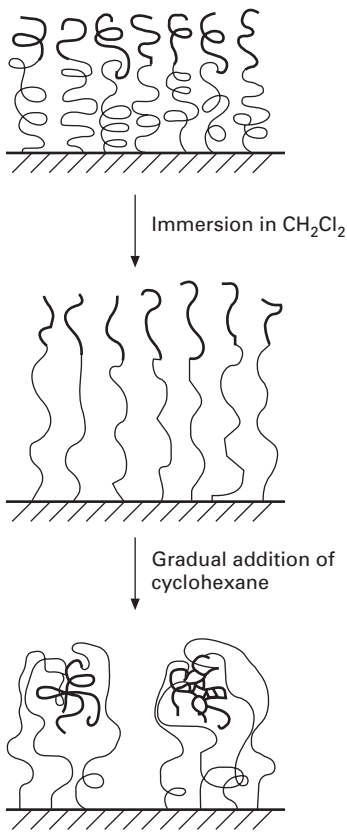

18.6 Morphology of the tethered poly(styrene–block–methylmethacrylate) brush. Reprinted with permission from Ref. 30. Copyright 2000 American Chemical Society.

the brushes grafted by the B blocks form dumbbell-like micelles with the B-polymer segregated to the grafting surface and the A-polymer micelles on the top. The brushes grafted by the A blocks form B-polymer micelles shielded by A-polymers. If solvent selectivity is improved for the A-polymers, the dumbbell-like micelles of the B-grafted brushes are transformed to structures that are similar to the mixed brushes in selective solvents. The B-polymers form pinned micelles which are congregated at the grafting surface. The micelles are shielded by the brush of the A-polymers. The block–copolymer brushes have a complex phase diagram affected by the ratio between the molecular weights of the A and B blocks and the grafting density.[29–32]

18.3 Polymer–polymer hybrid layers

Mixed and block–copolymer brushes are polymer–polymer hybrid thin films tethered to solid substrates. The well-defined architecture of end-tethered chains in polymer brushes allows for a deep study of the mechanisms of the brushes' response to their environment. Nevertheless, for practical applications a very similar mechanism can be approached using polymer layers when a polymer can be grafted by end groups, and also by side functional groups. The polymer chains randomly grafted by side functional groups will form loops and tails exposed to the solvent. Thus, two or more unlike polymers grafted by side chains will form polymer–polymer hybrid thin films with properties very similar to those for the mixed brushes. Practically, many combinations of polymer layer architectures could be used to design responsive hybrid layers (end tethers polymers A and grafted via side functional groups polymers B, two- and tri-block copolymers grafted via side functional groups of one of the blocks, etc.). Although many versions exist, in this chapter we will focus on the brush-like architecture which gives us a clear illustration of the responsiveness.

There are two main approaches employed for synthesizing mixed polymer brushes: 'grafting to'[33] and 'grafting from'.[34] The fabrication of binary mixed brushes consists of two repeating steps of the grafting procedure; the grafting of the first polymer is followed by the grafting of the second polymer. The 'grafting to' approach to synthesize binary polymer brushes is based on subsequent grafting of end-functionalized polymers to a solid substrate. Before grafting, a surface treatment is usually applied to introduce appropriate functional groups onto the substrate surface. A plasma treatment was used to introduce amino or hydroxyl functional groups on polymeric substrates[35, 36] or ω-functional silanes to introduce epoxy, amino and hydroxyl functional groups onto surfaces of inorganic oxides.[33, 34] Polished Si-wafers are frequently used to study the grafting polymers using ellipsometry. As an example, we describe here the grafting of a P2VP and polystyrene (PS) mixed brush. The

first step consists of chemisorption of 3-glycidoxypropyltrimethoxysilane (GPS) on cleaned Si-wafer (Si-wafer is protected by thin 1–2 nm native silica coating), which forms a layer with a very high concentration of epoxy groups on the surface. Its ellipsometric thickness around 0.7–1.1 nm corresponds to 1–1.5 theoretical monolayers of GPS. The second and the third steps consist of the grafting of carboxyl terminated poly(2-vinylpyridine) (P2VP-COOH) and polystyrene (PS-COOH), respectively.

The polymers are grafted from melt. A thin 10–50 nm PS-COOH film is spin-coated on the substrate and the polymer is grafted by annealing the sample at a temperature higher than the glass transition temperature (T_g) of the polymer. The non-grafted polymer is removed by Soxhlet extraction with tetrahydrofuran (THF). Afterwards, a 50 nm thick film of the second polymer P2VP-COOH is spin-coated on top of the PS-COOH brush and grafted upon heating above T_g. The kinetics of grafting of PS-COOH and P2VP-COOH in terms of the ellipsometric thickness of the layer can be estimated by sampling and measuring the thickness of the grafted brush. Most of the polymer is grafted in 2 h; afterwards the grafting slows down, approaching a plateau value in 16–20 h. In this example, the plateau values for homopolymer PS and P2VP brushes are around 7 nm. The grafting kinetics is useful to regulate the mixed brush composition. If we stop grafting PS-COOH as soon as we approach 3.5 nm thickness of the homopolymer brush, then we graft the second polymer P2VP-COOH for 16 h to approach the 7 nm thick mixed brush. Finally, the composition of the mixed brush is 1:1. Typically, the second polymer can be successfully grafted only if the first polymer has much smaller affinity to the solid substrate than the second. In this case the strong affinity of the second polymer to the solid substrate acts as a driving force for chains of the second polymer to penetrate the brush layer formed by the first polymer.

Binary brushes that are synthesized by the 'grafting to' method are macroscopically homogeneous but they exhibit phase segregation on a nanoscopic length scale. The composition of the brush (the amount of each polymer grafted) can be controlled by conditions of the grafting procedure: time, temperature and thickness of the spin-coated films. The drawback of the 'grafting to' procedure is that only a relatively small amount of polymer can be grafted onto the surface, although the number of grafted chains of polymers is much smaller than the number of functional reactive groups present on the surface. Diffusion of polymer chains to the surface is strongly limited by the already grafted polymer chains. The maximal thickness of binary brushes that could be achieved by the 'grafting to' method typically is around 10 nm, depending on molecular mass of the grafted polymers. Nevertheless, this method is very simple and robust. For many practical applications the grafting density achieved by the 'grafting to' method provides very pronounced responsive properties of the thin film.

Mixed polymer brushes of a very high grafting density can be prepared using the 'grafting from' approach by sequential one-after-another grafting of two incompatible polymers. Here we describe an example of the 'grafting from' procedure on the surface of polyamide (PA) plates and on the surface of a PA textile for the synthesis of PS and P2VP mixed brushes. Polyamides as semicrystalline thermoplastics have found numerous applications, particularly for the fabrication of excellent fibers due to their good thermal stability, flexibility and mechanical properties. Surface modification of PA is a widely used approach to regulate properties of fiber reinforced materials, textiles, etc. Responsive properties of a PA surface would extend the application of PA, particularly for cloth and biomedical materials. The aim of this example was to fabricate PA-based materials that change surface characteristics in response to environmental conditions. One of the possible routes to approach this goal comprises the grafting of mixed polymer brushes from a PA surface which can introduce adaptive and switching behavior in different surrounding media.

Here we describe the 'grafting from' PA-6 surfaces via free radical polymerization initiated by the thermal decomposition of an azo initiator (the chloroanhydride derivative of 4,4′-azobis(4-cyanopentanic acid) – abbreviated as ACPC) covalently attached to the PA substrate. To attach the azo initiator to the PA substrate, the PA surface was treated with low-pressure ammonia plasma. NH_3 plasma introduces N-containing functionalities such as amino (—NH_2), imino (—CH═NH), cyano (—C≡N) and other functional groups, and in addition oxygen-containing groups such as amido (—$CONH_2$) and hydroxyl groups due to post-discharge atmospheric oxidation. We used those functional groups to covalently bond the azo initiator to PA surfaces. Each step of the surface modification was controlled with ellipsometry, X-ray photoelectron spectroscopy (XPS), AFM, Fourier transform infrared spectroscopy in attenuated total reflection (FTIR-ATR) and contact angle measurements.

The PA samples were treated with NH_3 plasma for 60 s. The ratio between the number of atoms of oxygen and carbon ([O]:[C]) and nitrogen and carbon ([N]:[C]) in PA-6 calculated from the chemical composition equals 0.167. The surface composition determined from the XPS spectra gives the ratios [O]:[C] = 0.15 and [N]:[C] = 0.14, which is in good agreement with the chemical composition of the substrate. The plasma-treated samples of PA-6 show increased ratios [N]:[C] = 0.19, which prove the introduction of the N-containing functionalities. The azo initiator was covalently bound to the PA surface via the reaction of the amino and hydroxyl groups with ACPC. The reaction is well reproducible. The resulting layer of the initiator is about 2.1 ± 0.3 nm thick (as measured with ellipsometry in the reference experiment on the thin PA film deposited on the Si-wafer). This value corresponds to 5.7 $\times 10^{-6}$ mol/m^2 surface concentration of the initiator and to 0.5 nm average distance between the grafted initiator molecules.

Grafting of PS chains was performed by *in situ* radical polymerization initiated by the thermal decomposition of the azo initiator covalently attached to the PA surface. The amount of the grafted polymer and the residual initiator on the surface was regulated by polymerization time. The ungrafted polymer was washed out by a cold Soxhlet extraction. In the second polymerization step the residual amount of the azo initiator was used to carry out the graft polymerization of 2-vinylpyridine. The grafting of both polymers was proved with FTIR-ATR performed with the PA plates tightly pressed to the surface of the attenuated total reflection prism. The very well-pronounced differences in the spectra of individual polymers at 1400–1750 and 2750–3200 cm^{-1} allowed us to analyze the layer composition at least qualitatively. The characteristic bands of aromatic and aliphatic groups observed for the mixed brushes (obtained by the subtraction of the reference spectrum of the PA substrate from spectrum of the grafted brush) provide evidence for the grafting of PS and P2VP. In the spectra, we identified very pronounced PS bands at 1601 and 1493 cm^{-1} and the characteristic bands of P2VP at 1568 and 1590 cm^{-1}.

Responsive properties of the mixed brushes were investigated using contact angle experiments. The same samples of PA with the grafted PS/P2VP mixed brushes were exposed for 5 min to solvents of different thermodynamic quality for the polymers. After each treatment with a particular solvent the samples were dried in a flow of nitrogen and used for the contact angle investigations. The experiments were repeated several times with each sample to prove the reversibility of the switching of surface properties. In these experiments, we assume that the morphology of the dry film is directly correlated with the structure of the swollen film. The time of switching in a particular solvent is in the order of minutes (contact angle changes in 1–2 min and approaches to equilibrium in 5–10 min), which is much longer than the time to dry the film under nitrogen flux (several seconds). We may assume that we freeze the film morphology during solvent evaporation. At ambient conditions the polymers in the dry film are in a glassy state and the film morphology is stable for a long period of time.

The switching of morphologies upon exposure to different solvents is affected by the phase segregation at the nanoscopic scale as discussed above. The contact angle measurements have shown very pronounced switching of the surface energetic state. For example, if we expose the sample to toluene, the top of the layer is preferentially occupied by PS. In this case the contact angle approaches the value of 90°, while in ethanol and water (pH 3.0) the surface is dominated by P2VP with contact angles of 60° and 35°, respectively. The data clearly show that a top layer of the binary brush switches from the hydrophobic to the hydrophilic energetic state and vice versa upon exposure to selective solvent for one of the polymers.

The contact angles obtained on the mixed brush of 90° and 60° after toluene and ethanol, respectively, correspond to the same values of the contact

angles on the model PS and P2VP single homopolymer brushes, respectively. This fact is evidence that in a selective solvent the top layer of the mixed brush is formed due to the layered (perpendicular) segregation (Fig. 18.4b) and the top is occupied by the favorite polymer. In acidic water P2VP is protonated and charged. This layer is wetted by water much better than neutral P2VP. Wetting in this case is promoted by dissociation of the protonated P2VP below the water drop.

In the cases of nonselective solvents after exposure to chloroform or THF, both polymers are present on the top of the film (contact angle 80°) (Fig. 18.4a). Using the Cassie equation, we calculated that this contact angle corresponded to the 65% PS fraction on the top of the brush when the surface of the brush is constructed from laterally segregated domains of PS and P2VP.

Here we extend the study of the switching behavior on substrates with a complicated texture and present the results of contact angle measurements on the PA textile with the grafted PS/P2VP binary mixed brushes, comparing them with the wetting behavior on the PA plates with the same grafted brush. The fibers of about 200 μm in diameter forming the textile introduce an effect of a composite surface[37] where the drop of water is in contact partially with the surface of PA fibers and partially with air. In this case we observed the much more pronounced switching effect amplified by the surface texture of the PA textile (Fig. 18.7). The exposure of the textile sample to toluene results in the highly hydrophobic properties of the material with an advancing

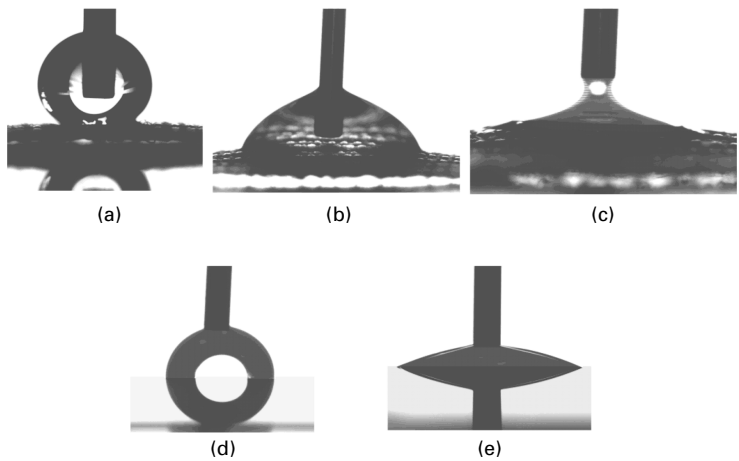

18.7 Video images of drops on substrates with grafted PS-P2VP brush from PA-6 textile: after exposure to toluene, Θ = 150° (a); ethanol, Θ = 50° (b); water, pH 3, wicking regime (c); from PA-6 plates after exposure to toluene, Θ = 90° (d) and water, pH 3, Θ = 20° (e). Reprinted with permission from Ref. 35. Copyright 2003 American Chemical Society.

contact angle of 152°, while upon exposure to ethanol the advancing contact angle is 50°, and after treatment with acidic water the film is fully wetted and water soaks into the textile sample. These pictures demonstrate that, in contrast, the flat PA surface is less hydrophobic (90°) and less hydrophilic (20°) upon exposure to toluene and acidic water, respectively.

Schematically this phenomenon is outlined in Fig. 18.8. The drop of water deposited on the mixed brush coated textile is in contact with the textile fibers and air. Each fiber is a twist of single fibers forming a yarn with a rough surface. Thus, the textile surface has a complicated hierarchical texture. Depending on the bare contact angle, on a flat surface the liquid might fill all the grooves of the rough substrate or might be in contact with the upper part of the relief and air can be trapped below a drop. The wicking criterion is determined as follows:[38]

$$\cos\Theta > \frac{(1-\phi_s)}{(r-\phi_s)}$$

$$\Theta_0 < \Theta \qquad [18.1]$$

where Θ_0 is the bare contact angle of water on a flat surface, ϕ_s is the solid surface fraction assigned with the upper part of the relief (in this case it is a fraction of the total area that is not in contact with the liquid), and r is the ratio between the increased contact area of the rough surface and the corresponding projected area. An example of this regime is shown in Fig. 18.7c.

If the bare contact angle is smaller than 90° but the wicking criterion is not fulfilled, the liquid fills the grooves of the rough surface only below a

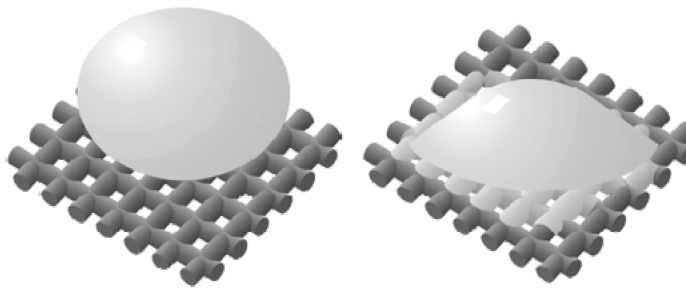

18.8 Schematic representation of a drop of water on PA textile: Θ >90°, Θ = 150°; air is trapped below the drop giving the Cassie regime if the brush was switched in a hydrophobic state (a). Θ <90°, water soaks into the textile sample if the brush was switched in a hydrophilic state (b). Reprinted with permission from Ref. 35. Copyright 2003 American Chemical Society.

droplet contacting with fibers and the contact angle corresponds to Wenzel's regime:[39]

$$\cos\Theta = \frac{r(\gamma_{vs} - \gamma_{ls})}{\gamma} = r\cos\Theta_0 \qquad [18.2]$$

where Θ is the contact angle of water on a rough surface. An example of this regime is shown in Fig. 18.7b.

If the bare contact angle is larger than 90°, air can be trapped below a drop and the liquid is only in contact with the upper part of the relief of the rough surface of fibers, resulting in the Cassie wetting regime given by:[40, 41]

$$\cos\Theta = -1 + \phi_s(1 + \cos\Theta_0) \qquad [18.3]$$

where ϕ_s is the fraction of the upper part of the relief (in this case, that is the fraction of the total area in contact with liquid), which itself depends on Θ_0. An example of this regime is shown in Fig. 18.7a.

Consequently, switching of the mixed brush on the surface of the textile material causes the transition between the Cassie regime (Fig. 18.8a, when the contact angle is larger than 90°) and the wicking regime (Fig. 18.8b, when wetting is characterized by a small contact angle and the wicking criterion is fulfilled). Therefore, the textile material with the grafted mixed brush demonstrated the behavior affected by the combination of two possible approaches to regulate surface wetting: chemical composition and roughness.

18.4 Polymer–particles hybrid layers

Direct grafting mixed or block–copolymer brushes on surfaces of various fibers and textile materials is a slow chemical process which cannot be easily introduced in existing technologies for treatment of fiber and textile surfaces. The situation was substantially improved with the following simple and elegant approach. The mixed or block–copolymer brushes can be grafted on the surface of colloidal particles, for example silica particles. Afterwards, the particles can be deposited on fibers and textiles from colloidal dispersions applying well-developed technologies for deposition of pigments on textile materials. In this approach the responsive particles (or smart particles) are used for the simple and robust modification of polymer surfaces.[42]

Here we describe an example of the fabrication and investigation of smart responsive nanoparticles by grafting block–copolymers. We grafted triblock copolymer of poly(styrene-*b*-2-vinylpyridine-*b*-ethyleneoxide) (P(S-b-2VP-b-EO) to silica particles 200 nm in diameter (Fig. 18.9). The particles were modified by 11-bromoundodeciltrimethoxisilane (BUDTMS), then the block–copolymer was grafted by a quaternization reaction to the particle surface. The grafting of the block–copolymer to the silica nanoparticles was proved by FTIR using the diffuse reflection technique. Very well-pronounced

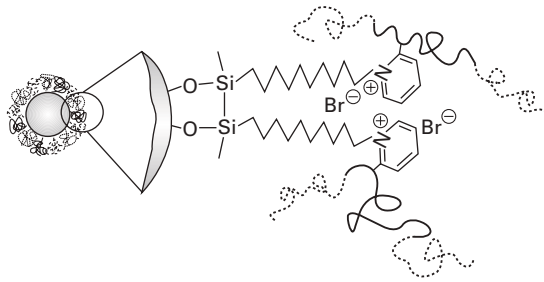

18.9 Tri-block copolymer grafted to the silica particles via a quaternization reaction between pyridine rings of the central P2VP blocks and 11-bromoundodeciltrimethoxisilane on the silica particle.

differences in the spectra of individual blocks of the block–copolymer allowed the analysis of the chemical composition of the smart silica particles. The characteristic bands of aromatic and aliphatic groups observed for the block–copolymer brushes were obtained by subtraction of the spectrum of the particles with chemosorbed BUDTMS from the spectrum of the particles with the grafted block–copolymer. In the spectra, we identified very pronounced PS block bands at 1601 and 1493 cm^{-1}, the characteristic bands of P2VP blocks at 1568 and 1590 cm^{-1}, and the characteristic bands of the PEO block at 1648 and 3378 cm^{-1}, which provided evidence for the grafting of P(S-b-2VP-b-EO). The quantitative analysis of FTIR data was used to estimate the grafted amount and the grafting density of the P(S-b-2VP-b-EO) on the silica surface as 6.7 mg/m^2 and 0.066 nm^{-2}, respectively.

In the next step, the smart particles were deposited on the substrate surface. In a reference experiment we used Si-wafers modified with the BUDTMS (Fig. 18.10). In this case, the smart particles were covalently attached to the Si-wafers via quaternization reaction between P2VP blocks and BUDTMS. However, the particles just physisorbed on Si-wafers or on the surface of PA textiles have demonstrated the same responsive behavior as chemically grafted particles. The data of contact angle measurements on these surfaces demonstrate well-pronounced switching from hydrophobic to hydrophilic wetting behavior (Table 18.1) upon exposure to different solvents. This behavior is similar to the behavior of block–copolymer brushes on a flat surface. However, the range of switching on the particle coated substrate is much larger than on the flat surface owing to the higher roughness of the material.

18.5 Hierarchical assembly of nanostructured hybrid films

The successful approach to smart responsive particles was further transformed into the principle of hierarchical self-assembly in the system when the particle

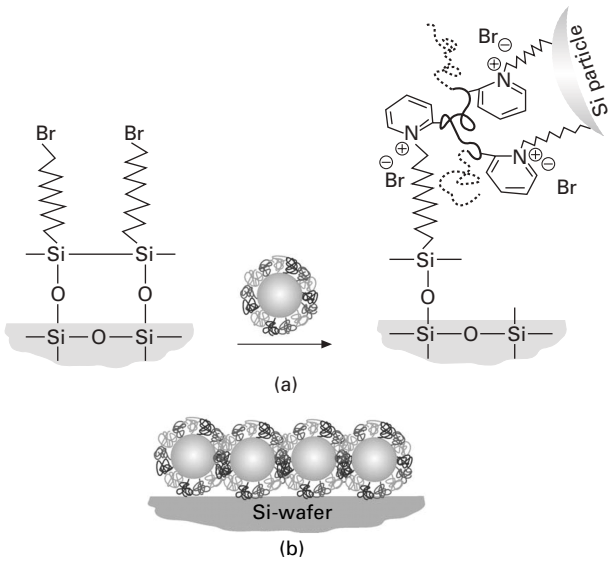

18.10 Schematic representation of grafting silica nanoparticles with tri-block copolymer brushes to the Si-wafer surface (a); a layer of the nanoparticles on Si-wafer (b).

Table 18.1 Wetting of block–copolymer brushes grafted to the nanoparticles on silica wafers

Sample	Contact angles of water (°)				
	Toluene	CH_2Cl_2	Ethanol	Water, pH 7	Water, pH 3
P(S-b-2VP-b-EO)	131	117	57	69	29

core was comparable in size or smaller than the thickness of the grafted mixed brushes. Recently, we reported on a unimolecular spherical mixed brush represented by the $P2VP_7$-PS_7 copolymer, consisting of seven poly(2-vinylpyridine) and seven polystyrene arms emanating from the same core.[43] The core of the unimer is formed by 106 cross-linked divinylbenzene molecules. The PS and P2VP arms (M_w(PS-arm) = 20 000 g/mol and M_w(P2VP-arm) = 57 000 g/mol, where M_w is the weight-average molecular weight) are randomly grafted to the core. The core is highly cross-linked and can be considered to consist of dense particles 3–6 nm in diameter embedded into the shell formed by PS and P2VP arms. The unimolecular spherical mixed brush demonstrates similar principles to that of environment-induced response. In an acidic environment at low concentrations, the copolymer forms unimolecular micelles with the PS segregated to the core and the protonated P2VP shell. Upon exposure to toluene, $P2VP_7$-PS_7 undergoes the inverse intramolecular

segregation: the P2VP arms form a dense core surrounded by the swollen PS shell. We applied this mixed spherical brush for grafting onto flat substrates.[44] The surface of silica substrate was chemically modified with Br-alkyl silane. Then the grafting was performed by a quaternization reaction of P2VP arms with surface Br-alkyl groups. The fabricated surfaces demonstrated an example of hierarchical transitions of the thin film morphology. This complex mechanism was approached using a very simple synthetic route to the responsive material via a one-step grafting procedure in contrast to much more complex procedures reported for the synthesis of mixed brushes.

To investigate the responsive behavior of the star–copolymer (smart particles) grafted layers, the samples were exposed to selective (toluene, ethanol, pH 2 water) and less selective (chloroform) solvents for 10 min. After the exposure to each solvent, the samples were dried and investigated with AFM, XPS and the contact angle method. A comparison can be made between the conformational transitions of single particles in very dilute solutions (where the transitions occur as a single-molecule event without effects of any kind of intermolecular interactions and the solid substrate) with cooperative transition in the dense layer confined by two interfaces and other particles grafted in close proximity to each other. In all solvents, the single unimers possess a core–shell morphology caused by the phase separation of the PS and P2VP arms to avoid unfavorable interactions in the given solvent. The size of the shell increases as solvent selectivity increases. The largest shell was observed upon treatment with pH 2 water where the P2VP arms are strongly stretched because of the electrostatic repulsion. Similar behavior was observed for the grafted monolayers of the particles in selective solvents toluene (for PS) and ethanol or pH 2 water (for P2VP). The PS and P2VP arms in toluene and ethanol, respectively, form nanosize clusters segregated to the unimer cores. That was proven by the XPS and water contact angle data (Table 18.2). Upon exposure to toluene, the contact angle value corresponds to the wetting of PS (90°), which completely occupies the top layer (the lowest fraction of N atoms in the XPS spectra). Upon exposure

Table 18.2 Advancing contact angles and XPS data for the $P2VP_7$-PS_7 star–copolymer layer surface after exposure to different solvents. Reprinted with permission from Ref. 44. Copyright 2005 American Chemical Society

Solvent	Contact angle(°)	Nitrogen, at. % (XPS, 30° angle of incidence)
Toluene	91 ± 1	5.47
Chloroform	78 ± 2	7.61
Ethanol	65 ± 1	9.20
H_2O, pH 2	15 ± 5	–

to ethanol or water, the contact angle value corresponds to the wetting of P2VP (63°) (in the case of acidic water, the contact angle value corresponds to the wetting of protonated P2VP), and the XPS spectra reveal the largest fraction of N atoms. Thus, in the monolayer each grafted single smart particle responds to outside changes via intramolecular phase segregation of PS, and P2VP arms form the first hierarchical level of response.

The cooperative character of the conformational transitions in the densely packed monolayer of smart particles makes up the second level of response (Fig. 18.11). The combination of the smart particles in one layer introduces new kinds of morphology. The core–shell transitions of unimers are transformed into transitions between different phase-segregated morphologies in the grafted monolayer in selective solvents. Clusters of the unfavored polymer are embedded in the layer of extended chains (matrix) of the favored polymer. In other words, the core–shell transitions of unimers are transformed into the interplay between lateral and layered phase segregation. The increase in

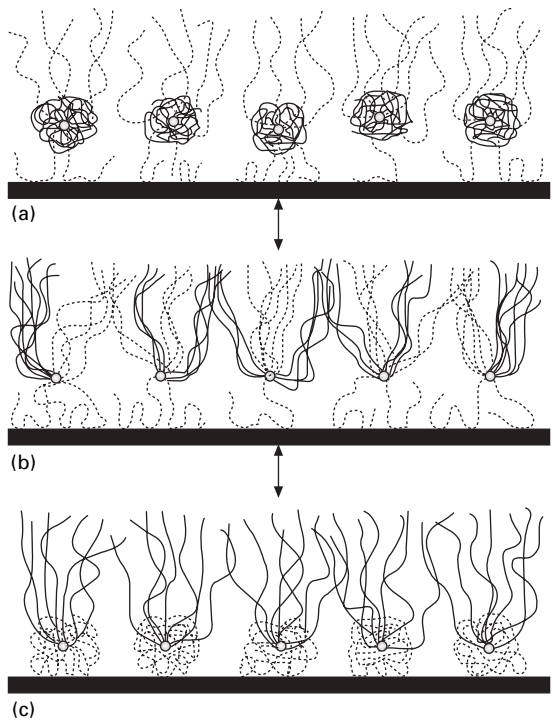

18.11 Schematic representation of the switching behavior of the $P2VP_7$-PS_7 star–copolymer layer chemically grafted to the surface upon exposure to solvents: (a) selective for P2VP (dashed lines); (b) nonselective; and (c) selective for PS (solid lines). Reprinted with permission from Ref. 44. Copyright 2005 American Chemical Society.

solvent selectivity results in an increase in upper layer thickness. However, the $P2VP_7$-PS_7 unimers possess new specific morphology in the grafted monolayer exposed to chloroform, where PS and P2VP arms segregate to different sides of the core. The result of the phase-segregation mechanism appears as a ripple morphology of the layer. Both the P2VP and PS arms are exposed to the top and form alternating stripes. This may be concluded from the AFM image, XPS and contact angle data. Chloroform is slightly selective for P2VP, and this promotes the formation of the ripple structures. The switching between different morphologies is a reversible process. We observed the transitions more than 10 times upon treatment of the sample with different solvents. It is noteworthy that the morphologies of the layer formed by the densely packed 'spherical brushes' are very similar to the morphologies of 'flat' mixed brushes.[7] In both cases, the response is expressed in the form of morphological transitions between the dimple and ripple segregated phases.

18.6 Future trends

Application of thin hybrid polymer monolayers for coating of smart textiles is in its earliest stages. The long initial period involved development of synthetic approaches and study of basic mechanisms of the responsive behavior. Most of these studies were performed using idealized model systems for theory and experiments. Further development of the field will face the problem of switching into an applied stream of research targeting the important properties of textiles, realistic technology, durability, etc. To this end the smart particle approach seems to be very promising. Development of this approach will effect no substantial changes in the existing technologies for modification of fibers and textile materials. This approach will need intensive investigations for synthetic routes of the fabrication of smart particles. Not all approaches can be automatically transformed from plane substrates onto particle surfaces. A number of problems will increase as an inverse function of the particle size. Another set of problems lies in the appropriate selection of polymers for the synthesis of a responsive shell of the particles. This selection will be strongly connected to the practical applications of the materials. The response kinetics is also a very important issue. The kinetics can be regulated by molecular weight and glass transition temperature of the grafted polymers. Investigations of the smart particles in dynamic conditions will be needed for precise adjustment of the response kinetics. For small particles, if the particle diameter is comparable with the grafted chain dimension, the phase segregation mechanism can be modified by the spherical geometry. This mechanism has not been investigated yet and should be studied carefully. The structure of the particle core can be also involved in designing responsive properties of the smart particles.

Further investigations should study correlations between responsiveness of the thin films and properties of textiles and cloth. Although many useful properties of responsive textiles can be imagined, it is important to identify how practically they could be explored for textile materials of different applications. Many different scenarios could be suggested to employ the responsiveness. Some examples are as follows. For a direct switching effect (textile hydrophilic in water and hydrophobic in air) the cloth will adsorb excess perspiration and it can then be easily washed in water, but in a dry state it will be hydrophobic with less friction and less adhesion. For an inverse switching effect (textile hydrophilic in air and hydrophobic in water) the cloth will be permeable for vapors, but an excess of water will block permeability of the materials for aqueous solutions. Experiments should discover which properties will be most attractive and important to consumers.

18.7 Sources of further information and advice

- Selected chapters on responsive polymer systems[1]
- Responsive thin polymer films[2]
- Polymer brushes[15, 16]
- Polyelectrolyte brushes[18]

18.8 Acknowledgment

Work described in this review was supported in part by the US ARO grant W911NF-05-1-0339, NTC award C04-CL06 and NSF award CTS 0456548.

18.9 References

1. Minko S., *Responsive Polymer Materials: Design and applications*, Ames, Blackwell Publishing, 2006.
2. Luzinov I., Minko S., and Tsukruk V. V., 'Adaptive and responsive surfaces through controlled reorganization of interfacial polymer layers', *Prog Polym Sci*, 2004 **29**(7) 635–698.
3. Roiter Y., and Minko S., 'Single molecule experiments at the solid–liquid interface: *in situ* conformation of adsorbed flexible polyelectrolyte chains', *J Am Chem Soc*, 2005 **127**(45) 15688–15689.
4. Holly F. J., and Refojo M. F., 'Wettability of hydrogels. I. Poly(2-hydroxyethyl methacrylate)', *J Biomed Mater Res*, 1975 **9** 315–326.
5. Ruckenstein E., and Lee S. H., 'Estimation of the equilibrium surface free-energy components of restructuring solid surfaces', *J Colloid Interface Sci*, 1987 **120** 153–159.
6. Ruckenstein E., and Lee S. H., 'Surface restructuring of polymers', *J Colloid Interface Sci*, 1987 **120** 529–536.
7. Lee S. H., and Ruckenstein E., 'Stability of polymeric surfaces subjected to ultraviolet-irradiation', *J Colloid Interface Sci*, 1987 **117** 172–178.

8. Mason R., Jalbert C. A., O'Rourke Muisener P. A. V., Koberstein J. T., Elman J. F., Long T. E., and Gunesin B. Z., 'Surface energy and surface composition of end-fluorinated polystyrene', *Adv Colloid Interface Sci*, 2001 **94** 1–19.
9. Lukas J., Sodhi R. N. S., and Sefton M. V., 'An XPS study of the surface reorientation of statistical methacrylate copolymers', *J Colloid Interface Sci*, 1995 **174**(2) 421–427.
10. Russell T. P., 'Surface-responsive materials', *Science*, 2002 **297**(5583) 964–967.
11. Zhang D., Ward R. S., Shen Y. R., and Somorjai G. A., 'Environment induced surface structural changes of a polymer: an in situ IR + visible sum-frequency spectroscopic study', *J Phys Chem B*, 1997 **101** 9060–9064.
12. Lewis K. B., and Ratner B. D., 'Observation of surface rearrangement of polymers using ESCA', *J Colloid Interface Sci*, 1993 **159**(1) 77–85.
13. Senshu K., Sh. Y., Mori H., Ito M., Hirao A., and Nakahama S., 'Time-resolved surface rearrangements of poly(2-hydroxyethyl methacrylate-block-isoprene) in response to environmental changes', *Langmuir*, 1999 **15** 1754–1762.
14. Milner S. T., 'Polymer brushes', *Science*, 1991 **251**(4996) 905–914.
15. Zhao B., and Brittain W. J., 'Polymer brushes: surface-immobilized macromolecules', *Prog Polym Sci*, 2000 **25**(5) 677–710.
16. Advincula R. C., Brittain W. J., Caster K. C., and Ruehe J., *Polymer Brushes*, Weinheim, Wiley-VCH, 2004.
17. Biesalski M., Johannsmann D., and Ruhe J., 'Synthesis and swelling behavior of a weak polyacid brush', *J Chem Phys*, 2002 **117**(10) 4988–4994.
18. Ruhe J., Ballauff M., Biesalski M., Dziezok P., Gröhn F., Johannsmann D., Houbenov N., Hugenberg N., Konradi R., Minko S., Motornov M., Netz R. R., Schmidt M., Seidel C., Stamm M., Stephan T., Usov D., and Zhang H., 'Polyelectrolyte brushes', in Schmidt, M., *Polyelectrolytes with Defined Molecular Architecture I*, New York, Adv. Polym. Sci.; Springer, 79–150, 2004.
19. Minko S., Luzinov I., Luchnikov V., Muller M., Patil S., and Stamm M., 'Bidisperse mixed brushes: Synthesis and study of segregation in selective solvent', *Macromolecules*, 2003 **36**(19) 7268–7279.
20. Minko S., Muller M., Usov D., Scholl A., Froeck C., and Stamm M., 'Lateral versus perpendicular segregation in mixed polymer brushes', *Phys Rev Lett*, 2002 **88**(3) 0355021–0355024.
21. Shusharina N. P., and Linse P., 'Oppositely charged polyelectrolytes grafted onto planar surface: mean-field lattice theory', *Eur Phys J E*, 2001 **6** 147–155.
22. Houbenov N., Minko S., and Stamm M., 'Mixed polyelectrolyte brush from oppositely charged polymers for switching of surface charge and composition in aqueous environment', *Macromolecules*, 2003 **36**(16) 5897–5901.
23. Biesheuvel P. M., and Stuart M. A. C., 'Electrostatic free energy of weakly charged macromolecules in solution and intermacromolecular complexes consisting of oppositely charged polymers', *Langmuir*, 2004 **20**(7) 2785–2791.
24. Zhulina E., and Balazs A. C., 'Designing patterned surfaces by grafting Y-shaped copolymers', *Macromolecules*, 1996 **29**(7) 2667–2673.
25. Julthongpiput D., Lin Y. H., Teng J., Zubarev E. R., and Tsukruk V. V., 'Y-shaped polymer brushes: nanoscale switchable surfaces', *Langmuir*, 2003 **19**(19) 7832–7836.
26. Granville A. M., Boyes S. G., Akgun B., Foster M. D., and Brittain W. J., 'Synthesis and characterization of stimuli-responsive semifluorinated polymer brushes prepared by atom transfer radical polymerization', *Macromolecules*, 2004 **37**(8) 2790–2796.

27. Zhulina E. B., Singh C., and Balazs A. C., 'Forming patterned films with tethered diblock copolymers', *Macromolecules*, 1996 **29**(19) 6338–6348.
28. Zhulina E. B., Singh C., and Balazs A. C., 'Self-assembly of tethered diblocks in selective solvents', *Macromolecules*, 1996 **29**(25) 8254–8259.
29. Zhao B., Brittain W. J., Zhou W., and Cheng S. Z. D., 'Nanopattern formation from tethered PS-b-PMMA brushes upon treatment with selective solvents', *J Am Chem Soc*, 2000 **122**(10) 2407–2408.
30. Zhao B., Brittain W. J., Zhou W. S., and Cheng S. Z. D., 'AFM study of tethered polystyrene-b-poly(methyl methacrylate) and polystyrene-b-poly(methyl acrylate) brushes on flat silicate substrates', *Macromolecules*, 2000 **33**(23) 8821–8827.
31. Zhao B., and Brittain W. J., 'Synthesis, characterization, and properties of tethered polystyrene-b-polyacrylate brushes on flat silicate substrates', *Macromolecules*, 2000 **33**(23) 8813–8820.
32. Boyes S. G., Brittain W. J., Weng X., and Cheng S. Z. D., 'Synthesis, characterization, and properties of ABA type triblock copolymer brushes of styrene and methyl acrylate prepared by atom transfer radical polymerization', *Macromolecules*, 2002 **35**(13) 4960–4967.
33. Minko S., Patil S., Datsyuk V., Simon F., Eichhorn K. J., Motornov M., Usov D., Tokarev I., and Stamm M., 'Synthesis of adaptive polymer brushes via "grafting to" approach from melt', *Langmuir*, 2002 **18**(1) 289–296.
34. Sidorenko A., Minko S., Schenk-Meuser K., Duschner H., and Stamm M., 'Switching of polymer brushes', *Langmuir*, 1999 **15**(24) 8349–8355.
35. Motornov M., Minko S., Eichhorn K. J., Nitschke M., Simon F., and Stamm M., 'Reversible tuning of wetting behavior of polymer surface with responsive polymer brushes', *Langmuir*, 2003 **19**(19) 8077–8085.
36. Minko S., Muller M., Motornov M., Nitschke M., Grundke K., and Stamm M., 'Two-level structured self-adaptive surfaces with reversibly tunable properties', *J Am Chem Soc*, 2003 **125**(13) 3896–3900.
37. Öner D., and McCarthy T. J., 'Ultrahydrophobic surfaces. Effects of topography length scales on wettability', *Langmuir*, 2000 **16**(20) 7777–7782.
38. Bico J., Tordeux C., and Quere D., 'Rough wetting', *Europhys Lett*, 2001 **55**(2) 214–220.
39. Wenzel R., 'Resistance of solid surfaces to wetting by water', *Ind Eng Chem Res*, 1936 **28** 988–994.
40. Cassie A. B., and Baxter S., 'Wettability of porous surfaces', *Trans Faraday Soc*, 1944 **40** 546–551.
41. Bico J., Marzolin C., and Quere D., 'Pearl drops', *Europhys Lett*, 1999 **47**(2) 220–226.
42. Motomov M., Sheparovych, R., Lupitskyy, R., MacWilliams, E., Minko, S., Responsive colloidal systems: Reversible aggregation and fabrication of superhydrophobic surfaces. *J Colloid Interface Sci* 2007, **310**(2), 481–488.
43. Gorodyska G., Kiriy A., Minko S., Tsitsilianis C., and Stamm M., 'Reconformation and metallization of unimolecular micelles in controlled environment', *Nano Lett*, 2003 **3**(3) 365–368.
44. Lupitskyy R., Roiter Y., Tsitsilianis C., and Minko S., 'From smart polymer molecules to responsive nanostructured surfaces', *Langmuir*, 2005 **21**(19) 8591–8593.

19

Structure–property relationships of polypropylene nanocomposite fibres

C. Y. LEW, University of Oxford, UK and
G. M. McNALLY, Queen's University Belfast, UK

19.1 Introduction

Montecatini (Roder, 1999) first commercialised polypropylene as a synthetic fibre-forming material in 1957, nearly two decades later than the production of polyamide fibre by E. I. du Pont de Nemours & Co. in 1939 (Carraher, 2003) and polyester fibre by ICI in 1941 (Whinfield, 1946). This was because the stereochemistry required to develop the spinnability properties for polypropylene was not achieved until 1954 with the independent discovery of stereospecific titanium halide-based coordination catalysts by Edwin Vandenberg (Vandenberg and Salamone, 1992) and Giulio Natta (Natta *et al.*, 1955).

The high molecular weight (M_w) and broad molecular weight distribution (MWD) arising from the heterogeneous Ziegler–Natta polymerization limited the earlier melt spinning of polypropylene to relatively low take-up speeds, usually less than 1000 m/min, due to high viscoelasticity and resultant susceptibility to spinline cohesive fracture (Ziabicki, 1976). Higher-speed spinning of isotactic polypropylene was later made possible with visbreaking technology developed by Exxon, facilitating the reduction of M_w and MWD by extensive chain-scission through twin-screw kneading in the presence of a peroxide species (Steinkamp and Grail, 1975). Recent progress in constrained geometry-catalysed technology using chiral metallocene catalysts has led to the polymerisation of highly stereospecific polypropylenes with even narrower M_w and MWD (Brintzinger *et al.*, 1995), thus further improving spinnability.

Studies of propylene random copolymers have recently gained importance over isotactic polypropylene in applications requiring high clarity, flexibility and low-temperature performance (Maier and Calafut, 1998). Traditionally, the enhancement in mechanical performance of melt-spun fibres relies primarily on the control of molecular chain orientation and crystalline structure development through take-up speed, drawing ratio and quenching conditions. Heterogeneous particulate reinforcement of polymers often leads to phase separation, increases the melt viscosity and creates hydrodynamic instabilities,

which affect the spinline stability and molecular orientation of the molten filament.

Several reinforcement techniques have been introduced for the fabrication of composite fibres, such as: (i) the introduction of thermotropic liquid crystalline polymers (TLCP) to produce a matrix–fibril structure, (ii) use of multiphase polymer blends and hard/soft segmented thermoplastics, and (iii) bicomponent extrusion, where different polymers are brought in contact as separate streams just before the spinnerette to produce a sheath–core structure (Salem, 2000). However, the inapplicability of these techniques to high-commodity commercial polymers and other serious drawbacks has limited the appeal. For instance, fabrication of TLCP is very expensive and post-processing may destroy its unique matrix–fibril structure. Incomplete microphase separation in some polymer blends often leads to a less desirable morphology in multiphase fibres and bicomponent spinning is sensitive to differences in viscosity between the polymers.

The use of smectite layered-silicate for reinforcing commercial fibre matrix was first reported in 2000 by Giza *et al*. (2000a, b) and has recently attracted greater attention, in both academia and industry (Ergungor *et al*., 2002; Koo *et al.*, 2002; Chang *et al*. 2003, 2004; McCord *et al*., 2004; Siochi *et al*., 2004; Yoon *et al*., 2004; Zhang *et al*., 2004). The fabrication of nanocomposite fibres involves exfoliating the layered silicate particles and integrally dispersing them in the host polymer matrix. Nanocomposite systems could potentially offer an overall property improvement without compromising the melt spinnability, flexibility and density of the host matrix. Furthermore, the nanocomposites would preserve a homogeneous polymer-filler phase compared with the heterogeneous morphology obtained in conventionally filled thermoplastic composites.

The kinematics and dynamics of deformation that occur in the polymer melt leaving the spinneret during fibre spinning are affected by extensional flow characteristics and the associated elongational viscosity. The relationship between elongational viscosity and shear viscosity for Newtonian fluids defined by Trouton's rule states that the extensional viscosity is over three times greater than the shear viscosity, while for non-Newtonian polymer melts it is considerably greater (Trouton, 1906). Pavlikova *et al*. (2003) reported on the enhanced layered-silicate exfoliation through solid-phase drawing of melt-spun polypropylene/hectorite fibres. More recently, Guan *et al*. (2005) observed that the intercalation of layered-silicate was further improved following the melt-spinning process, which can be related to the strong elongational stress. Lew (2004) reported that exfoliation of layered-silicate can be promoted by the action of elongational deformation during the melt-drawing process of polypropylene, where the extent of exfoliation increased with drawing speed. McConnell *et al*. (2006) also observed improved exfoliation of layered-silicate in poly(ethylene-terephthalate) matrix under

the influence of elongational stress; however the degree of exfoliation decreased with increasing melt spinning speed.

This chapter aims at exploring in greater detail than hitherto the effect of extensional flow deformation on the exfoliation behaviour of layered-silicate by investigating the structure and properties of a series of polypropylene nanocomposite fibres, obtained through melt-spinning processing, compared with their corresponding compounded feedstocks and injection-moulded specimens. A range of maleic anhydride (MA) oligomers were used to reduce physical phase separation between the hydrophobic matrix and the hydrophilic layered-silicate, and to study the effect of compatibiliser properties on the structure–property relationships of the resultant nanocomposites.

19.2 Materials, processing and characterisation techniques

The host polymer was a metallocene-catalysed propylene–ethylene random copolymer (PP), tradename Metocene X70293, supplied by Basell in pellet form, with a melt-flow index of 40 g/10 min (ASTM D1238). The layered-silicate was synthetic tetrasilisic fluoromica, tradename SOMASIF MAE, with a cation-exchange capacity of 1.2 meq/g, manufactured by CO-OP Chemical Co. Ltd. The layered-silicate was derived from heat treating talc with alkali silicofluoride followed by isomorphous counterion-exchange with tri-(hexadecyl-octadecyl-octadecenyl)-methyl ammonium cations. A range of MA-grafted isotactic propylene oligomers were used as compatibilisers (Table 19.1).

A range of PP/layered-silicate mixtures were prepared by cryo-grinding the PP pellets into powder form, turbo-blending with 3.5 pph fluoromica and thereafter, mixed with predetermined percentages of compatibilisers (Table 19.2). The mixtures were compounded using a Killion KN150 single-screw extruder, fitted with a Davis Standard DSBM-T Spiral Maddock screw. The mixtures were compounded twice, at 15 rpm and 45 rpm screw speed and the barrel temperature profile was ramped from 175 to 200 °C. The low-speed first pass was intended to improve distributive mixing and extend the melt

Table 19.1 Specifications of maleic anhydride-grafted propylene (MAPP) oligomers

MAPP	M_w	M_w/M_n	T_m (°C)	Acid number (mg KOH/g)	Functionality (%)	MAPP/MA (molar ratio)
E43	9100	2.33	156.0	47	8.2	0.32
G3003	52000	1.91	163.8	8	1.4	0.24
G3015	47000	1.89	161.6	15	2.6	0.16
P3150	332000	10.7	164.3	3	0.5	1.57

Table 19.2 Composition of MAPP and MA in the samples

Sample code	MAPP	MA (%)	Final MA (%)
PPEX	E43	4.17	0.342
PPEZ	E43	12.5	1.025
PPG5	G3015	12.5	0.325
PPG3	G3003	12.5	0.175
PPB3	P3150	12.5	0.063

intercalation time, while the second pass at higher rotation would promote delamination of the intercalated layered-silicate.

The pelletised feedstock pellets were melt-spun at a constant shear rate of $300\,s^{-1}$, at take-up speeds of 80 and 400 m/min, from a 16:1 *L/D* ratio, 1 mm diameter die, at 160 ºC into single filaments targeted at 150 and 50 µm diameter respectively. Fibres spun at 80 and 400 m/min are referred to as *'lsv'* and *'hsv'* respectively. Spinning was performed using a Rosand RH7 capillary rheometer equipped with a digitally controlled high-speed haul-off unit. For comparison, the feedstocks were also injection-moulded into tensile specimens (ASTM D638) using an Arburg 320S Allrounder injection-moulding machine. The injection-moulding temperature and pressure were 180–215 °C and 1200 bar with the mould maintained at 45 °C.

The structure of layered-silicates in the nanocomposites was analysed using a Bruker AXS D8 Discover diffractometer (CuKα radiation), scanned at step size of 0.04° and step time of 0.8 s. X-ray diffraction (XRD) was performed on the surface of injection-moulded samples, the compounded feedstock and the melt-spun filament bundles, twisted to about 2 mm in diameter. The morphology of the nanocomposite fibres and the injection-moulded samples was examined using a digital Philips FEI Technai F20 high-resolution transmission electron microscope (HRTEM), operated at 200 kV. The presented HRTEM images for each of the fibre samples were representative from at least four different ultra-microtomed specimens of the fibre, taken at random sections along the filament. The fibres' surface textures, associated with spinline stability and cold-fractured surface morphologies related to phase homogeneity, were studied using a JOEL JSM 6400 scanning electron microscope (SEM). Rheological data were recorded using a Rosand RH7 capillary rheometer. Optical birefringence (refractive index) of the fibres was analysed using an Olympus BX50 microscope, equipped with a pair of mutually perpendicular cross-polarisers and a 30 order Berek compensator. The birefringence (double refractive index) Δn was determined from the ratio of optical retardation Γ over the filament diameter d. The infrared deformation response of fibre molecular bonding was studied using a Perkin-Elmer Spectrum 1000 Fourier transform infrared (FTIR) spectrometer, scanned at resolution of $4\,cm^{-1}$ for 25 scans on average. The

tensile properties of the fibres were determined using an Instron 4411 Universal extensometer.

19.3 Structure and morphology

Figure 19.1 shows the wide-angle XRD patterns of pristine layered-silicate and its structures in the injection-moulded specimens. The corresponding XRD patterns of the compounded feedstock and melt-spun fibres are shown in Fig. 19.2 and 19.3. The pristine layered-silicate exhibited six characteristic peaks, at 2.9, 4.4, 5.0, 5.8, 7.3 and 10.2°. These characteristic peaks were nearly absent in the injection-moulded, melt-spun and compounded PPEX, thus suggesting that the compatibiliser imparted favourable mixing thermodynamics which promoted exfoliation. PPEX was maleated with a highly functionalized/low M_w, MA oligomer (8.2% functionality, 9100 M_w) at a low concentration (4.2%). High functionality (and hence acid value) of

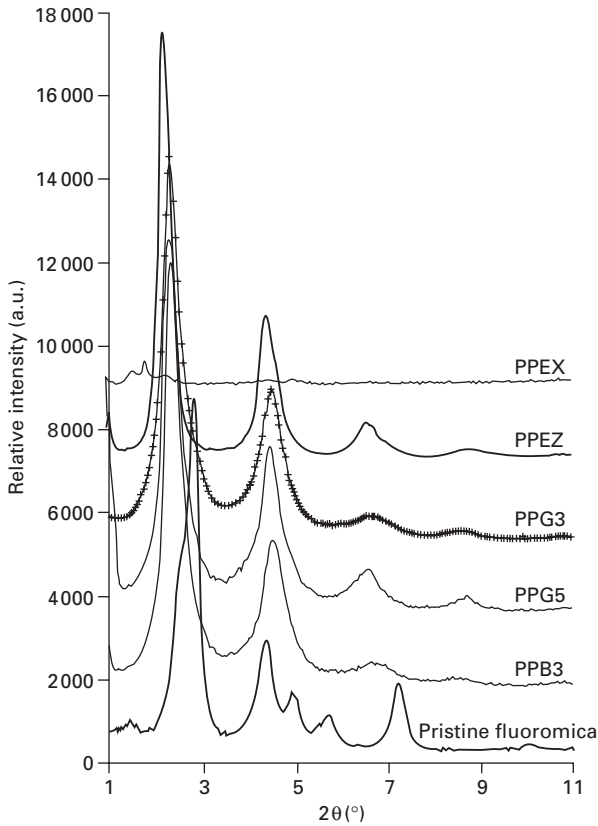

19.1 Wide-angle XRD patterns of injection-moulded nanocomposites.

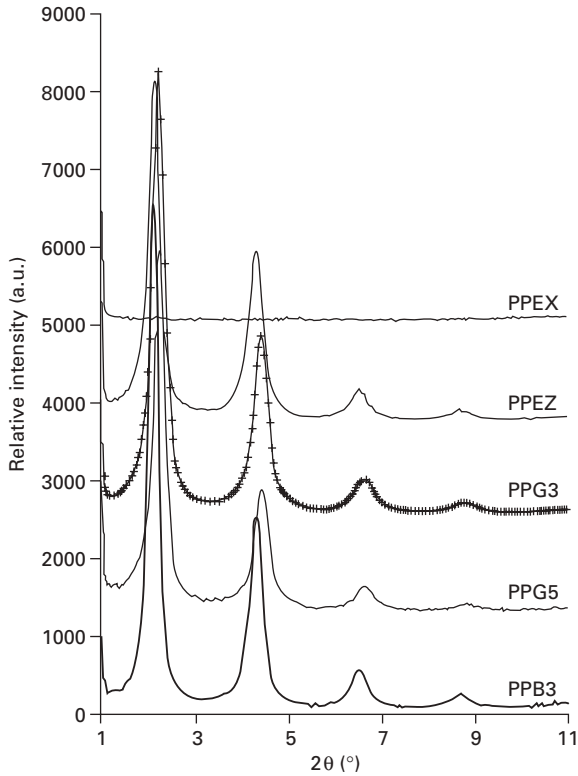

19.2 Wide-angle X-ray patterns of nanocomposites in feedstock compound form.

an MA oligomer improved the mixing enthalpy (Reichert *et al*., 2000), while low M_w enhanced its dispersibility and wetting efficiency, therefore creating a favourable condition for exfoliation to occur. In addition, the low concentration of the polar MA compatibiliser minimised physical phase separation with the host PP matrix.

In contrast, PPEZ also incorporated the same oligomer, but did not exhibit good exfoliation at a concentration that was three times higher (12.5%). The higher loading of the MA oligomer in PPEZ led to phase separation as observed later in the SEM morphology (Lew, 2004) with the neat PP, or caused a reduction in the optimum shear viscosity required to delaminate the layered-silicate tactoids (Kawasumi *et al.*, 1997; Kim, 2000). Furthermore, Manias *et al*. (2001) also reported that overloading of the MA oligomer could render a polymer system so robust that the layered-silicate will not mix well with the polymer given that the oligomer would agglomerate around the layered-silicate particles.

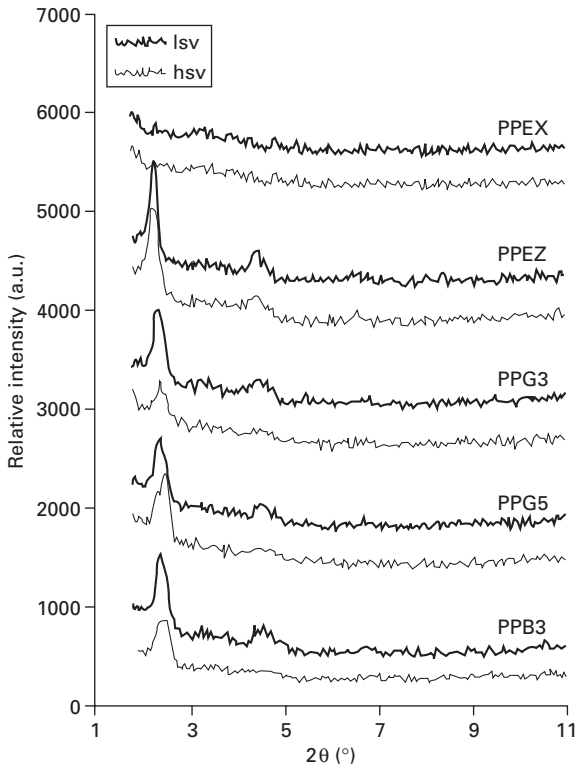

19.3 XRD patterns of melt-spun nanocomposite fibres.

The XRD spectra show the layered-silicate retains four interlayered peaks in the injection-moulded specimens and the compounded feedstock. The higher peak intensity recorded for the injection-moulded samples is attributed to the strong flow orientation effect (McNally *et al.*, 2003). Although the peak reflection patterns for the injection-moulded and compounded samples are very similar, the 2θ peak angles for the feedstock compound were slightly lower than those of the corresponding injection-moulded specimens. In addition, the injection-moulded PPEX displayed three mildly adjoined peaks at 1.54, 1.78 and 2.22° which were not found in the feedstock. These two phenomena suggest shear-induced demixing (Madbouly, 1999), a not so rare phenomenon sometimes seen in a nanoparticle-filled polymer system when subjected to high shear flow (Dennis *et al.*, 2001).

In contrast, the XRD spectra for the nanocomposite fibres recorded only two peaks at 2θ position of ~2.2 and 4.4°. The disappearance of the third and fourth order peaks (at 6 to 9° region) further suggest exfoliation of layered-silicate during the melt-spinning process. This may be associated with the elongational deformation of the the PP matrix during melt-spinning, which

can be greater than conventional shear-induced deformation by a factor of up to a hundred (Cogswell, 1975), and therefore draws on a more effective stress to delaminate the layered silicate.

Considering the differences in surface characteristics (texture and dimension), the disappearance of the third and fourth order XRD peaks of the fibres could be attributed to the beam scattering effect on the filament due to its surface curvature compared with the flat surface of the injection-moulded and feedstock compound. Comparisons between the first and second order retained peaks of the fibres suggested that the disappearance of the third and fourth order peaks was attributable in part, if not solely, to improved exfoliation of the layered-silicate, based on the following observations. The 2θ peaks of nanocomposite fibres spun at 400 m/min (*hsv*) appeared to be more depressed in shape (i.e. greater degree of exfoliation) than their corresponding *lsv* fibres spun at 80 m/min. Since elongational deformation during spinning of the *hsv* was greater than *lsv* because of the higher take-up speed, this would corroborate that the more depressed peaks (exfoliation) observed for *hsv* could be ascribed to the more effective elongational deformation derived from the higher melt drawing speed.

The third and fourth order peaks of the injection-moulded PPB3 appeared slightly more depressed in shape than PPG3, PPG5 and PPEZ. This manifestation may be ascribed to the high MA oligomer concentration with very high M_w (332 000) and low functionality (0.5%). Fornes *et al.* (2001) extruded nanocomposites using polyamide 6 of different M_w and also observed that a higher matrix M_w, because of its greater interlayer penetration stress, was more effective in exfoliating the layered-silicate. Similarly, the high MA oligomer concentration together with its high M_w in PPB3 may be responsible for the shift of all the peaks to the lower 2θ angles (i.e. enhanced intercalation) observed for the PPB3 feedstock compound.

19.3.1 Morphology

Figure 19.4 shows the HRTEM images of the *hsv* fibres and injection-moulded nanocomposites. Overall, the relative thickness and dispersion of the layered-silicates in the PP matrices are consistent with the XRD trend. For example, the highly delaminated silicate platelets observed in the PPEX matrix are manifested as a level plateau in its XRD spectrum; an indication of full exfoliation. The observed smaller lateral dimension of layered-silicates in the *hsv* matrix relative to their corresponding *lsv* fibres would corroborate the more repressed XRD peaks seen for the *hsv* fibres. This further suggests the influence of extensional flow deformation on the exfoliation of layered-silicate.

The appearance of tactoid layered-silicate in the PPEZ matrix may be attributed to high-concentration (12.5%) incorporation of low M_w (9100)

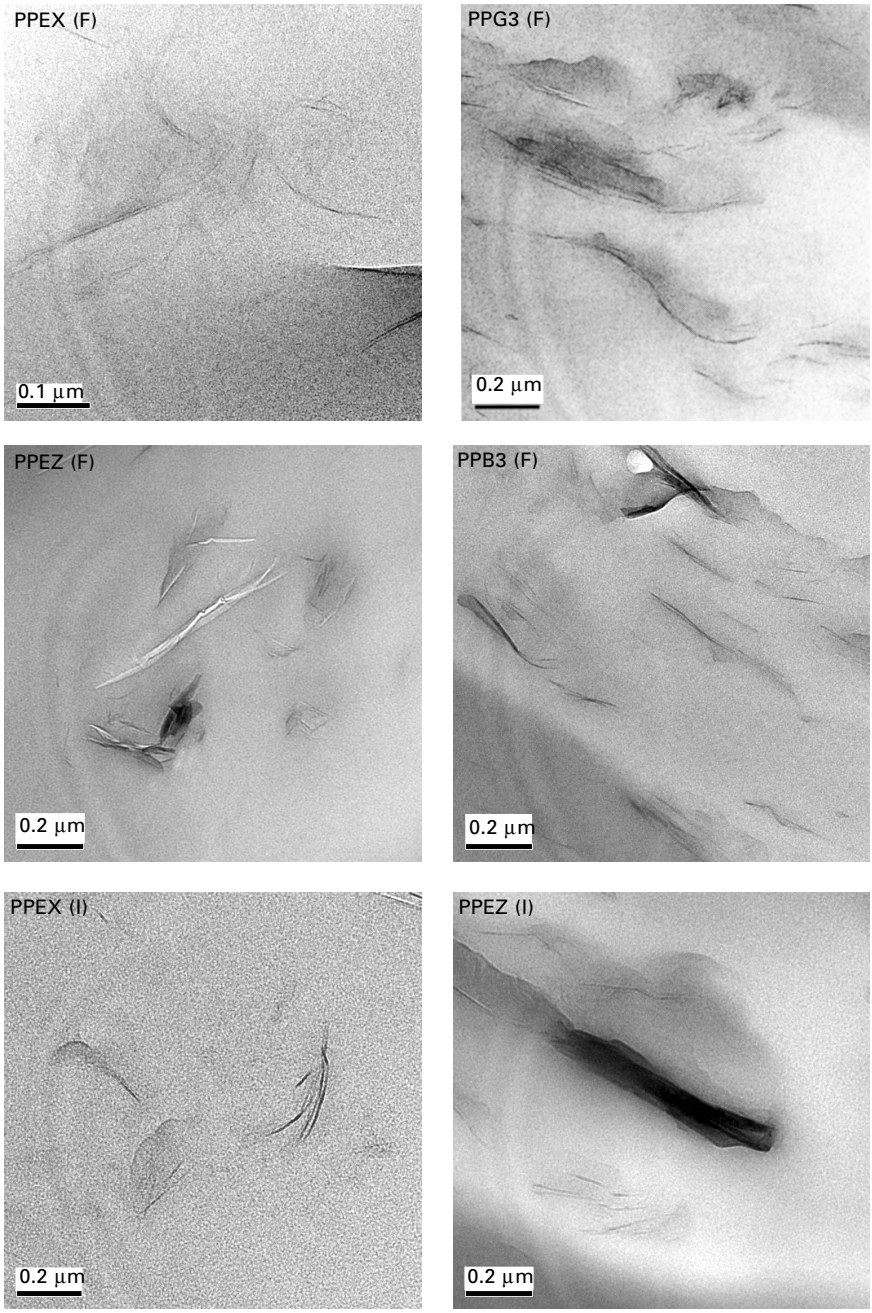

19.4 HRTEM images of *hsv* fibres (F) and injection-moulded (I) specimens.

MA oligomer, thus lowering the overall melt viscosity and hence the shear stress to break up the layered-silicate crystallites. Furthermore, the high MA functionality (6.0%) of the oligomer may cause conflux of layered-silicate particles by the compatibiliser species. Two possible consequences may arise as an effect. Envisage the formation of a strong hydrogen bond and van der Waals interaction between the carbonyl (C═O) group and the Si—O/Si—OH groups drawn from excess enthalpic interaction and thus developed into polar globules. These would energise more of the close MA oligomers to populate about the polar localities, therefore reducing the MA dispersibility and leading to a PP/oligomer phase separation. Furthermore, too much enthalpic interaction between the MA and the layered-silicate may reduce the translational entropy and miscibility of the compatibiliser with the interlayer aliphatic tails of the alkylammonium surfactant and, hence, overall energetic conditions for intercalation.

19.4 Phase homogeneity and spinline stability

The cold-fractured surface morphologies of the various fibres, associated with the matrix phase homogeneity are shown by the SEM photomicrographs in Fig. 19.5. The relatively smooth morphology exhibited by PPEX, close to that of the neat PP, is an indication of the presence of significantly exfoliated silicate layers that preserved a homogeneous PP phase. In contrast, PPEZ

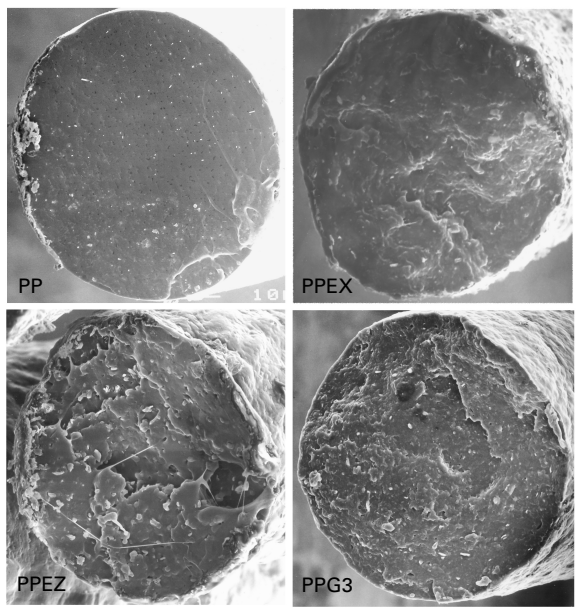

19.5 SEM fracture morphology of *Isv* fibres (×1000 magnification).

displayed an extremely jagged and micro-cracked surface with strong evidence of clay tactoids, which, as suggested by the XRD and HRTEM results, are attributed to poor exfoliation. PPG3, which as expected, exhibited an intermediate degree of exfoliation between PPEX and PPEZ, displayed a fracture morphology somewhere between that of the two samples.

The surface textures of the various melt-spun *hsv* fibres were associated with their spinline stability. The PPEX fibre featured a smoother circumference than the neat PP fibre, which is usual for a filled polymer system. Given that the development of fibre surface texture is largely dependent on its spinline stability and crystallisation behaviour, this would imply a favourable alteration of the linear viscoelastic response of the PP that had led to better spinning properties and crystallisation attributes.

On the contrary, the PPEZ fibre and PPB3 fibre (Lew, 2004) exhibited an uneven and jagged surface texture. Zhang *et al*. (2004) ascribed these flaws, which they observed in the polypropylene/montmorillonite nanocomposite fibres, to the presence of clay platelets or aggregates that dramatically altered the heterogeneous crystallisation process. This explanation is consistent with the aggregate of tactoids seen in the HRTEM image of PPEZ. In addition, the very high compatibiliser loading (12.5%), as well as low (9100), and high (332 000) M_w in PPEZ and PPB3 respectively would result in a significant broadening of the MWD and an increase in the viscoelasticity of PP melt, therefore becoming more sensitive to melt cohesive fracture.

According to Ziabicki (1976), the broadening in MWD and hence elasticity can cause significant change in the heterogeneity of spinning melt, instability of flow within the spinneret channel, hydrodynamic instability of spinline and alteration of crystallisation behaviour, which may be responsible for defects and irregularities on the undrawn fibre surface. In addition, the presence of impurities (tactoids) in PPEZ is quite obviously responsible for the observed knots on its surface. PPG3 and PPG5 (Lew, 2004) which are not shown, displayed an intermediate surface texture between those of PPEX and PPEZ. This would agree with the observed trend since both PPG3 and PPG5 possess an M_w and functional level between those of PPEX, PPEZ and PPB3.

It is not uncommon for the presence of bulk nanofiller particles in a conventional polymer system to lead to a reduction in melt spinnability or even provoke the formation of aggregates, owing to instabilities, such as localisation and phase segregation. However, in this work, because the layered-silicate had already been intercalated and partially exfoliated via compounding prior to melt-spinning, the resultant particles would exhibit an improved aspect ratio and anisotropy. This, in effect, should lead to an enhanced mesoscopic reorientation ability of the silicate platelets in the shear flow direction, which, in turn, could promote the realignment of the polymer chain (Giannelis *et al*., 1999).

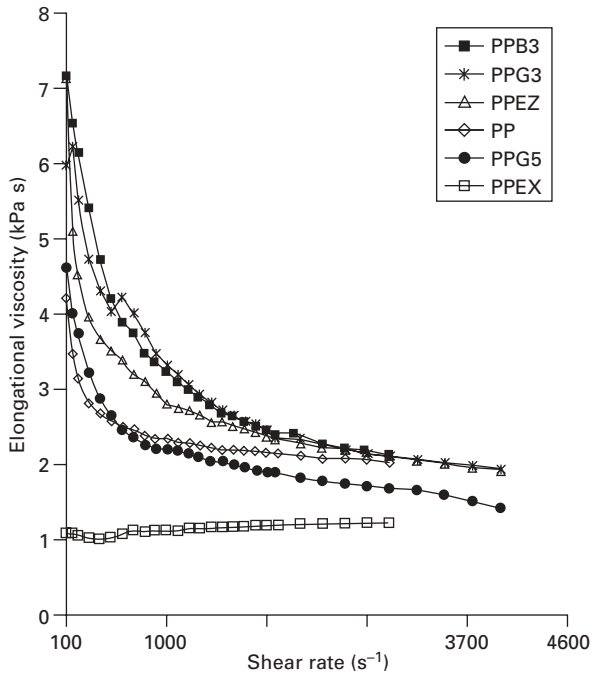

19.6 Plots of elongational viscosity *vs.* shear rate.

The rheological curves in Fig. 19.6 recorded a significant decrease in the elongational (extensional) viscosity for PPEX. Furthermore, it is intriguing that the PPEX melt would exhibit a Newtonian-like response in the range of shear rates studied, rather than the non-Newtonian behaviour that would be expected for a viscoelastic (polymer) system. From this viewpoint, PPEX, from its Newtonian-like behaviour as well as its adequate melt strength to resist viscoelastic fracture, could notionally be spun at extremely high speeds to achieve a very high tenacity and optical birefringence. The enhanced fibre surface texture of PPEX compared with the virgin PP fibre is another indication of its improved spinning property.

This viscosity reduction for PPEX may be attributed to the enhanced plasticising effect of the PP matrix imparted by a nanodispersion effect of the highly exfoliated silicate platelets and alklyammonium species. In a highly exfoliated state, as indicated by its XRD and HRTEM results, contact between the PP matrix and the soft-waxy alkylammonium phase tethered to the silicate layers surface was increased significantly and therefore led to an enhanced plasticising effect. The use of alkylammonium as an alternative to conventional plasticiser to impart melt processing flexibility (i.e. plasticising effect) is well documented (Wittcoff *et al.*, 2003). Xu *et al.* (2004) reported on the ability of layered-silicate to act as a plasticiser carrier. The increased

volume of silicate layers, and therefore plasticiser carriers attributed to extensive exfoliation in PPEX, could have contributed to the enhancement of the plasticising effect.

Although the cause of the plasticising effect may be attributed to grafted alkylammonium species, several authors have reported on the unique effect of ungrafted pristine nanoparticles to plasticise a polymer matrix, leading to viscosity reduction. This is achieved either via a chain slippage effect or through formation of nanosize free volume in the polymer melt (Cho and Paul, 2001; Roberts *et al.*, 2001; McNally *et al.*, 2003; Mackay *et al.*, 2003). However, the enhanced melt spinnability of PPEX is more likely to be associated with the Newtonian-like modification of its melt viscoelastic response and is thus a free melt fracture characteristic. However, the reasons for this radical alteration of viscoelastic behaviour in PPEX are not clear and will be the subject of further investigation.

The considerable increase in elongational viscosity recorded for PPB3 is likely to be attributed to the excessive loading (12.5%) of a very high M_w (332 000) compatibiliser, therefore increasing the overall system viscosity. However, the MA oligomer (12.5% E43) used in PPEZ had an M_w (9100) that was significantly lower than that of the neat PP, but also recorded a substantial increase in viscosity. In this case, the increase in viscosity is associated with the presence of silicate tactoids, as observed previously in the HRTEM. The presence of tactoids would restrict the flow of PP melt such as in a conventionally filled polymer system. Kawasumi *et al.* (1997) reported that excessive loading of an MA oligomer, especially a highly polar one (such as in the PPEZ) in the PP matrix could lead to pronounced phase separation and result in an increase of the polymer melt viscosity, similar to that observed in a heterogeneous system.

19.5 Optical birefringence and infrared activation

The polarised monofilament images and double refractive index measured for *lsv* fibres melt-spun at lower take-up speed did not exhibit significant variation in birefringence. The observed dark spots along the core of *lsv* monofilaments would manifest the presence of isotropic type crystal formed through melt nucleating (Buchko *et al.*, 1999). Nucleation of the isotropic crystal is attributed to lower cooling rate associated with lower spin speed and hence more favourable chain relaxation process. A similar crystal feature was also exhibited by the *hsv* PPEZ, PPG3, PPG5 and PPB3 which comprised a predominantly intercalated layered-silicate structure. However, this feature is not seen for the highly exfoliated *hsv* PPEX and neat PP fibres, which displayed an intense core brightening associated with enhanced molecular chain conformation. This is confirmed by their considerably higher refractive index plots shown in Fig. 19.7. The absence of isotropic crystal in the exfoliated

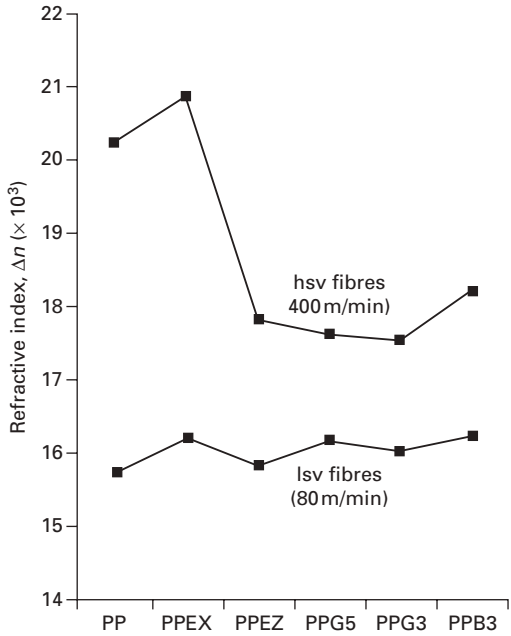

19.7 Plots of optical birefringence.

PPEX compared with the intercalated nanocomposite fibres may be due to enhanced nanodispersion of the silicate platelets. In this respect, despite the fact that the exfoliated silicate platelets may increase point nucleating density, they reduce the volumetric space required for the nuclei to a spherulite growth. In addition, the nanodispersed silicate platelets would lead to a significant volume increase in the silicate layers in the polymer matrix, thus restricting the global self-diffusion ability of the polymer chain.

The enhanced birefringence seen for the *hsv* PPEX fibre may also be because of the anisotropic ordering of silicate platelets. The presence of highly exfoliated silicate platelets would suppress the entropy associated with relaxation of the polymer chain. The higher birefringence of PPEX further corroborated enhanced melt spinnability of the *hsv* PPEX as indicated by the SEM and elongational viscosity plots. Because the enhancement in birefringence was only recorded for the PPEX fibre spun at higher take-up speed, this strongly suggests the influence of extensional stress deformation on exfoliation of layered-silicate.

At an angle of 2θ between 13 and 29° in the fibre XRD spectra (not shown in Fig. 19.1; Lew, 2004), the equatorial reflection of the PP α-crystalline phase for PPEX fibre was greatly suppressed. This observation indicates that the improved PPEX birefringence may also be attributed to a decrease in the isotropic crystalline phase located towards the fibre circumference and an

increase in the growth of the anisotropic '*shish kebab*' phase (Salem, 2000). It is also possible that the suppressed α-crystalline phase was due to the lateral migration of the highly exfoliated silicate platelets towards the fibre outer region during the spinning process and obstructed the diffraction of the X-ray beam from the PP crystal. Siochi *et al*. (2004), in their study of polymer carbon nanotubes fibres, reported an increased nanotube concentration from the centre towards outer fibre surface. This phenomenon may be related to the tendency of neutrally buoyant particles to migrate towards an equilibrium position between the wall and flow centre due to wall effects, velocity profile curvature and shear force (Segrè and Silberberg, 1961; Qi *et al*., 2002). Huang *et al*. (1997) simulated motion of a single anisotropic circular disc particle in a planar Poiseuille flow using the finite element technique and also demonstrated that, in a neutral case, the Segrè–Silberberg phenomenon was observed in which the equilibrium position for the particle would shift closer to the wall for a higher velocity flow.

19.5.1 Infrared activation

Figure 19.8 shows the FTIR spectra of the *lsv* and *hsv* fibres. Wavebands of ~1763 and ~1710 cm^{-1} represent the asymmetric stretching of the hydrogen-bonded carbonyl group (C=O) of the cyclic anhydride and the hydrolysed maleic acid, which are reversible on addition or removal of water (Barra *et al*., 1999; Bettini and Aganelli, 2000; Premphet and Chalearmthitipa, 2001). Two registered bands at 969 and 99 cm^{-1} are attributed to the vibrational stretching of the helical C—C backbone of the PP in the amorphous region (Verleye *et al*., 2001). The 1039 cm^{-1} band refers to both the symmetric stretching of Si—O and also deformation of PP, while the 1353 and 1371 cm^{-1} bands are assigned to the in-plane bending vibration of CH_2 and CH_3 bonds. The 1069 cm^{-1} band results from stretching of the Si—O bond in the tetrahedral coordinated silica plane (Gilman *et al*., 1999; Kang *et al*., 2000; Yeh *et al*., 2002; Kim *et al*., 2003). The spectra show a unique IR activation response for the PPEX fibre, which is very different from IR patterns exhibited by PPEZ, PPG3, PPG5 and PPB3. PPEX exhibited a waveband pattern that was consistent with those of the neat PP spectra as if the layered-silicate were absent in the matrix. This would suggest that PPEX, because of its highly exfoliated layered-silicate and uniform dispersion, had developed a homogeneous PP/layered-silicate phase, whereas the less exfoliated samples had yielded a more heterogeneous phase.

Firstly, the 1069 cm^{-1} Si—O band and the 1003 cm^{-1} band are absent in the nanodispersed PPEX and neat PP, but are visible in other systems. Secondly, no alteration was registered for the 1039 cm^{-1} band of PPEX and PP, but it rose in intensity and merged with the 1003 cm^{-1} band in other, less homogeneous, systems that exhibited evidence of clay tactoids. Rzanek-

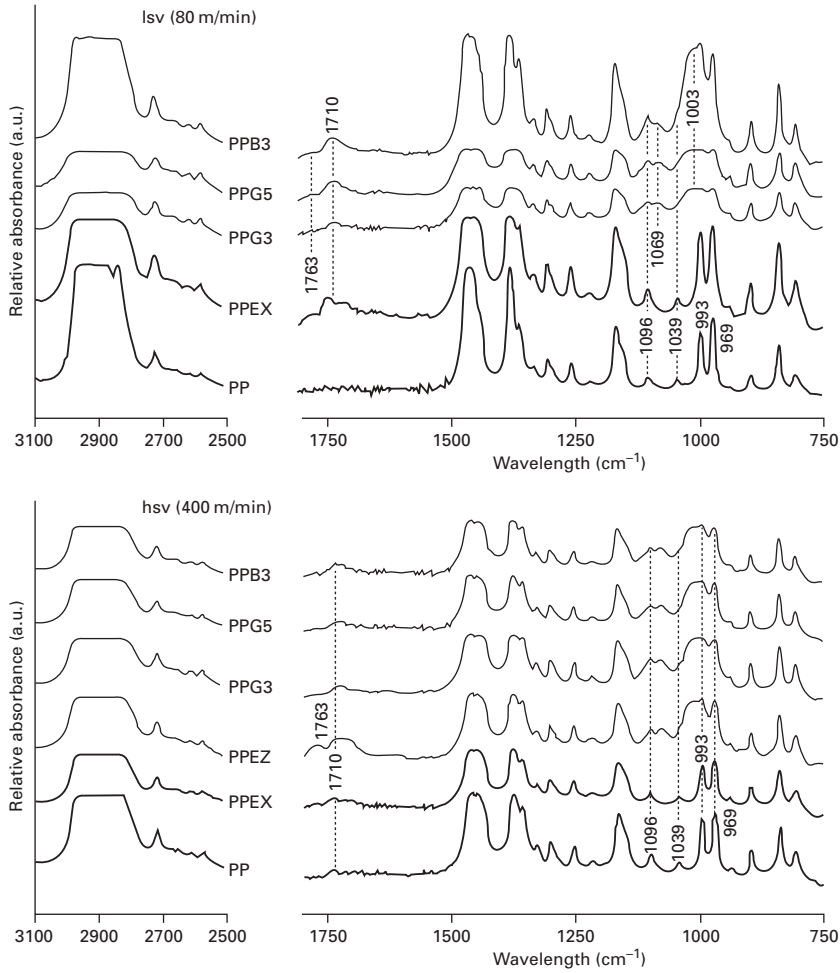

19.8 FTIR spectra of the *lsv* and *hsv* fibres.

Boroch *et al*. (2002) reported a similar observation of the 1039 cm^{-1} Si—O IR absorption band in their study of a range of organosilicon deposited film's. When the film's surface was further characterised using atomic force microscopy, they observed that the intensity of the Si—O IR band was weaker for films with improved phase homogeneity and was stronger for films with more heterogeneous surface deposition, exhibiting evidence of fine organosilicon aggregates.

The manifestation of the 1003 cm^{-1} Si—O vibration band for predominantly phase-intercalated PPEZ, PPG3, PPG5 and PPB3 may be ascribed to a systematic distortion of the tetrahedral symmetry silicate plane structure by dipolar interaction between the Si—O or Si—OH and carbonyl group of the anhydride

species, or with the alkylammonium cations ($NH_4^{\delta+}$). Peak *et al.* (1999) previously demonstrated, in the absorption study of a goethite-based clay system, that increasing the absorption of protonated surfactants (e.g. cationic alkylammonium) would render a more severe distortion effect on the tetrahedral SiO_4 symmetry due to an electrostatic effect, causing a split in their v_3 (asymmetric stretch) absorption band and triggering activation of the usually IR-inert v_1 bond vibration. The absence of this 1003 cm^{-1} band in PPEX therefore can be associated with its homogeneous exfoliated layered-silicate phase, where the effect of electrostatic distortion by onium cations was significantly reduced compared with other matrix/onium intercalated layered-silicate systems.

19.6 Crystallisation behaviour and mechanical performance

Figure 19.9 shows the endothermic differential scanning calorimetry (DSC) traces of the various fibres, with their corresponding peak melting temperature, the principal and secondary crystalline enthalpy of fusion attributed to melting of the host PP copolymer and MA oligomer respectively. The DSC traces of the PPG3, PPG5 and PPB3 fibres demonstrated two fusion peaks. In contrast, the second endotherm ascribed to the compatibiliser phase is absent in the PPEX fibre which exhibited DSC traces consistent with that of the virgin PP fibre consisting of a homogeneous phase. The absence of the second endotherm peak in PPEZ, on the other hand, may be ascribed to inhibition of nucleation activity or crystal growth by the highly MA-grafted low M_w oligomer incorporated where the pendant anhydride branching would interfere with, and restrict, the lamellae folding process.

In contrast to most reports on the nucleating effect of layered silicates that often find an increase in the PP crystallinity of their nanocomposite systems (Ma, 2001; Xu *et al.*, 2002; Li *et al.*, 2003), the crystalline portion of the nanocomposite fibres, except for PPEX, was considerably lower than the neat PP and the magnitude of reduction was more significant for fibres exhibiting less exfoliated morphology. In general, this reduction in the crystalline phase may be associated with an anti-nucleation effect of the layered-silicate, as implied from its suppressed melt crystallisation temperature (Lew, 2004). In addition, the increase in viscosity measured for PPEZ, PPG3, PPG5 and PPB3 due to the presence of predominantly intercalated layered-silicate phase may cause an increase in the diffusional activation energy of the PP chains, thus reducing their crystallinity.

The nucleation rate of a polymer is the product of a mass transport and nucleation parameter (Avrami, 1939), where the transport factor is related to a chain's self-diffusion; therefore the reduction in crystalline phase and crystallisation temperature could be explained by the coupling of functional carbonyl anhydride molecules with the reactive silanol sites on the silicate

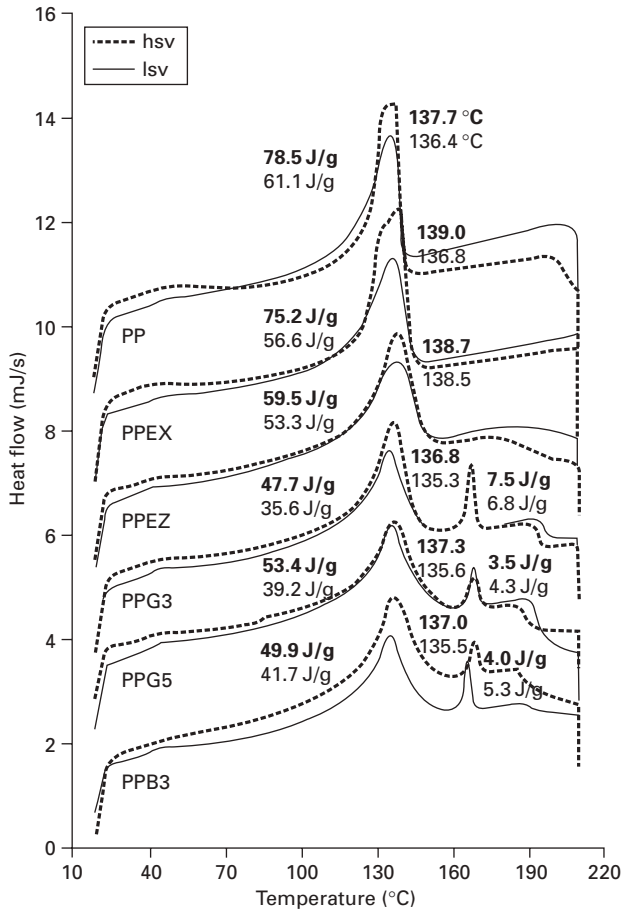

19.9 DSC endothermic traces of nanocomposite fibres.

surface, thus inhibiting lamellae formation for the compatibiliser. In addition, nanodispersion of exfoliated silicate platelets, owing to their larger surface area, may constrain the chain mobility and hence global self-diffusion of the host PP matrix. Lew *et al*. (2004) and Gopakumar *et al*. (2002) observed a similar reduction in the crystallinity of polyethylene layered-silicate nanocomposites incorporating MA oligomer and ascribed it to restriction in polymer matrix mobility through association with exfoliated layered-silicate or pendant anhydride. The higher melting enthalpy measured for PPEX could be due to increased formation of the anisotropic '*shish kebab*' phase as can be seen from the previous birefringence results. However, owing to the very large specific area of the exfoliated silicate platelets, the entropy of the melt matrix to initiate nucleation was greatly constrained and hence explained for the lower quiescent crystallisation temperature (Lew, 2004). In contrast to

the melt-spun nanocomposite fibres, the influence of the layered-silicate on the crystallinity of injection-moulded nanocomposites was not as significant; recorded melt enthalpy values were: PP (69.2 J/g), PPEX (66.8 J/g), PPEZ (69.5 J/g), PPG3 (70.1 J/g), PPG5 (67.6 J/g) and PPB3 (76.1 J/g).

The melting enthalpy, associated with crystallinity for *hsv* fibres spun at greater take-up speed, despite registering lower XRD peak intensity (associated with lower fraction of crystalline phase), was significantly higher than for their corresponding *lsv* fibre. Given that the *hsv* fibre exhibited considerably higher birefringence, the higher melting enthalpy measured for *hsv* fibres may be ascribed to higher thermal energy required for the melting of the *shish kebab* phase. The slightly higher peak melting temperature registered for the *hsv* fibres relative to their corresponding *lsv* fibres may be attributed to the greater activation energy required to induce mobility to the better oriented core crystalline structure.

19.6.1 Mechanical performance

Figure 19.10 shows the tensile properties graphs of the various *hsv* fibres, melt-spun at 400 m/min. The graphs for *lsv* fibres, melt spun at 80 m/min

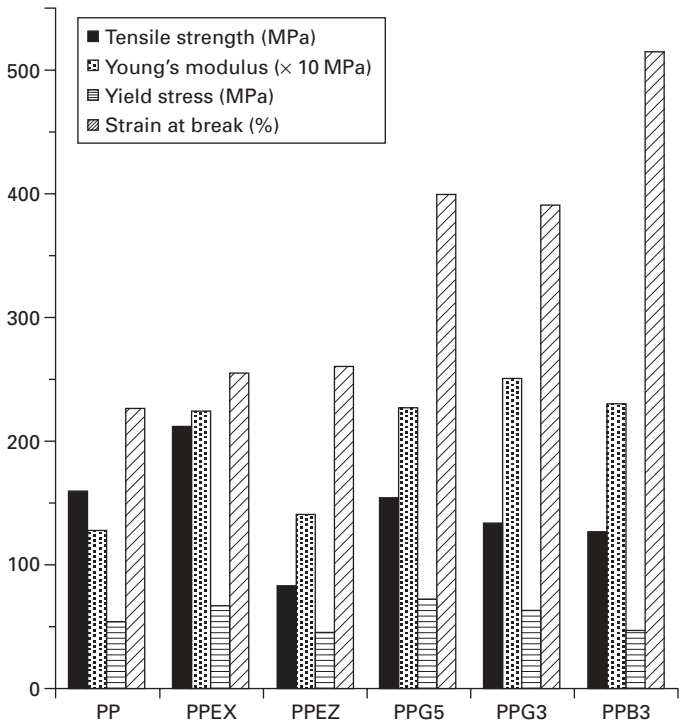

19.10 Mechanical properties of *hsv* fibres.

(not shown here; Lew, 2004), exhibited lower values for all the corresponding properties compared with the *hsv*, except having significantly higher strain at break. Because the *lsv* fibres were spun at lower take-up speed, the degree of extensional flow stress deformation and hence chain orientation was lower. As a result, *lsv* will therefore contain a larger percentage of (stretchable) amorphous phase and isotropic crystal line phase compared with the more highly aligned '*shish*' core crystalline phase in the *hsv*.

Substantial correlation is observed between the previous birefringence study and the tensile properties of the fibre samples, especially the tensile strength, which appeared to be dependent on the birefringence. For instance, PPEX, which displayed the highest birefringence value, also recorded the highest tensile strength and the neat PP exhibited second highest tensile strength for a similar reason. All other nanocomposite fibres exhibited tensile strengths lower than the neat PP fibre. The very poor tensile strength recorded for PPEZ is attributed to the presence of layered-silicate tactoids which could accelerate the rate of void propagation. Despite that PPG3, PPG5 and PPB3 exhibited greater improvement than PPEX in some of the tensile performances, PPEX alone exhibited a combination of overall improvement in tensile strength, Young's modulus, yield stress and stress at break. The substantial increase in stress at break for PPB3 on the other hand is attributed to the presence of the very high M_w (332 000) and broad MWD compatibiliser.

Kim *et al*. (2001) proposed that the tensile deformation mechanism of injection-moulded nanocomposites consists of three main stages. In brief, the first two stages comprise microvoid formation, owing to debonding of the intercalated matrix, followed by a splitting and realignment of layered-silicates. The criticality of the first and second deformation stages is less significant for PPEX fibre because the layered-silicates were already highly exfoliated as shown by the XRD and HRTEM results, and already oriented in the fibre axis (flow) direction. The third deformation stage could be adapted to explain the observed overall improvement in tensile properties for the PPEX fibre. During the third tensile deformation stage, silicate platelets bonded to the '*shish*' fibrillar core and the overgrowth lamellae '*kebab*' would interfere with the chain slip and fragmentation process. As the tensile deformation continued, the silicate platelets resist stress-induced recrystallisation of the disintegrated fibrils and the matrix/silicate interaction relaxes the stress imposed on the PP chain, while the soft alkylammonium tethered to the silicate platelets would impart a plasticising effect, thus reducing the slip friction between matrices and prolonging the fibre rupturing process.

The greater break strain recorded for the PPG3, PPG5 and PPB3 fibres may be attributed to the second deformation stage, which allows for splitting and reorientation of the intercalated layered-silicate stacks as described. The higher amounts of microvoids created during this stage would lead to an improved toughening mechanism (McNally *et al*., 2003).

19.7 Exfoliation by extensional flow deformation

Fornes *et al.* (2001) proposed that the layered-silicate exfoliation during an extrusion process was initiated by the break-up of taller silicate stacks into smaller stacks, following a layer-by-layer peeling mechanism of the top and bottom silicate stack platelets by the extrusion shear stress. They also reported that this mechanism was proportional to the polymer M_w (viscosity), in which higher effective shear stress associated with higher M_w would lead to a more exfoliated morphology.

Contrary to conventional shear deformation via an extrusion process, the elongational stress deformation associated to the spin speed in fibre extrusion can, in many instances, being inversely proportional to the M_w and MWD. This is because, although higher M_w polymers will produce higher spinline tension associated with the elongational viscosity, the molten filament is also more susceptible to spinline fracture and thus less spinnable. On the other hand, lower M_w polymers, providing they possess sufficient melt strength, are more spinnable at much higher take-up speeds and hence would experience greater elongational stress and chain alignment. A recent schema proposed to describe the exfoliation mechanism of layered-silicate under the influence of extensional flow stress deformation can be found in the literature (Lew, 2004).

Correlations drawn from the experimental results have led to the postulation that melt-spinning and hence extensional flow stress per se will not evoke exfoliation of layered-silicate in a pristine state. However, interestingly, melt-spinning is found to greatly promote exfoliation and nanodispersion of a precedently intercalated layered-silicate. This postulation is in part based on the XRD and HRTEM results and further corroborated by the following observations and contentions.

Firstly, the two peaks attributed to the third and fourth orders of basal spacing of the layered-silicate seen in the XRD spectra for the injection-moulded specimens and feedstock compounds were absent in the fibre spectra. Because the disappearance of the third and fourth order peaks could be an effect of exfoliation or because of low X-ray beam intensity, it is not possible to distinguish which of the two effects is more prevalent. However, the first and second order peaks of the *hsv* fibres manifested a more depressed peak shape and exhibited a lower peak intensity compared with the *lsv* fibres, but, in theory, the *lsv* fibre should exhibit a greater peak intensity because of the larger circumference and hence area exposed for beam diffraction. It is quite apparent, therefore, that the disappearance of the third and fourth order peaks, and the suppressed peak shape and intensity for the first and second order peaks, are mainly attributed to further exfoliation of the precedently intercalated layered-silicate through an extensional deformation effect during the melt-spinning process.

Secondly, because the XRD spectra of PPEX did not show any peak in the compounded feedstock form, its absence in the fibre spectra could not be taken as convincing evidence of layered-silicate exfoliation associated with the melt-spinning. However, given that the HRTEM images of PPEX fibre have manifested layered-silicates of thinner lateral dimension and more uniform dispersion than the injection-moulded PPEX, this would imply the occurrence of exfoliation during the melt-spinning process.

Finally, the larger lateral dimension of layered-silicates observed in the feedstock compounds and the injection-moulded samples compared with the corresponding melt-spun fibres would confirm that the extensional flow stress associated with melt-spinning had indeed extended the exfoliation of the layered-silicate. The above analyses would lead to the following proposal of the exfoliation mechanism of layered-silicate during the melt-spinning process and its schematic diagram is given in the literature (Lew, 2004).

- The coiled polymer chains intercalated in the layered-silicate disentangle, enabling the layered-silicates to begin to realign themselves in the flow direction. The polymer chains residing in the intercalated layered-silicate spacing will also be oriented in the flow direction.
- Drawdown of the melt stretches the polymer chains and promotes further penetration of the co-entangled polymer chains into the layered-silicate spacing.
- Under the very high elongational deformation rates, the silicate interlayers begin to shear apart and are subsequently delaminated by the polymer chains that reside in the silicate interlayers.
- The exfoliated silicate platelets improve the slippage of the polymer chains during drawdown from the capillary, enhance the melt stability and result in highly regular chain orientation in the spinline direction. Depending on the extent of exfoliation, the exfoliated silicate platelets preserve the chain alignment by suppressing molecular relaxation in the fibre traverse axis, leading to an overall improvement in the birefringence and mechanical performance of the fibre, as shown by the PPEX fibre.

19.8 Conclusions

Propylene–ethylene copolymer nanocomposites, in fibre or injection-moulded form, were produced from precompounded PP/organoclay feedstocks, maleated with a range of isotactic propylene MA oligomers of different M_w, MWD and functionality. The XRD and HRTEM results revealed that a highly nanodispersed and exfoliated layered-silicate phase was obtained when the PP was loaded, with a very low M_w, low MWD and highly functionalised oligomer at low/optimum concentration (4.2%). The low M_w would induce a favourable wetting property and ease of dispersion in the PP melt while

high functionality improves enthalpic interaction with the layered-silicate. Low MWD reduces the tendency to viscoelastic fracture during the spinning process and low concentration is important to prevent phase separation with the PP matrix.

Comparison of the compounded nanocomposite feedstocks and melt-spun fibres revealed the action of elongational stress on the PP matrix during the melt-spinning process would extend exfoliation of already intercalated layered-silicate and enhances its nanodispersion, similar to observations by Guan *et al*. (2005). This is further corroborated by the SEM, birefringence and rheological analyses in which the PPEX nanocomposite exhibited more desirable fibre features than the virgin PP fibre, characterised by its enhanced melt spinnability, surface texture, birefringence and mechanical properties, while maintaining a homogeneous PP phase.

PPEX melt had demonstrated a Newtonian-like modification which is unusual for a polymer system, given that the PP is viscoelastic and a viscoelastic system should develop a non-Newtonian flow behaviour. Therefore, this Newtonian-like modification of the PPEX melt is most likely to be attributed to a unique molecular level interaction between the PP matrix and the exfoliated silicate platelets. This could potentially lead to infinite increase of the melt-spin speed and hence the fibre tenacity.

19.9 References

Avrami, M. (1939), 'Kinetics of phase change. I general theory', *J Chem Phys,* **7** (12), 1103–1112.

Barra, G. M. O., Crespo, J. S., Bertolino, J. R., Soldi, V., Pires, A. T. N. (1999), 'Maleic anhydride grafting on EPDM: Qualitative and quantitative determination', *J Braz Chem Soc*, **10** (1), 31–34.

Bettini, S. H. P., Agnelli, J. A. M. (2000), 'Evaluation of methods used for analysing maleic anhydride grafted onto polypropylene by reactive processing', *Polym Testing*, **19** (1), 3015.

Brintzinger, H. H., Fisher, D., Mulhaupt, R., Rieger, B., Waymouth, R. M. (1995), 'Stereospecific olefin polymerization with chiral metallocene catalysts', *Angew Chem Int Ed*, **34** (11), 1143–1170.

Buchko, C. J., Chen, L. C., Shen, Y., Martin, D. C. (1999), 'Processing and microstructural characterization of porous biocompatible protein polymer thin films', *Polymer*, **40** (26), 7393–7407.

Carraher, C. E. (2003), *Giant Molecules: Essential materials for everyday living and problem solving*, 2nd edn, John Wiley & Sons Inc.

Chang, J. H., An, Y. U., Kim, S. J., Im, S. (2003), 'Poly(butylene terephthalate)/organoclay nanocomposites prepared by *in situ* interlayer polymerization and its fiber (II)', *Polymer*, **44** (19), 5655–5661.

Chang, J. H., Kim, S. J., Joo, Y. L., Im, S. (2004), 'Poly(ethylene terephthalate) nanocomposites by *in situ* interlayer polymerization: the thermo-mechanical properties and morphology of the hybrid fibers', *Polymer*, **45** (3), 919–926.

Cho, J. W., Paul, D. R. (2001), 'Nylon 6 nanocomposites by melt compounding', *Polymer*, **42** (3), 1083–1094.

Cogswell, F. N. (1975), 'Polymer melt rheology during elongational flow', in White, J. L. *Fiber and Yarn Processing*, *Appl Polym Symp No. 27*, John Wiley & Sons Inc.

Dennis, H. R., Hunter, D. L., Chang, D., Kim, S., White, J. L., Cho, J. W., Paul, D. R. (2001), 'Effect of melt processing conditions on the extent of exfoliation in organoclay-based nanocomposites', *Polymer*, **42** (23), 9513–9522.

Ergungor, Z., Cakmak, M., Barut, C. (2002), 'Effect of processing conditions on the development of morphology in clay nanoparticle filled nylon 6 fibers', *Macromol Symp*, **185** (1), 259–276.

Fornes, T. D., Yoon, P. J., Keskkula, H., Paul, D. R. (2001), 'Nylon 6 nanocomposites: the effect of matrix molecular weight', *Polymer*, **42** (25), 9929–9940.

Giannelis, E. P., Krishnamoorti, R., Manias, E. (1999), 'Polymer-silicate nanocomposites: model systems for confined polymers and polymer brushes', *Adv Polym Sci*, **138**, 107–147.

Gilman, J. W., Kashiwagi, T., Nyden, M., Harris, R. H. Jr. (1999), *New Flame Retardants Consortium Final Report*, NISTIR 6357, NIST, pp. 1–26.

Giza, E., Ito, H., Kikutani, T., Okui, N. (2000a), 'Fiber structure formation in high-speed melt spinning of polyamide 6/clay hybrid nanocomposites', *J Macromol Sci – Phys*, **39 B** (4), 545–559.

Giza, E., Ito, H., Kikutani, T., Okui, N. (2000b), 'Structural control of polyamide 6/clay nanocomposite fibers by in-line drawing process', *J Polym Eng*, **20** (6), 403–425.

Gopakumar, T. G., Lee, J. A., Kontopoulou, M., Parent, J. S. (2002), 'Influence of clay exfoliation on the physical properties of montmorillonite/polyethylene composites', *Polymer*, **43** (20), 5483–5491.

Guan, G. H., Li, C. C., Zhang, D. (2005), 'Spinning and properties of poly(ethylene terephthalate)/organomontmorillonite nanocomposite fibers', *J Appl Polym Sci*, **95** (6), 1443–1447.

Huang, P. Y., Feng, J., Hu, H. H., Joseph, D. D. (1997), 'Direct simulation of the motion of solid particles in Couette and Poiseuille flows of viscoelastic fluids', *J Fluid Mech*, **343**, 73–94.

Kang, S., Kim, J., Park, M. Hong, S. I. (2000), 'Effects of surface modification of silicas on the properties of organic/inorganic nanocomposites', *Polym Preprints*, **41** (1), 596–597.

Kawasumi, M., Hasegawa, N., Kato, M., Usuki, A., Okada, A. (1997), 'Preparation and mechanical properties of polypropylene–clay hybrids', *Macromolecules*, **30** (20), 6333–6338.

Kim, G. M., Lee, D. H., Hoffmann, B., Kressler, J., Stöppelmann, G. (2001), 'Influence of nanofillers on the deformation process in layered silicate polyamide-12 nanocomposites', *Polymer*, **42** (3), 1095–1100

Kim, K. N., Kim, H. S., Lee, J. W. (2000), 'Mixing characteristics and mechanical properties of polypropylene–clay composites', *Proc ANTEC 2000*, **3**, 3872–3876.

Kim, T. H., Lim, S. T., Lee, C. H., Choi, H. J., Jhon, M. S. (2003), 'Preparation and rheological characterization of intercalated polystyrene/organophilic montmorillonite nanocomposite', *J Appl Polym Sci*, **87** (13), 2106–2112.

Koo, C. M., Ham, H. T., Kim, S. O., Wang, K. Y., Chang, I. J. (2002), 'Morphology evolution and anisotropic phase formation of the maleated polyethylene-layered silicate nanocomposites', *Macromolecules*, **35** (13), 5116–5122.

Lew, C. Y. (2004), Polymer-clay nanocomposites: preparation, processing and properties, Doctoral Thesis, Queen's University Belfast.

Lew, C. Y., Murphy, W. R., McNally, G. M. (2004), 'Preparation and properties of polyolefin-clay nanocomposites', *Polym Eng Sci*, **44** (6), 1027–1035.

Li, J., Zhou, C., Gang, W. (2003), 'Study on nonisothermal crystallization of maleic anhydride grafted polypropylene/montmorillonite nanocomposite', *Polym Testing*, **22** (2), 217–223.

Ma, J., Qi, Z., Hu, Y. (2001), 'Synthesis and characterization of polypropylene/clay nanocomposites', *J Appl Polym Sci*, **82** (14), 3611–3617.

Mackay, M. E., Dao, T. T., Tuteja, A., Ho, D. L., van Horn, B., Kim, H. C., Hawker, C. J. (2003), 'Nanoscale effects leading to non-Einstein-like decrease in viscosity', *Nature Mater*, **2**, 762–766.

Madbouly, S., Ohmomo, M., Ougizawa, T., Inoue, T. (1999), 'Effect of the shear flow on the phase behaviour of polystyrene/poly(vinyl methyl ether) blend', *Polymer*, **40** (6), 1465–1472.

Maier, C., Calafut, T. (1998), *Polypropylene. The definitive user's guide and databook*, Plastics Design Library.

Manias, E., Touny, A., Wu, L., Strawhecker, K., Lu, B., Chung, T. C. (2001), 'Polypropylene/montmorillonite nanocomposites. Review of the synthetic routes and materials properties', *Chem Mater*, **13** (10), 3516–3523.

McConnell, D., Hornsby, P. R., Lew, C. Y., Qua, E. H. (2006), 'Structure-property of PET nanocomposite fibres', *ANTEC 2006*, accepted.

McCord, M. G., Matthews, S. R., Hudson, S. M. (2004), 'Extrusion and analysis of nylon/montmorillonite nanocomposite filaments', *J Adv Mater*, **36** (1), 44–56.

McNally, T., Murphy, W. R., Lew, C. Y., McNally, G. M., Turner, R. J., Brennan, G. P. (2003), 'Polyamide-12 layered silicate nanocomposites by melt blending', *Polymer*, **44** (9), 2761–2772.

Natta, G., Pino, P., Corradini, P., Danusso, F., Mantica, E., Mazzanti, G., Moranglio, G. (1955), 'Crystalline high polymers of α-olefin', *J Am Chem Soc*, **77** (6), 1708–1710.

Pavlikova, S., Thomann, R., Reichert, P., Mülhaupt, R., Marcincin, A., Borsig, E. J. (2003), 'Fiber spinning from poly(propylene)–organoclay nanocomposite', *J Appl Polym Sci*, **89** (3), 604–611.

Peak, D., Ford, R. G., Sparks, D. L. (1999), 'An *in situ* ATR-FTIR investigation of sulfate bonding mechanisms on goethite', *J Coll Interface Sci*, **218** (1), 289–299.

Premphet, K., Chalearmthitipa, S. (2001), 'Melt grafting of maleic anhydride onto elastomeric ethylene-octene copolymer by reactive extrusion', *Polym Eng Sci*, **41** (11), 1978–1986.

Qi, D. W., Luo, L. S., Aravamuthan, R., Strieder, W. (2002), 'Lateral migration and orientation of elliptical particles in Poiseuille flows', *J Statistical Phys*, **107** (1/2), 101–120.

Reichert, R., Nitz, H., Klinke, S., Brandsch, R., Thomann, R., Mülhaupt, R. (2000), 'Poly(propylene)/organoclay nanocomposite formation: Influence of compatibilizer functionality and organoclay modification', *Macromol Mater Eng*, **275** (1), 8–17.

Roberts, C., Cosgrove, T., Schmidt, R. G., Gordon, G. V. (2001), 'Diffusion of poly(dimethylsiloxane) mixtures with silicate nanoparticles', *Macromolecules*, **34** (3), 538–543.

Roder, H. (1999), 'Polypropylene – a material of the future', *Prog Polym Sci*, **24** (8), 1205–1215.

Rzanek-Boroch, Z., Schmidt-Szalowski, K., Janowska, J., Dudziński, K., Szymańska, A.,

Misiak, M. (2002), 'Thin films obtained by PE-CVD method from hexamethyldisiloxane under atmospheric pressure', *Proc International Synposium on High Pressure Low Temperature Plasma Chemistry*, Pühajärve, Estonia, 415–419.

Salem, D. R. (2000), *Structure Formation in Polymeric Fibres*, Hanser Gardner Publications Inc.

Segrè, G., Silberberg, A. (1961), 'Radial Poiseuille flows of suspensions', *Nature*, **189**, 209.

Siochi, E. J., Working, D. C., Park, C., Lillehei, P. T., Rouse, J. H., Topping, C. C., Bhattacharyya, A. R. and Kumar, S. (2004), 'Melt processing of SWCNT–polyamide nanocomposite fibers', *Composites Part B: Engineering*, **35** (5), 439–446.

Steinkamp, R. A., Grail, T. J. (1975), US Patent no. 3 863 265.

Trouton, F. T. (1906), *Proc Royal Soc*, **77** (A), 426.

Vandenberg, E. J., Salamone, J. C. (1992), *Catalysis in Polymer Synthesis*, Oxford University Press.

Verleye, G. A. L., Roeges, N. P. G., Moor, M. O. D. (2001) *Easy Identification of Plastics and Rubbers*, Rapra Technology Ltd, Chapter 3, pp. 28–29.

Whinfield, J. R. (1946), *Nature*, **158**, 930.

Wittcoff, H. A., Reuben, B. G., Plotkin, J. S. (2003), *Industrial Organic Chemicals*, 2nd edn, John Wiley & Sons Inc.

Xu, W., Ge, M., He, P. (2002), 'Nonisothermal crystallization kinetics of polypropylene/ montmorillonite nanocomposites', *J Polym Sci, Part B: Polym Phys*, **40** (5), 408–414.

Xu, W. B., Zhou, Z. F., Ge, M. L., Pan, W. P. (2004), 'Polyvinyl chloride/ montmorillonite nanocomposites: Glass transition temperature and mechanical properties', *J Thermal Anal Calorimetry*, **78** (1), 91–99.

Yeh, J. M., Chen, C. L., Chen, Y. C., Ma, C. Y., Lee, K. R., Wei, Y., Li, S. (2002), 'Enhancement of corrosion protection effect of poly(*o*-ethoxyaniline) via the formation of poly(*o*-thoxyaniline)–clay nanocomposite materials', *Polymer*, **43** (9), 81–86.

Yoon, K. H., Polk, M. B., Min, B. G., Schiraldi, D. A. (2004), 'Structure and property study of nylon-6/clay nanocomposite fiber', *Polym Int*, **53** (12), 2072–2078.

Zhang, X., Yang, M., Zhao, Y., Zhang, S., Dong, X., Liu, X., Wang, D. and Xu, D. (2004), 'Polypropylene/montmorillonite composites and their application in hybrid fiber preparation by melt-spinning', *J Appl Polym Sci*, **92** (1), 552–558.

Ziabicki, A. (1976), *Fundamentals of Fibre Formation*, John Wiley & Sons.